APPLICATION OF POLYELECTROLYTE MULTILAYER REVERSE OSMOSIS MEMBRANE IN SEAWATER DESALINATION

BY

Farid Fadhillah

A Dissertation Presented to the

DEANSHIP OF GRADUATE STUDIES

KING FAHD UNIVERSITY OF PETROLEUM & MINERALS

DHAHRAN, SAUDI ARABIA

In Partial Fulfillment of the
Requirements for the Degree of

DOCTOR OF PHILOSOPHY

In

CHEMICAL ENGINEERING

APRIL, 2012

KING FAHD UNIVERSITY OF PETROLEUM & MINERALS

DHAHRAN, SAUDI ARABIA

DEANSHIP OF GRADUATE STUDIES

This dissertation, written by Farid Fadhillah under the direction of his dissertation advisor and approved by his dissertation committee, has been presented to and accepted by the Dean of Graduate Studies, in partial fulfilment of the requirements for the degree of DOCTOR OF PHILOSOPHY in Chemical Engineering.

Dissertation Committee

Thesis Advisor
Prof. Dr. S.M. Javaid Zaidi

Co- Advisor
Dr. Zafarullah Khan

Member
Dr. Mazen M. Khaled

Department Chairman
Dr. Usamah A. Al-Mubaiyedh

Member
Prof. Dr. Basel Abu Sharkh

Dean of Graduate Studies
Dr. Salam A. Zummo

Member
Prof. Dr. Paula T. Hammond

23/4/12
Date:

DEDICATED TO

MY BELOVED PARENT AND PARENT IN LAW, MY WIFE DESTI AND

MY THREE SONS: ABDULLAH, ABDURRAHMAN, AND ABDURRAZZAQ

ACKNOWLEDGMENT

I would like to thank to my dissertation advisor, Prof. S.M. Javaid Zaidi and my dissertation co- advisor, Dr. Zafarullah Khan for their support, superb mentoring, wonderful patience, and excellent advice for almost three years of my Ph.D. research. I would like to thank to Dr. Mazen Khaled for providing his lab and research facilities so I had very nice and comfortable place to work. I would like to thank to Prof. Basel Abu shark for his input. I would like to thank to Prof. Paula Hammond for her technical input and suggestion during my stay at MIT and through monthly video conference and also to Dr. Fevzi Cebeci for his guidance at the beginning of my work with Layer by Layer (LbL) Assembly. I would like to acknowledge Prof. Takeshi Matsuura for his help in preparation of nanoclays modified thin film composite polyamide membrane. It was an honour for me to be able to work with the experts in this interesting topic.

I would like to acknowledge Center of Excellence for Scientific Research Collaboration with MIT and King Abdulaziz City for Science and Technology (KACST) for financially supporting my research. I would like to acknowledge Dr. Faizurrahman for his great help in setting up the permeation cell. I would like to thank Dr. Libby shaw of center of material science and engineering (CMSE) MIT and Dr. Rachid Sougrat of King Abdullah University of Science and Technology Core lab for their help in imaging and characterization.

I would also like to thank to my parent and my parent in law for their support and pray, also to my wife and my sons who inspire and encourage my work.

I would also like to thank to all of my research group members from MIT: Dr. Fevzi, Dr. Gozde, Jason, Simon, Rong and Damien. Special thanks to Asif Matin for his friendship since the beginning of my study at KFUPM, for facing the hardship together at MIT and for working together in the project for three years.

I would like to acknowledge Department of Chemical Engineering, of Mechanical Engineering, and of Chemistry for providing an excellent research environment. I would like to acknowledge King Fahd University of Petroleum and Minerals (KFUPM) for providing me generous assistant ship and travel financial support from Dhahran to Boston.

I would like to thank to all my Indonesian community especially Mr. Ahmad Ridha, and Mr. Putu Danu Raharja, all CHE technicians, staffs, and janitors for their help during my Ph.D. research.

TABLE OF CONTENTS

CHAPTER SIX

CHAPTER SEVEN

LIST OF TABLES

LIST OF FIGURES

DISSERTATION ABSTRACT

Name : Farid Fadhillah

Title : Application of Polyelectrolyte Multilayer Reverse Osmosis Membrane in Seawater Desalination.

Major Field : Chemical Engineering

Date of Degree : April 2012

Alternate adsorption of polyanion and polycation onto a substrate through layer by layer (LbL) assembly provides a convenient mean of depositing ultrathin film with controlled thicknesses and compositions. Spin assisted layer by layer (SA-LbL) assembly was introduced to reduce processing time and improve layering quality. This dissertation explores the use of SA-LbL assembly in particular for fabricating reverse osmosis (RO) membrane.

The effect several parameters such as molecular weight of polyelectrolyte, concentration of polyelectrolyte solution, spin speed, and ionic strength of polyelectrolyte solution has been thoroughly investigated. However; the effect of pH for this particular technique has not been investigated yet whereas pH is one of the most important parameter for controlling film properties. This dissertation also investigated the effect of pH coupled with other parameters such as spin speed and concentration.

Four different polyelectrolyte membrane systems such as poly(diallyldiamine ammonium chloride) (PDAC) /poly(vinyl sulfate) (PVS); poly(allylamine hydrochloride)

(PAH)/PVS; Poly(ethylene imine) (PEI)/Poly(acrylic acid) (PAA), and PAH/PAA were deposited on polysulfone (PSF) ultrafiltration membrane as a support. Characterization using atomic force microscope (AFM), Fourier transform infra red (FTIR), and contact angle show the existence of the coating on PSF membrane. The membrane performance in terms of salt rejection and water flux was also examined using cross-flow permeation cell for short term testing (7 hours). PAH/PAA was selected and tested for longer period (48 hours) to examine the film stability. Effects of various RO operating conditions such as pressure, temperature and salt concentration of feed water on permeation characteristic of the PAH/PAA membrane were also thoroughly investigated. The testing and characterization shows that PAH/PAA membranes are quite stable and still intact with the PSF support however their performance becomes poorer as the feed water salt concentration is increased.

In this dissertation, hand-made RO polyamide (PA) was also fabricated using interfacial polymerization technique and tested as comparison. Nanoclays were incorporated in PA membrane to enhance membrane performance. The test demonstrates that the performance of PAH/PAA membrane is comparable to that of hand-made RO PA. While clay modified PA performs somewhat better than PAH/PAA and unmodified PA membranes.

DOCTOR OF PHILOSOPY DEGREE

KING FAHD UNIVERSITY OF PETROLEUM & MINERALS

DHAHRAN, SAUDI ARABIA

ملخص الرسالة

الإســــــــــــم: فريد فضيله

عنوان الرسالة: تطبيقات أغشية التناضح العكسي باستخدام طبقات محلول متعدد الالكتروليت في تحلية مياه البحر

التخصـــــص: هندســـة كيميـــــائية

تأريخ الدرجة : أبريل 2012

الامتزاز البديل باستخدام متعدد الانيون ومتعددالكاتيون على سطح من خلال تجميع طبقة على طبقة, يوفر اداة ملائمة

لترسيب غشاء رقيق بسماكات وتراكيز مسيطر عليها.تركيب طبقة على طبقة بمساعدة النسج استعمل لتقليل زمن التصنيع وتحسين جودة التصفيف.اكتشف في هذا البحث استخدام تركيب طبقة على طبقة بمساعدة النسج في تصنيع أغشية التناضح العكسي.

تأثير عوامل مختلفة مثل الوزن الجزيئي لمتعدد الالكتروليت وتركيز محلول متعدد الالكتروليت وسرعة النسج والقوة الايونية لى محلول متعدد الالكتروليت درست بشكل تام . الا أنه حتى الان لم يتم دراسة تأثير درجة الحموضة على هذة التقنية والذي يعتبرمن اهم العوامل للسيطرة على خصائص الغشاء. في هذا البحث تم دراسة تأثير درجة الحموضة مع متغيرات مختلفة كسرعة النسج والتركيز.

أربعة أنظمة مختلفة من أغشية متعدد الالكتروليت مثل متعدد (diallyldiamine ammonium chloride) (PDAC) /(poly(vinyl sulfate) (PVS) وPAH/PVS) poly (allylamine hydrochloride) و Poly(ethylene imine) (PEI) /Poly(acrylic acid) (PAA) و PAH/PAA رسبت على غشاء رقيق من polysulfone (PSF) والذي استخدم كدعامة.

التأكد من وجود التغطية على غشاء PSF تم باستخدام مجهر القوة الذرّي (AFM) و مطياف الأشعة تحت الحمراء (FTIR) و زاوية السطح البيني. وقد تم أيضا اختبار أداء الاغشية من حيث رفض الملح وتدفق المياه باستخدام خلية النفاذية ذات التدفق العرضي لاختبار المدى القصير(7ساعات), بينما أختبر PAH/PAA لفترة زمنية أطول (48ساعة) لدراسة استقرارية الفيلم.

تم أيضا دراسة التناضح العكسي بشكل واف تحت ظروف تشغيلية مختلفة مثل الضغط ودرجة الحرارة وتركيز الملح في اللقيم على خصائص النفاذية لأغشية PAH/PAA . أظهرت نتائج الاختبارات والتوصيف أن أغشية PAH/PAA أكثر أستقرارا عند استخدام (PSF) كدعامة , الا أن أداءها قل عند ما زاد تركيز الملح في اللقيم.

تم أيضا في هذا البحث تصنيع RO polyamide (PA) يدويا باستخدام تقنية البلمرة البينية واختبر كمقارنة. كما تم أيضا أدماج nanoclays في أغشية PA لتحسين أداءها. أظهرت الإختبارات بأن أداء أغشية PAH/PAA مشابة لاغشية RO PA المصنعة يدويا, بينما أداء اغشية PA المعدلة باستخدام Nanoclays كان أفضل من أغشية PAH/PAA وأغشية PA الغير معدلة .

درجة الدكتوراه في الفلسفة

جامعة الملك فهد للبترول والمعادن

الظهران, المملكة العربية السعودية

CHAPTER ONE

INTRODUCTION & BACKGROUND

1.1. WATER SCARCITY AND SOLUTION

Nowadays, water shortage is a common problem in almost all countries all around the world. In 2004, WHO/UNICEF has reported that there was more than 1.1 billion people lack access to improve-drinking water supplies as can be seen in Figure 1.1. The number of people who have little or no sanitation was even more than two times larger. Both problems result in deaths attributable to diarrheal disease [1].

Problem with fresh water can also be seen from water stress index (WSI) which is actually ratio of total annual freshwater withdrawals to hydrological availability. Moderate and severe water stresses occur above a threshold of 20 and 40%, respectively [2]. As can be seen from Figure 1.2., all countries in Middle East, North Africa, South Asia, part of Europe, and western part of America have very high stress water index and this problem is expected to grow worse in the coming years [3]

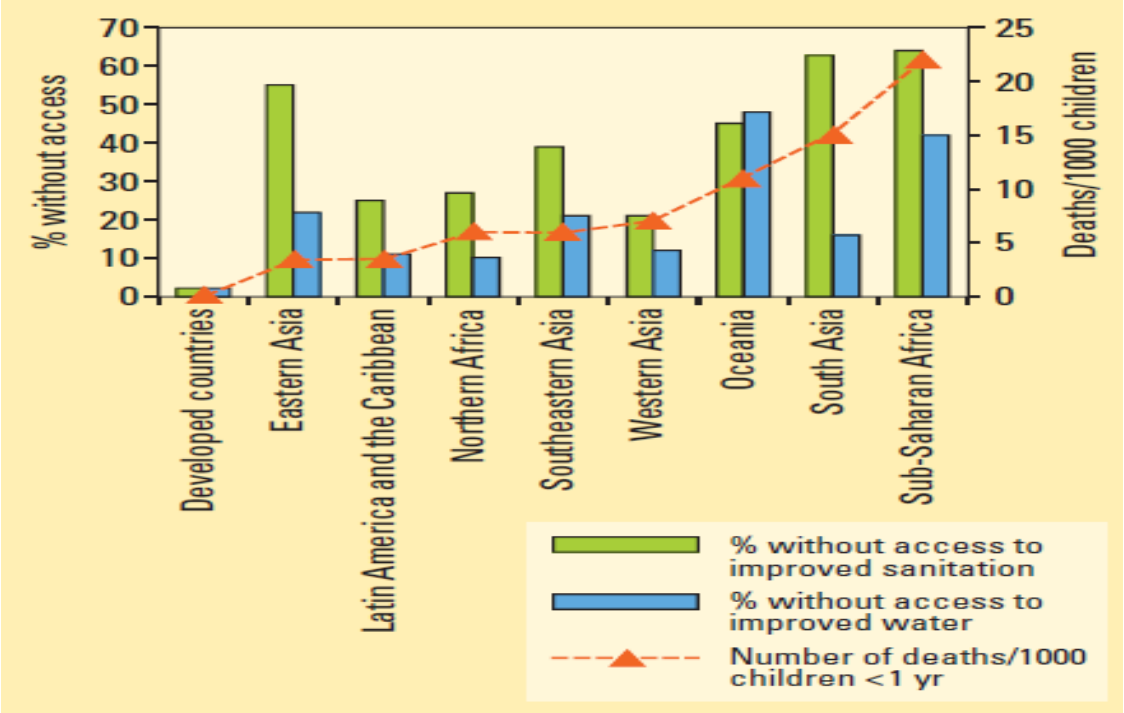

Figure 1.1. comparison between lack of access to improved water and sanitation and deaths attributable to diarrheal disease [1].

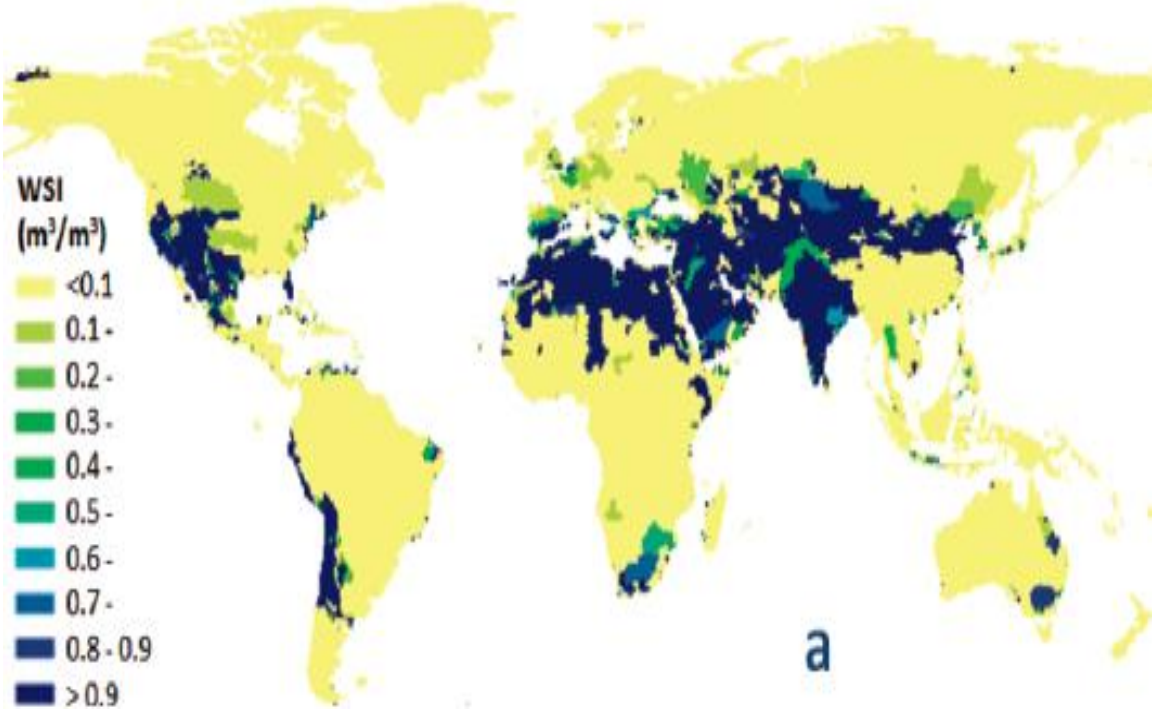

Figure 1.2. Water stress index in 2009 [2].

There have been several methods developed to address the fore mentioned problem, such as through water disinfection, water decontamination, water re-use and reclamation and water desalination. All methods are complementary each other and typically they all can be found in water treatment plant. However, of those methods, it is only desalination that can provide fresh water for drinking from traditional sources such as ground water, sea water and other saline aquifers [3]. Meanwhile, water re-use and reclamation is mainly used to provide fresh water for other purposes such as irrigation, power plant cooling water, industrial process water, and ground water recharge [4]. The significance of desalination is because all those traditional sources account for 97.5 % of all water on the earth. Therefore capturing even a tiny portion of that water can have significant impact in reducing the water scarcity [3].

1.2. MEMBRANE BASED DESALINATION TECHNOLOGY

1.2.1. CURRENT MEMBRANE BASED DESALINATION TECHNOLOGY ITS DRAWBACKS

Desalination is a general term for any process of removing salt from water to produce fresh water. Fresh water is defined as containing less than 1000 mg/L of salt or total dissolved solid (TDS) however some countries may apply lower standard such as 500 mg/L of salt or TDS [4]. Desalination technologies can be divided into two main groups, namely thermal based and membrane based desalination. The most used technology for thermal based desalination is multi stage flash (MSF) while RO is the most used tehcnology in membrane based desalination. As can be seen from Figure 1.3. MSF process became highly popular and many commercial plants were built worldwide using

this technology during the last three decades, particularly in the Arabian Gulf where fuel is readily available. However RO more dominated in other areas where fuel cost is expensive. Both technologies have continuously developed in terms of process design thus the unit cost of water produced by both techniques reduce significantly. It can be seen from Figure 1.4 and Figure 1.6 that the unit cost of water by MSF reduces significantly over the last three decades that is from US$ 5 /m3 to about US$ 1.004 /m^3 [5]. However for middle east condition the unit cost in 2005 can be as low as US$ 0.52/m^3 because of low fuel price [6]. While the unit cost of RO for seawater reduces from US$ 4.8 /m^3 to US$ 1 /m^3 [5].

Thermal based desalination can be better dealing with high salinity water and produce water with much lower TDS or salt concentration but this technology is more energy intensive for example MSF requires thermal energy of 12 kWh/m^3 water and electrical energy of 35 kWh/m^3 water compared to RO that requires only electrical energy of 0.4-7 kWh/m^3 water [7]. Aside from this disadvantage, corrosion is also major problem that typically found in thermal based desalination plant, not to mention the high capital and operational costs that limit the adoption of thermal based desalination in many areas [3].

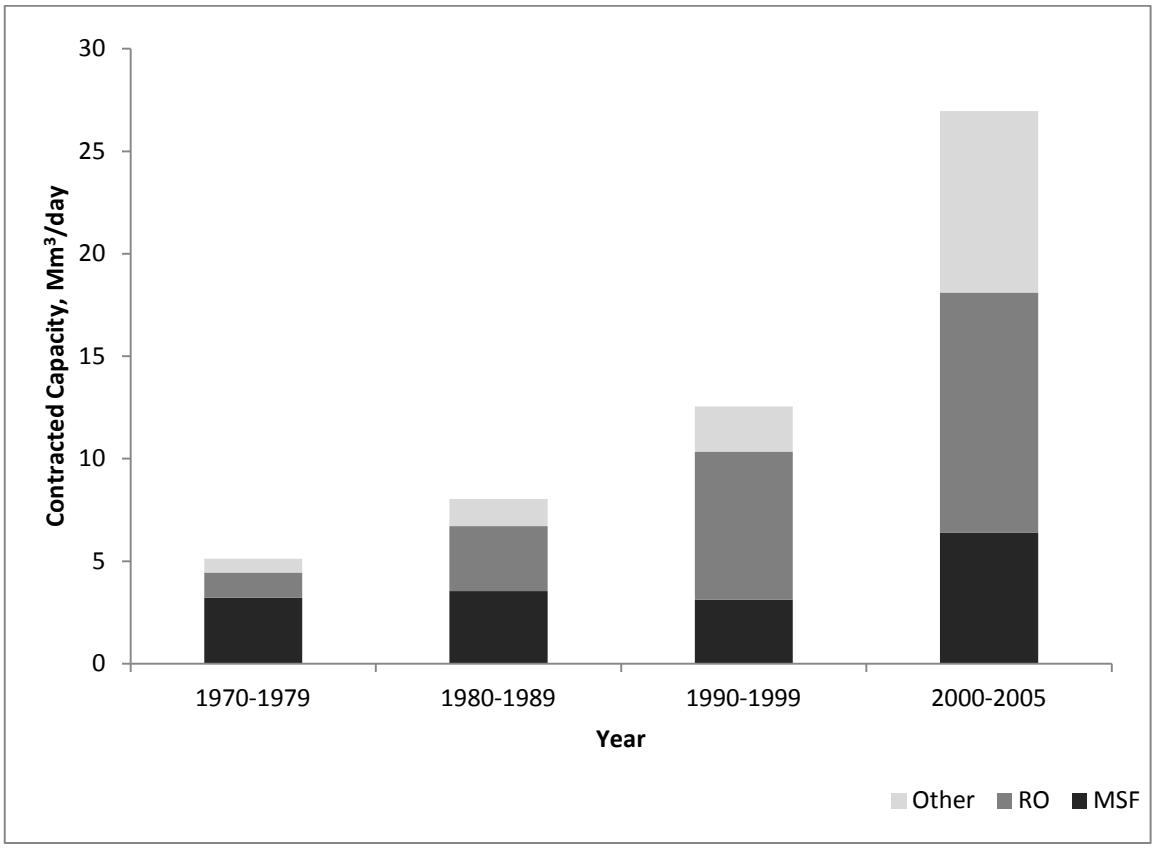

Figure 1.3. Contracted Desalination Capacity World wide (adapted from [8]).

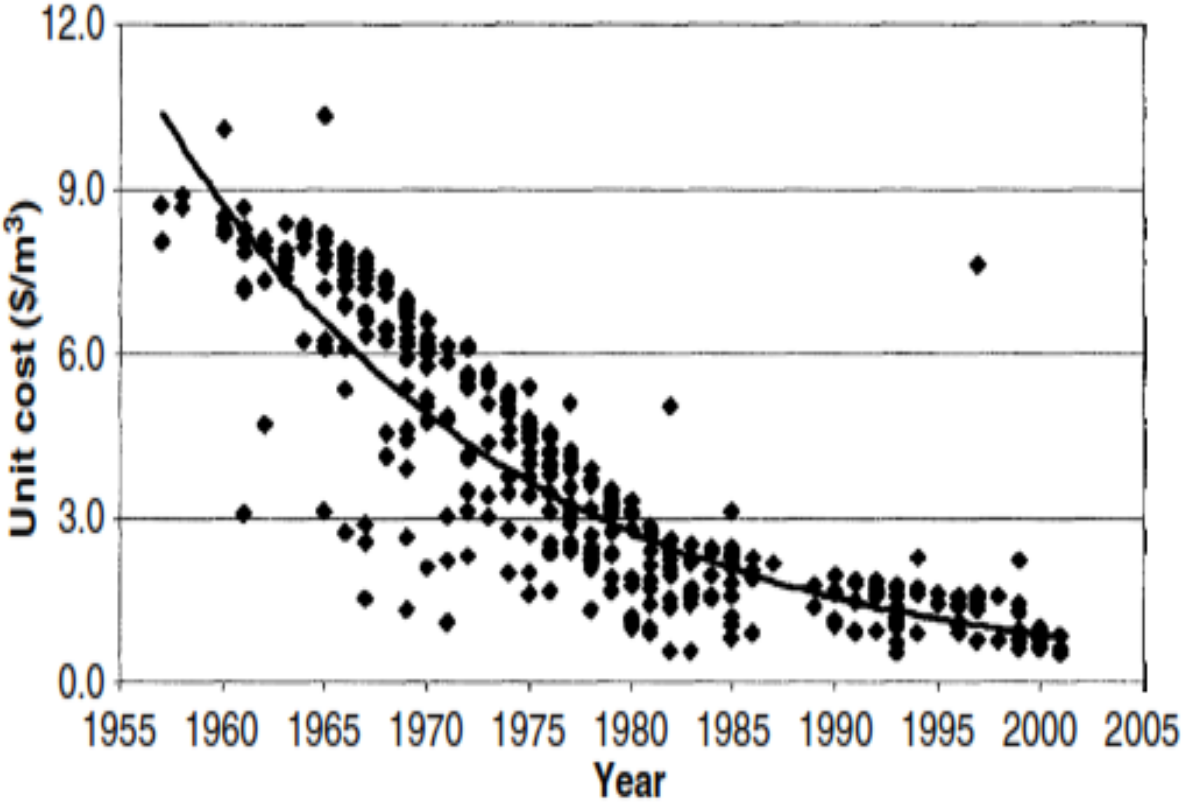

Figure 1.4. Unit cost of water produced using MSF [8].

The RO desalination is expected to grow in a faster rate than MSF and other thermal based desalination and will dominate the desalination technology in the near future. The data shows that in 2001, 51% of new installed capacity used RO and in 2003, 75% of new installed capacity used RO [4]. This trend also occurs in Middle East region for example, in Saudi Arabia, in which MSF and other thermal based is still dominating with 65% share over RO with 35% share in 2003 but the growth rate of RO process is 6.7% per year which is almost twice higher than that of MSF.

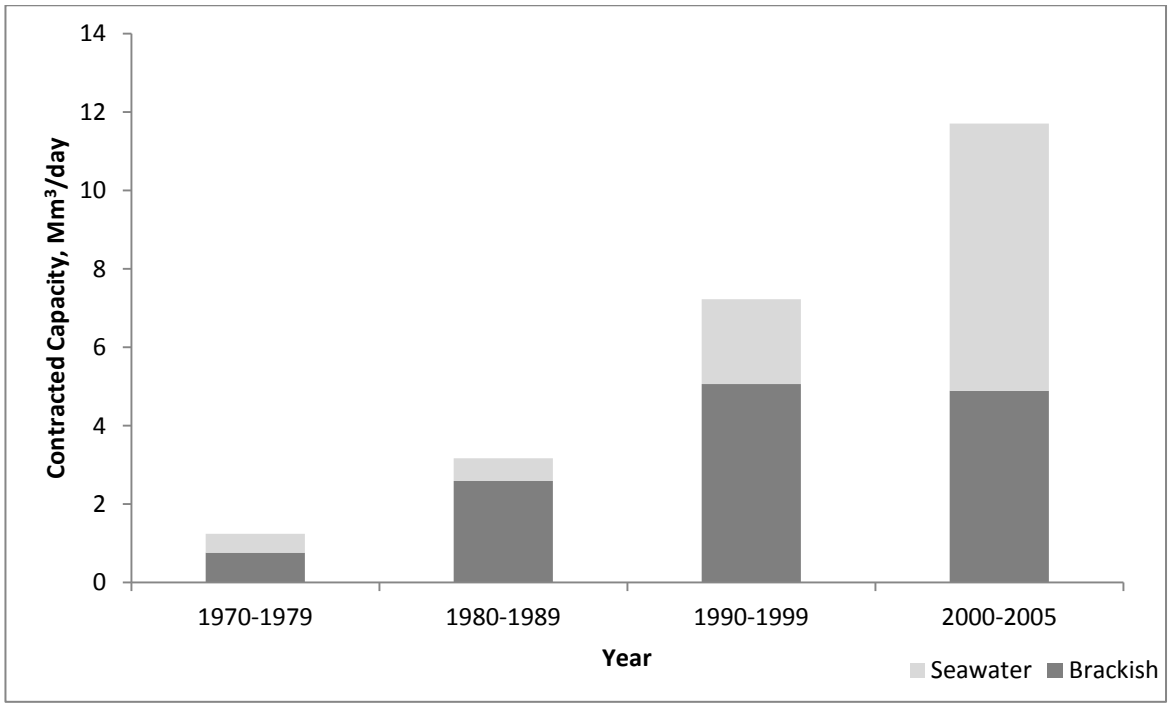

Figure 1.5. Contracted RO desalination capacity Worldwide (adapted from [8])

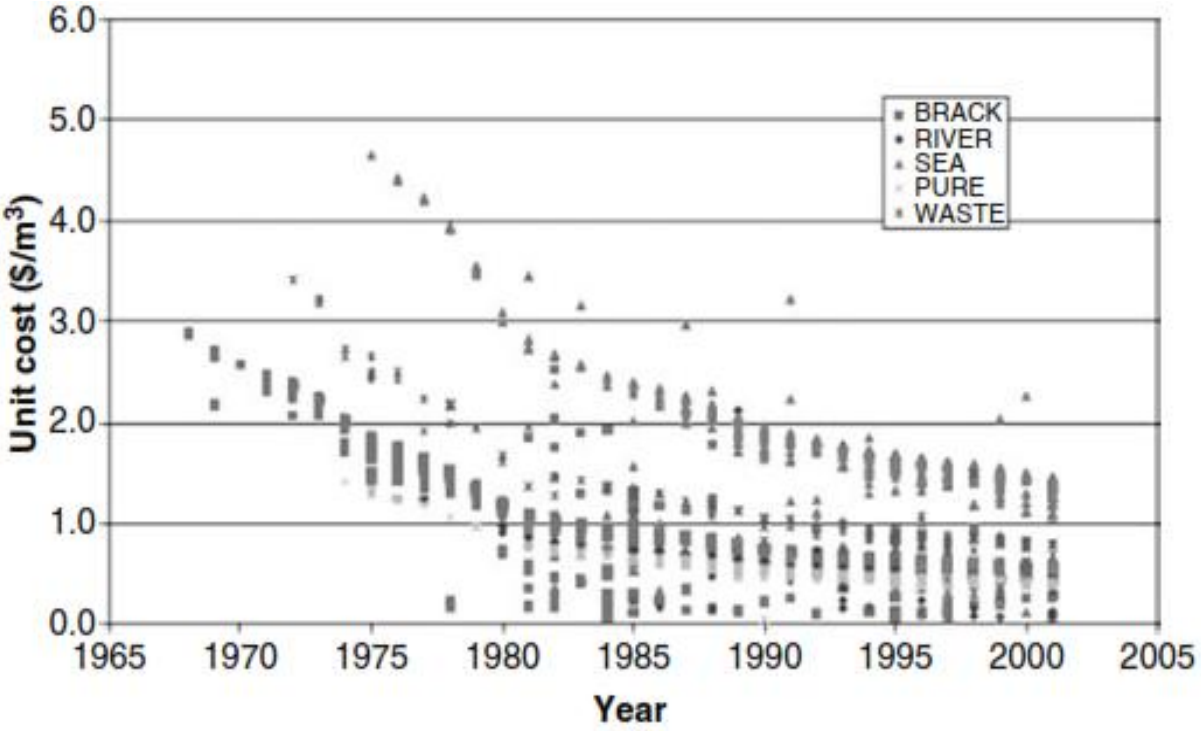

Figure 1.6. Unit cost of water produced through RO processes. [8]

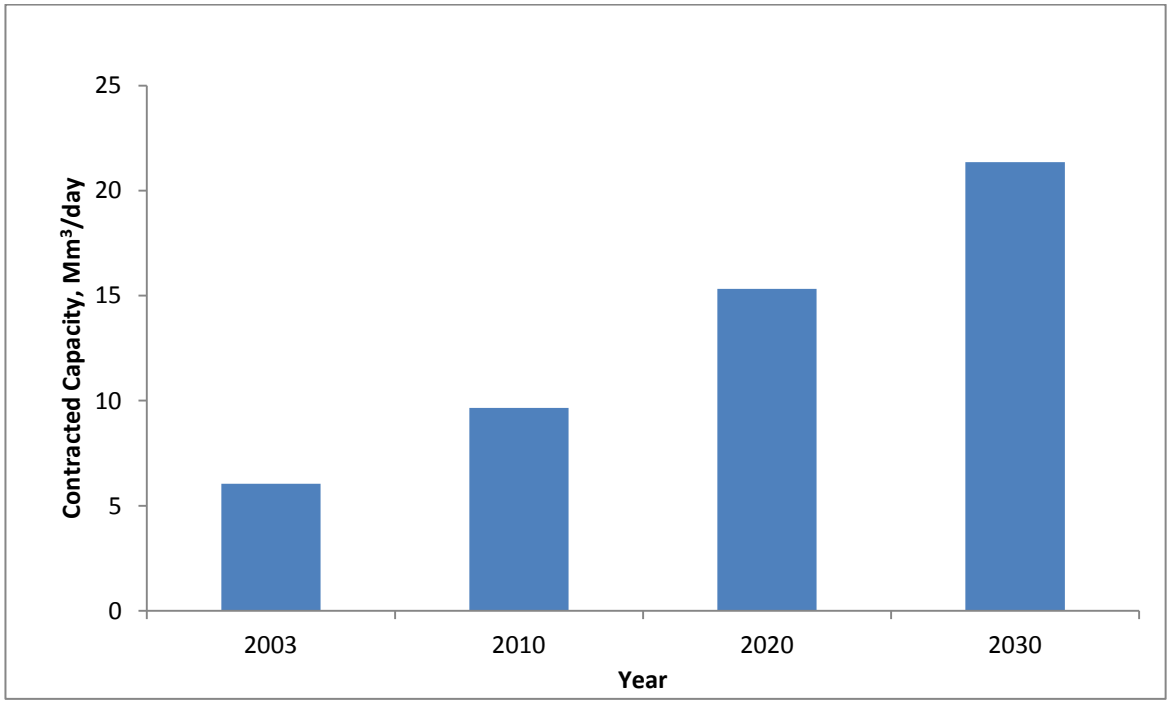

Figure 1.7. Contracted desalination capacity in Saudi Arabia (adapted from [8])

The first RO membrane ever used in the industry was made of cellulose acetate fabricated through phase inversion technique. This asymmetric membrane was industrial standard for almost 15 years since 1960. At that time, CA membrane already showed much better performance compared to any symmetric membrane. Unfortunately CA membrane is easily compacted, good feed source for microorganism and hydrolyzed in the presence of water [7]. The new membrane was developed with totally new concept. This is later known as thin film composite membrane which was developed by Cadotte in the beginning of 1970s and then due to much better performance and properties compared to CA, TFC becomes industrial standard and used for the first time in Jeddah RO plant, Saudi Arabia [7].

TFC RO membrane is made through interfacial polymerization (IP) of two highly reactive monomers i.e. methyl phenylene diamine (MPD) and trimesoyl chloride (TMC) on top of polysulfone (PSF) support. MPD dissolves in aqueous phase while TMC dissolves in organic phase such as n-hexane. Polyamide (PA) is formed once MPD diffuse across the interface of aqueous and organic phase and reacts with TMC in the organic phase. In order the film thickness to build up, MPD must continually diffuse through already formed polyamide and react with TMC in the interface between polyamide and organic phase. Therefore, typical RO membrane as available in the market today consists of three layers, namely polyester (PE) web, PSF, and PA. PSF and PE layers are typically around 40 μm and 130 μm thick, respectively and highly porous and provide the mechanical strength of whole membrane while PA is rather non-porous with 0.3 – 3 μm thickness and serves as active layer which is responsible for salt rejection [9].

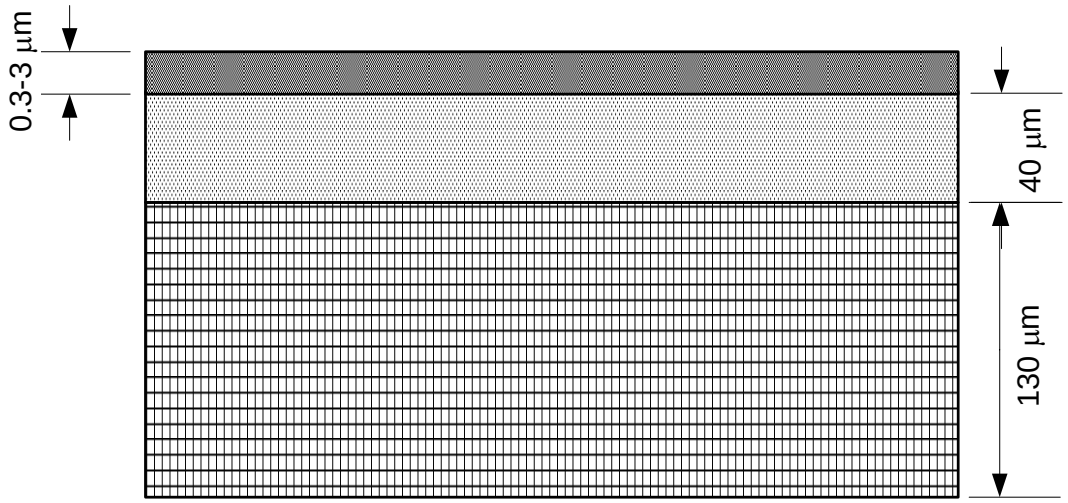

Figure 1.8. Schematic Diagram of a Thin Film Composite Membrane

Thin film composite RO membrane offers advantages over typical asymmetric RO membrane for instance each individual layer can be optimized for its particular function. However it does have some disadvantages as well. The difficulty in controlling the film thickness and film morphology is one of major disadvantages meanwhile the two parameters determines the performance of the membrane such as permeability, salt rejection as well as fouling resistance properties. This problem arises due to the nature of interfacial polymerization process. Aside from that, IP can only be applied for limited polymer such as polyamide and polycarbonate, thus there has been no significant development of this sort of membrane for the last 3 decades from chemistry point of view. The use of organic solvent is also another issue from safety and environmental point of view. A true thin film fabrication technique is supposed to offer the flexibility in controlling such parameters and can be applied for different materials. Therefore, it is imperative to use real thin film fabrication technology in order to explore many different materials that may have better characteristic than PA.

1.2.2. MEMBRANE BASED DESALINATION PLANT And MODULE

A flow sheet of a reverse osmosis based desalination plant is shown in Figure 1.9. The abstraction of feed water can be realised either through coast- and beach wells or through open seawater intake systems. Coast- and beach wells provide better quality water with less turbidity, algae and total dissolved solids than open seawater intakes, but require more space. In brackish water desalination, wells are used to abstract feed water.

Pre-treatment includes all activities to adjust the intake water in constitution and pH-value. Particulate matter is removed from the feed-water and chemicals are added to

prevent scaling and fouling. The pumping system is required to overcome height differences within the distribution chain and to apply the necessary pressure to the feed. The membrane is capable of separating salt from water with a rejection of 98–99.5%, depending on the membranes in use.

The energy recovery system is responsible for the transfer of potential energy from the concentrate to the feed. Current energy recovery systems such as work exchangers operate with efficiencies of up to 96%. In post-treatment, permeate is re-mineralised, re-hardened, disinfected by chlorination and adjusted to drinking water standards. A control system maintains a continuous and reliable production.

The membrane either cellulose acetate or polyamide must be packed into a membrane module. Hollow fine fiber was the most used configuration in the early years of RO membrane. At the time when Permasep HF-Permeators from Dupont for desalination of seawater were introduced in to the market in the 1970's they had some advantages compared to seawater spiral wound elements which explain their success in the RO-market at this time [10]. This is mainly due to Permasep HF-Permeators are self supporting membranes. This simplified the hardware for fabrication compared to flat-sheet membranes which have to be assembled with spacers and supports. In addition the hollow fibers were able to operate up to 82.7bar (1,200 psi), which allowed to reach relatively high recoveries, like 60 percent at 25°C and 38,000 mg/L feed TDS (total dissolved solids).

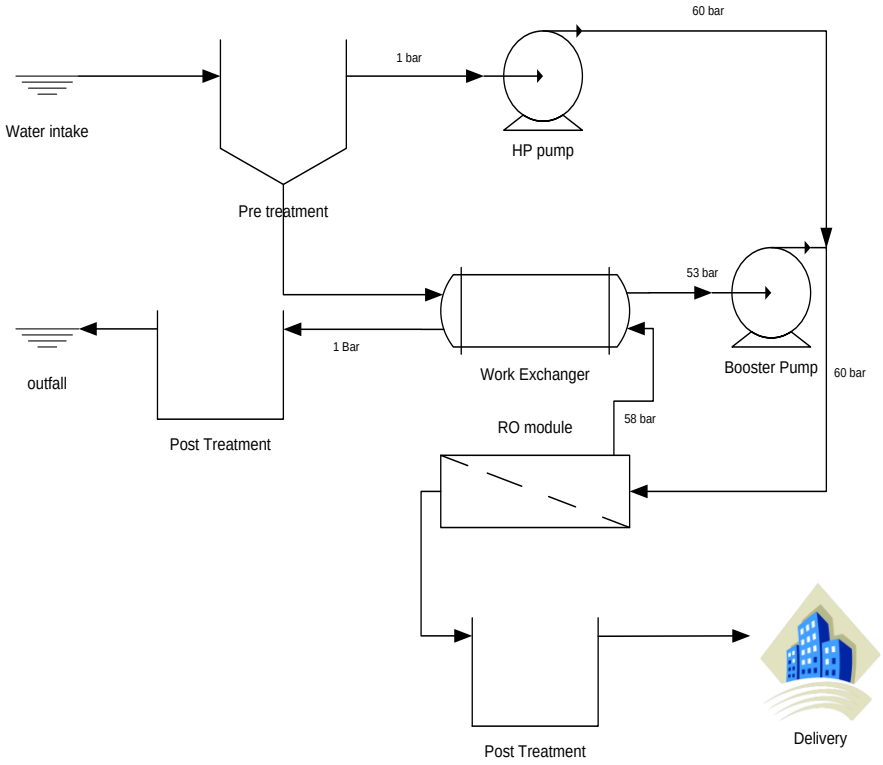

Figure 1.9. Schematic Diagram of Reverse Osmosis Plant with Energy Recovery system (adapted [7])

A major disadvantage of the Permasep HF Permeator was its tendency to foul and plug due to low free space between the hollow fibers and due to dead zones in the Permeator. In addition fouling and scaling was difficult to remove due to the low cross flow velocities and a relatively limited pH-range (4 – 11). These constraints required a high RO-feed water quality (SDI < 3) which resulted in higher pretreatment costs and some operational difficulties. To keep the rejection of the Permasep HF Permeator constant it generally had to be coated by poly vinyl methyl ether and tannic acid. These chemicals had to be reapplied frequently, the later chemical even after every membrane cleaning cycle [10].

The DuPont hollow fiber, which had been leading the RO market in the 1980s and early 1990s, started to lose ground to polyamide spiral wound modules in the 1990s. This was due to the increasingly fierce competition of a larger quantity of spiral wound module suppliers such as FilmTec / Dow, Rohm & Haas / Hydranautics, Toray, Fluid Systems /Koch, TriSep and Osmonics / General Electrics, which significantly reduced module pricing and advanced module concepts. The DuPont concept lost its appeal and the business became increasingly unattractive, which led to the exit of DuPont from hollow fine fiber module production [11].

Despite its cylindrical configuration, the spiral-wound reverse osmosis module is essentially a flat-sheet, cross flow device (see Figure 1.10). The feed water passes through the module axially, while permeate moves in the spiral, radial direction toward the permeate collection tube. The membrane interposed between these streams remains the technological center piece of the module, but other aspects of module engineering are increasingly critical to performance. The increased focus on module engineering is driven

in part by the desire for cost reduction, but more often by the desire to extract the full value of the latest membrane technologies. The promised membrane benefits can only be fully realized when module designs focus on energy efficiency and the preservation of membrane salt rejection. There are five major non-membrane components of the spiral wound module i.e. Feed spacer, permeate spacer, permeate tube, permeate carrier , and endcap.

By far the most common feed spacer configuration used in reverse osmosis membrane modules is the biplanar extruded net. Most RO feed spacers are made from polypropylene, which offers the preferred combination of extrudability, low cost, and chemical inertness. Thicknesses between 0.6 and 0.9 mm are typical. The feed spacer has two functions. It provides an open channel for the flowing feed water by maintaining separation between the membrane sheets. It also promotes mixing within the feed channel, moving salt and other rejected substances away from the membrane surface [11].

The permeate spacer provides a conduit for the collection and transport of permeate from the membrane to the permeate tube. Woven polyester fabric is the most common spacer in commercial use. The tricot weave is often chosen for its structural rigidity, smoothness, and fluid-channeling characteristics. The tricot is sandwiched between two sheets of membrane and sealed on three edges by glue, as shown in Figure 1.10, to create an envelope that is often referred to as a membrane leaf.

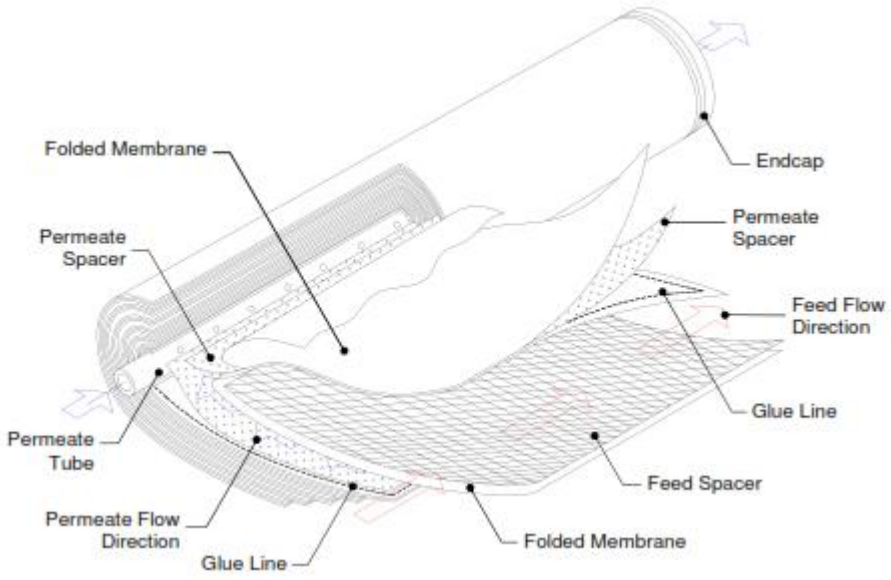

Figure 1.10. Spiral Wound RO Module [11, 12]

The permeate tube collects permeate from the spacer materials inside a module. In multi module pressure vessels, the tubes are connected in series, and serve as a conduit for the transport of permeate to an external manifold. The permeate tube also provides important diagnostic access during operation, permitting conductivity sensors and sampling probes to be inserted in search of membrane defects and leakage. Tube configurations have been largely unchanged in 20 years of RO module development, although materials and methods of tube fabrication have been updated. Tubes for standard modules of 40-inch length are usually extruded. Secondary machining operations add sideholes and tightly-toleranced sealing surfaces. Tubes for shorter modules are sometimes injection-molded. Although most tubes for 8-inch diameter modules have inside diameters near 2.5 cm, a large-diameter tube has been offered in commercially available low-energy brackish water and nanofiltration elements. The 3.5 cm inside diameter reduces pressure drop, which is a significant contributor to unwanted permeate backpressure in low-pressure RO systems [11].

The endcap is a highly engineered, injection-molded plastic component that plays several important roles within the module [11]. Here is a partial list of those roles:

- Leaf retention – The endcap prevents telescoping (relative axial movement) of the membrane leaves, and is sometimes referred to as an anti-telescoping device (ATD).
- Load transmission – The endcaps transmit axial load from module to module and also into the rigid fiberglass shell of the module.
- Bypass prevention – The endcap holds a brine seal, which prevents feed water from bypassing the module by entering the annulus between the module and inside wall of

the pressure vessel. The connection between fiberglass shell and endcap helps to prevent bypass around the brine seal.

- Permeate connection – In some cases, the endcap has been designed to include features for interlocking and permeate sealing between modules.

1.3. MULTILAYER THIN FILM

Multilayer thin film actually falls into category of nanolayered film which belongs to nanostructured film category. By definition, nanostructured film is any matter with film-form that has structural features on the nanometer scale. These features can be nanoporous, nanoparticle, thickness that is on the nanometer scale or surface roughness ranged at the nanometer scale [13].

The preparation of such film seems to be similar at some extent for instance they are synthesized primarily using substrates which can be flat, curved solid including spheres. The most important thing is there must be good affinity between the substrate and the incoming building units or precursors of thin film. The interaction between the substrate and the precursors may be different from one system to another for instance Langmuir-Blodget (LB) and Layer by Layer assembly make use of physisorption such as electrostatic force between the two however in the case LbL assembly particularly, many other surface interaction can also be used. Other examples are Self Assembly Monolayer (SAM) which is using chemisorption or other surface reaction [13].

1.3.1. LANGMUIR-BLODGET (LB) FILM

Of ultra thin film techniques, LB can be considered as the oldest. This technique was carried out systematically by Langmuir (1917) [14] and further developed by Blodget

(1935) [15] by transferring Langmuir films which was long chain carboxylic acid on to solid surface. Thus, LB films are obtained through a two step process: (1) self-assembly on liquid surfaces as a Langmuir monolayer by the help of external mechanical force. This monolayer consists of amphiphilic molecules on a water surface. Due to amphiphilic character, those molecules will orient themselves so that the hydrophilic head are dispersed in water surface while hydrophobic tail will protrude to the air. (2) deposition on solid surfaces by two ways either by withdrawing the substrate from water if the substrate hydrophilic or immersing it if the substrate hydrophobic (see Figure 1.11). [13]

First application of LB film for separation processes appeared in 1968 in which the researcher used low molecular weight substances such as fatty acid and 3b-cholestanol. In their work, they fabricated multilayer LB film for gas separation [16]. The application of such film for liquid permeation was done 25 years later in which the researchers prepare composite membranes using the LB technique to deposit multilayers of amphiphiles or amphiphilic polymers on porous supports [17]. However the LB separation layers provide poor molecular mobility and low flexibility. Even the use of amphiphilic polymers with short alkyl groups did not substantially improve separation efficiency. More recently, Regen and coworkers employed calixarene amphiphiles to form selective membranes by the LB technique [18, 19] Although Regen's are very impressive, fabrication of these materials on a large scale will likely be very difficult.

However this technique apparently is powerful to form and deposit monolayer or even multilayers on a substrate but it is basically suffering from practical point of view. Firstly, the need of amphiphilic constituents limits films composition while only a few such constituents are available. Additionally, no chemisorption is involved during the

formation of LB films. The primary driving force is the physisorption of the building unit as that are spread and self assembled by an external mechanical force on the solid surfaces. Such driving force will result in a fragile system and obviously not applicable for our case here which is RO.

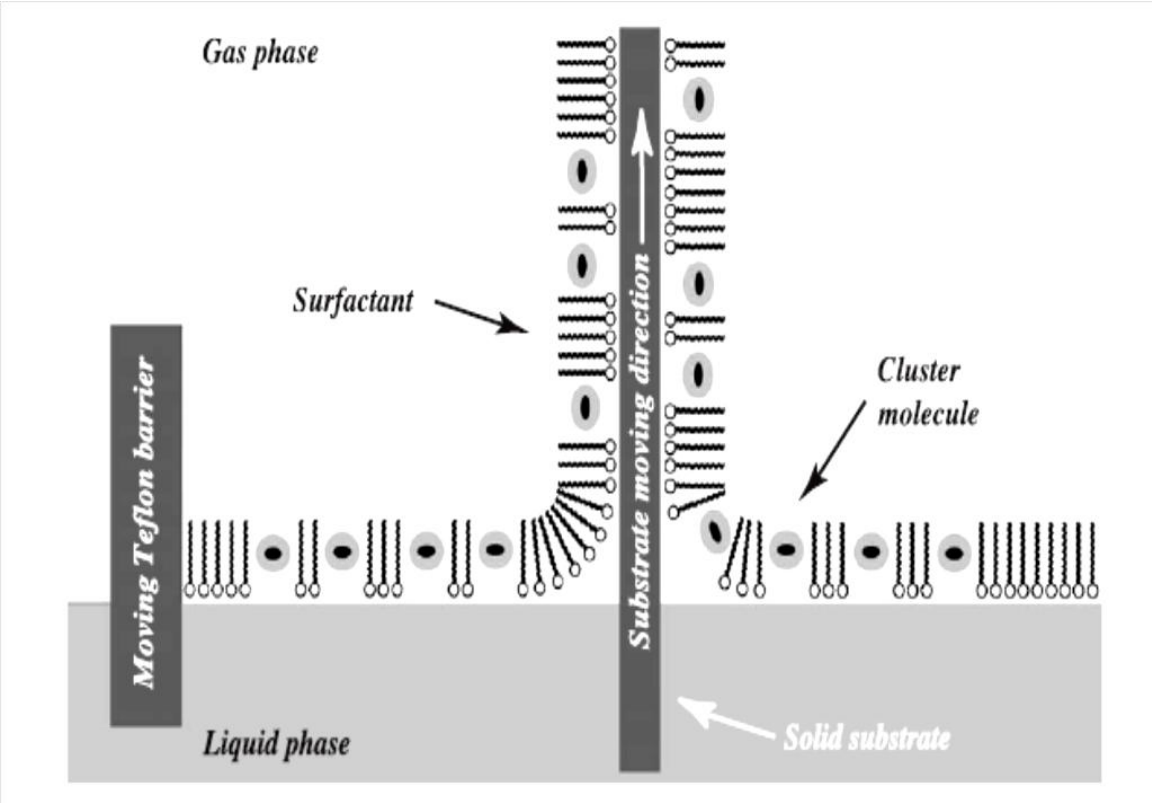

Figure 1.11. Schematic illustration of the fabrication procedure of organized 2-D molecular nanostructures containing ligand-stabilized nanoclusters via formation of mixed Langmuir monolayer at the gas–liquid interface with subsequent monolayer deposition by LB technique. [20]

1.3.2. SELF ASSEMBLY MONOLAYER

A more recent step in the development of ultrathin films was the discovery of self-assembled monolayer (SAM). The principle behind formation of these monolayers is simple; a molecule containing a head group that adsorbs to a surface, e.g. thiols on gold, assembles on the substrate under the constraints of intermolecular forces and adsorption site geometry. Unlike LB films, formation of SAM does not require any pre-assembly, so their synthesis is simple and convenient. Additionally, because they are bound to a surface, SAM is more robust than LB films.

The most common family of SAM is organothiols adsorbed on gold and the first systematic study of these materials was done by Nuzzo and Allara in 1985. By employing thiols with different tail groups, SAM can be easily used to modify surface properties. In addition to Au, other substrates such as Al/Al_2O_3, Si/SiO_2 and Cu have also been used to support SAM. The application of SAM in membrane was firstly done by Martin and his co-workers by using gold nanotubes [21-23]. Forming SAMs of different functionalized alkanethiols in the interior of gold nanotube pores makes it possible to control and modulate the size of the molecules that can pass through the nanotubes. For instance, pores coated with hydrophobic, long-chain alkanethiols selectively pass toluene in preference to pyridine; this selectivity can be reversed by changing the lining of the pore to the more hydrophilic mercaptoethanol [24]. A two-molecule permeation experiment with a hexadecanethiolate-lined pore (2.0 nm diameter) showed that the flux of toluene was 165 times higher than that of pyridine [25]. Other organic materials such as proteins can also be separated by using gold nanotubes coated with PEG-thiolates [26, 27]. Gold

nanotubes coated with zwitterionic cystein can be used to control the ion flux through the tubes as shown in the below figure [28, 29].

The main drawback to SAM is the limited film thickness available from monolayer formation. Additionally, although self-assembled coatings are more convenient and stable than LB films, the stability of Au-Thiol films is still an issue at high temperatures as well as substrate requirements also restrict the applications of these films. Most of the application of this film are for tailoring surface properties of metal, metal oxide or semiconductor [30].

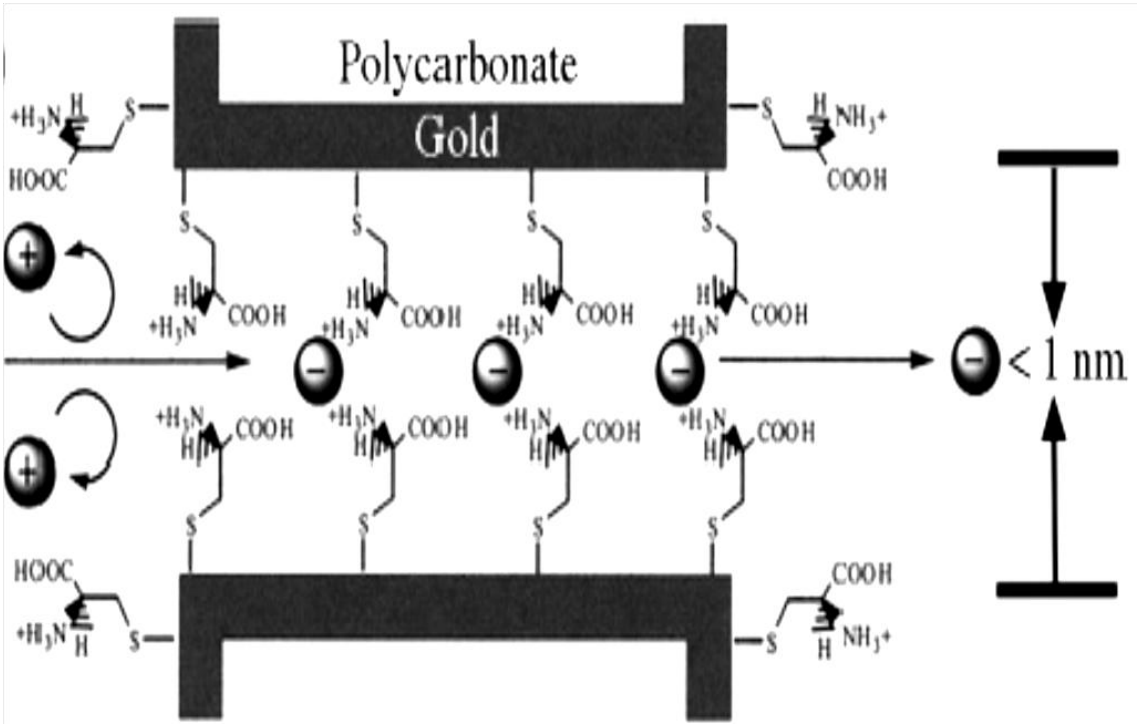

Figure 1.12. Schematic Diagram of Gold Nanotubes coated with SAMS containing Cystein [30]

1.3.3. LAYER BY LAYER ASSEMBLY

1.3.3.1. LAYER BY LAYER

It was discussed earlier that LB and SAM films have several limitations such as substrate requirement, chemistry of materials, fabrication equipment, etc. Thus, even though the techniques can provide access to nanoscale thin film, the implementation of both techniques for fabricating RO membrane is extremely difficult.

Iler in 1966 introduced a novel technique in which colloidal oppositely charged particles can be assembled into layer by layer film [31]. However, It was only after Decher re-introduced the similar technique for polyelectrolytes multilayer assembly, the technique became very popular in colloidal and interfacial science [32]. After various testing and proofing particularly for different multilayer precursors [33-37], the systematic way was then reported in 1997 and become the most cited article in nature or in science in field of chemistry for ten years (1998-2008) [38]. The classic approach to assemble polyelectrolyte multilayer thin film is by alternately dipping the substrate into two oppositely charged polyelectrolytes. If the substrate has positive charges on its surface then the first layer can be formed by dipping it into polyanion solution and followed by dipping it into polycation solution. Rinsing is always needed in between to remove weakly bound polyions [38].

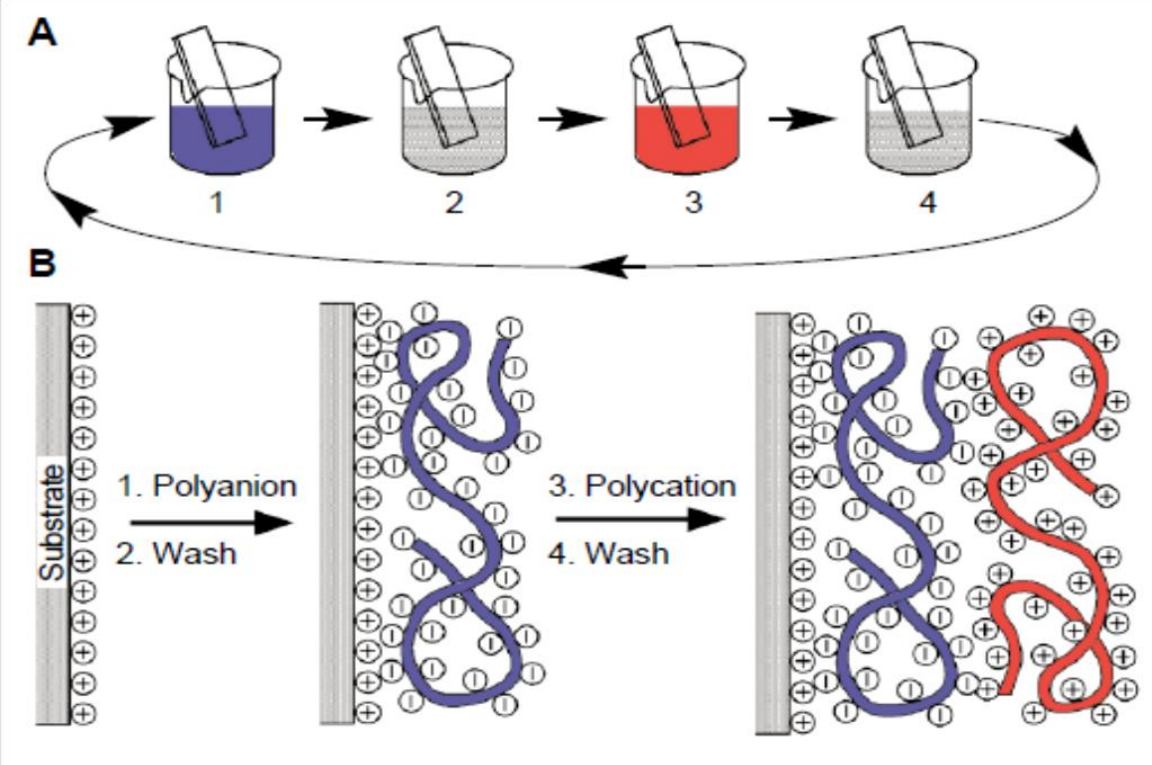

Figure 1.13. Schematic Diagram of Dip Layer by Layer Assembly (Adapted from[38])

This technique was initially invented by making use of electrostatic interaction between the two oppositely charge polyelectrolytes or colloidal particles. Such interaction force is very strong (500 – 1,000 kJ/mol) and long range (up to ~50 nm) and comparable to covalent bond which is somewhat strong and short-range [13]. However, nowadays LbL assembly can also be formed via donor/acceptor [39, 40], hydrogen bonding (citation), adsorption/drying cycles (citation), covalent bonds (citation), stereocomplex formation or specific recognition (citation). The precise structure of each layer depends on a set of control parameters such as polyelectrolyte concentration, adsorption times, ionic strength [41], pH [42], or temperature [43].

The deposition technique has also undergone transformation from dipping into spraying and spinning. Spray assisted LbL (SrA-LbL) was introduced by Schlenoff [44] by employing poly(diallyl dimethyl ammonium chloride) and poly(styrene sulfonate) on silicon wafer. The result showed that both techniques produce the film with quite similar thickness and identical transport properties for approximately 10 s deposition time. Slow polyelectrolyte assembly, seen also for d-LbL, coupled with inefficient use of polymer solution where 99% of the polymer solution is rinsed off, are the main drawbacks of SrA-LbL. However, if the size of the substrate is the concern then this technique is more suitable than d-LbL [44]. Krogman *et al* developed full automatic system and they showed that processing time is 25-fold faster than that of d-LbL to achieve the same film quality [45-47]. The technique can also be used to conformally coat individual fiber within a textured surface of hydrophobic textile [46].

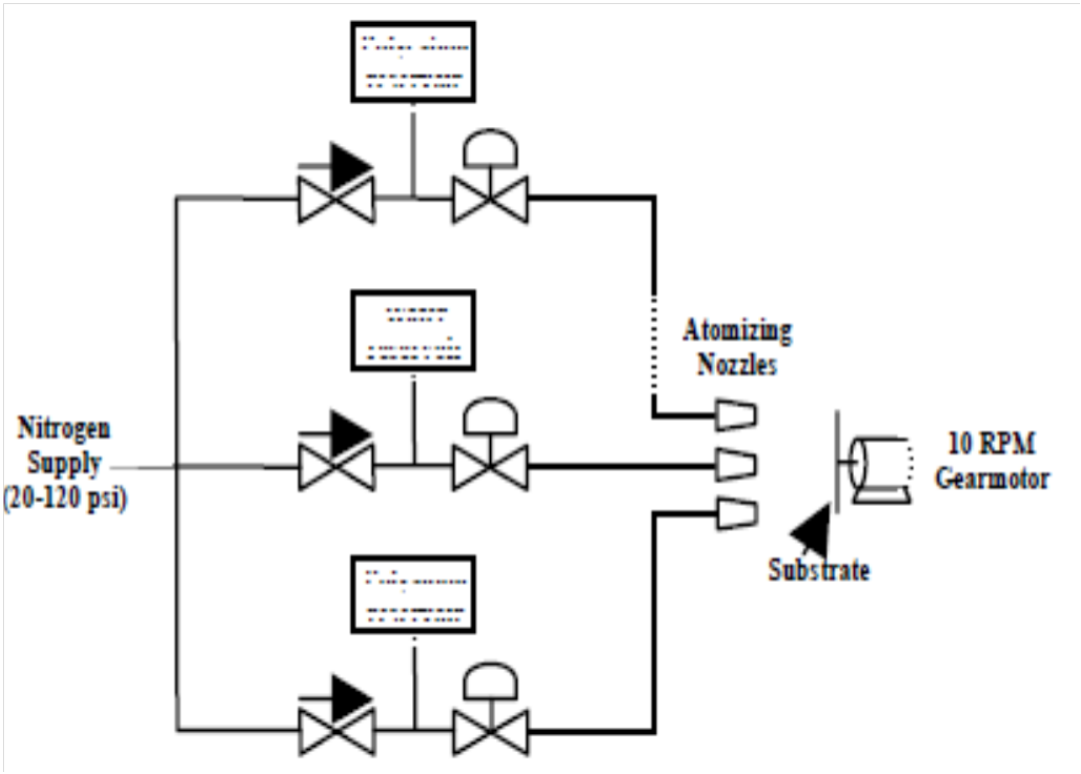

Figure 1.14. Schematic diagram of Spray-Layer by Layer Assembly (adapted from [46])

Spin Assisted LbL (SA-LbL) was introduced by Hong *et al* in 2001 [48, 49] and Chiarelli *et al* in the same year [50]. The major difference between d-LbL and SA-LbL is the way polyelectrolytes are deposited on the substrate. It is known that in the case of d-LbL, substrate is immersed in polyelectrolyte solutions (see Figure 1.13), while in the case of SA-LbL, small amount of polyelectrolyte is injected onto spinning substrate (see Figure 1.15).

It was reported that the SA-LbL film is several times thicker than d-LbL film for the same number of bilayers which is due to different adsorption mechanism. In the case of d-LbL polymer chain will be adsorbed on the substrate under influence of electrostatic force and then followed by chain rearrangement. Meanwhile, in the case of SA-LbL, due to high speed spinning, the adsorption, the rearrangement of polyelectrolyte chains and water removal occur simultaneously. Quick water removal increases polyelectrolyte concentration in very short time and also removes screening effect by water molecules. This in turn promotes faster adsorption and stronger electrostatic force thus more polymer chains are adsorbed within short time. Therefore, the SA-LbL film is thicker than d-LbL film [48]. Air shear force that occurs due to the relative movement between spinning substrate and air enhance the planarization of multilayer film and significantly reduce the surface roughness of the film. This feature is indirect evidence that SA-LbL film has highly ordered internal structure [48].

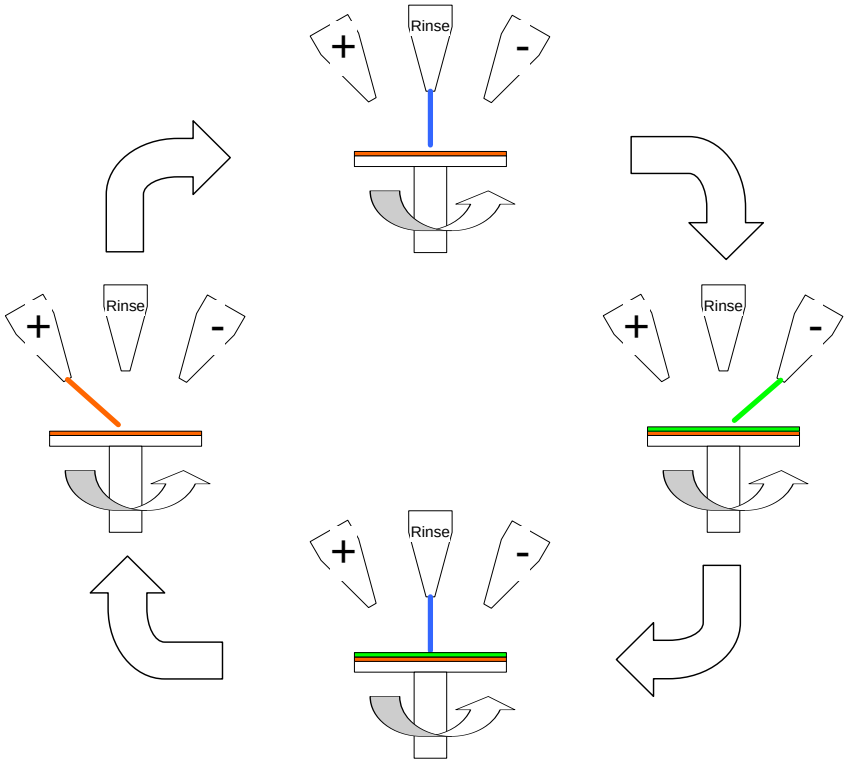

Figure 1.15. Schematic Diagram of Spin-Layer by Layer Assembly (Adapted from [[51])

Recent work by Tsukruk *et al* in 2009 has proven experimentally the highly ordered internal structrure of SA-LbL film by using neutron reflectivity [52]. This highly ordered internal structure that is difficult to achieve in conventional d-LbL or even SrA-LbL, can be obtained in much shorter time than conventional d-LbL hence it makes SA-LbL can be considered more "technologically friendly" [52].

SA-LbL assembly also produces LbL film with much improves elastic properties and robustness. SA LbL films also show extremely low creep and a unique "self-recovery" ability upon releasing them from deformation close to the ultimate strain [53]. Such self-recovery behavior is essential for fabricating devices with long lifetimes, robustness, and reproducible dynamic properties [54-56]. This enhanced mechanical integrity is also due to strong shear forces coupled with fast solvent removal in the course of assembly [52].

1.3.3.2. POLYELECTROLYTE

Our work is mainly focused on fabrication of polyelectrolyte multilayer film for separation membrane. Thus it is worthwhile to introduce polyelectrolytes and their main characteristic. A polyelectrolyte is a macromolecular that will dissociate into high charged polymer in water or any other ionizing solvent. Smaller oppositely charged counter ions are usually present to neutralize the charges on the repeating unit of the polymer to preserve electroneutrality. Because of those charges along the polymer backbone, the polymer chain tends to be straight or most extended if it is dissolved in low ionic strength solution and to be coiled if it is dissolved in high ionic strength solution. This chain form is mainly governed by intramolecular repulsion force of the unscreened charges on each monomeric unit in polymer backbone. The higher the ionic strength the lesser the unscreened charges on each monomeric unit, hence the chain become coiled.

The effect of salt can be seen clearly when two opposite charged polyelectrolytes form a complex. In salt free solution, level of aggregation is very high due to no screened charges in two polyelectrolytes. This leads polyelectrolytes to have stiff structure and each charges of polyanion can be compensated by charges of polycation to form aggregates quickly. When the ionic strength is increased, the level of aggregation reduces quite significant due to the screening of the Coulomb repulsion along the charged chains and causes more coiled structure. Obviously, complex formation or aggregation between the two opposite charged polymer becomes more difficult [57, 58].

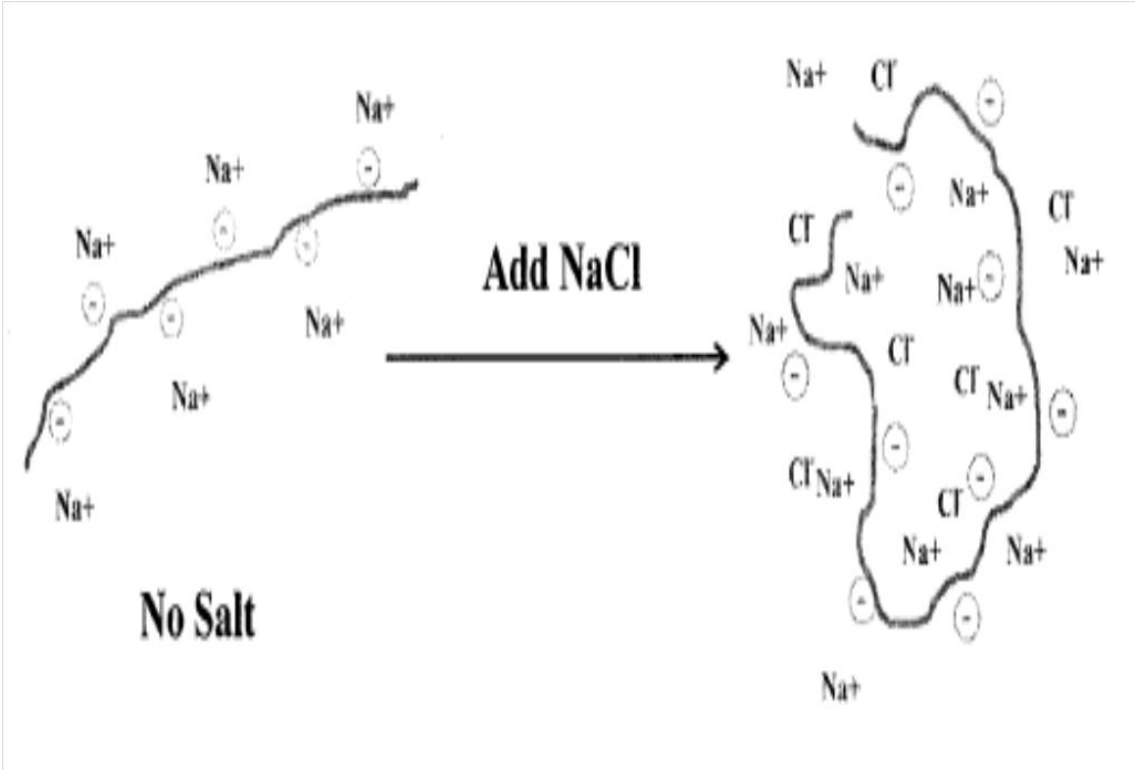

Figure 1.16. Schematic Diagram showing the effect of salt on polyelectrolyte chain

Similar to any ionized materials, polyelectrolytes also have different degree of ionization depends up on the pH of the solution. Strong polyelectrolytes tend to dissociate completely regardless the pH of the solution while weak ones dissociate more or less depending up on the pH of the solution. When polyelectrolytes are in their fully ionized condition, they will adopt most extended or stiff structure in the absence of salt. Meanwhile, more coiled structure is obtained when polyelectrolytes are partly ionized. This is shown indirectly from roughness of polyelectrolyte complexion in LbL assembly. Those polyelectrolytes that are deposited in partly ionized condition produce rough film while the ones that are deposited in fully ionized condition create rather smooth film in the absence of salt [42].

1.4. WATER AND SALT TRANSPORT In REVERSE OSMOSIS MEMBRANE

Understanding of water and salt transport through RO membrane is very important to design RO system. The most commonly used model in RO membrane transport is known as solution diffusion model (SDM) which is appeared in the 19^{th} century. However at that time other models such as pore flow model (PFM) was much more popular because it was closer to normal physical experience. The use of SDM in explaining membrane transport mechanism became more popular in 1940s particularly to explain transport of gases through polymeric membrane [59]. It was the discovery of asymmetric cellulose acetate membrane for seawater desalination by Loeb and Sourirajan in early 1960s that aroused interest of many researchers in this area to investigate the transport mechanisms through such membrane [60]. Later they modified the mechanism for thin film composite polyamide membrane. In addition, membrane transport also includes the discussion of

concentration polarization which is caused by the accumulation of solutes in the vicinity of membrane surface [61].

1.4.1. CONCENTRATION POLARIZATION

During the course of the RO process, water continually passes through the membrane while very little salt or solute passes. They will accumulate on membrane surface creating a phenomenon that is so-called concentration polarization. This accumulation of solutes in the vicinity of membrane surface will basically lead to higher concentration of those than that in the bulk [61]. Concentration polarization occurs in two direction, first from surface to the bulk solution while the other is from surface to the permeate side. The accumulation of solutes will generate concentration gradient that drives solute molecules away from the membrane. This first effect is commonly called as solute back transport [62]. Since at steady state, the salt flux is typically very small therefore, the salt transport from the bulk to the membrane surface is equal to the diffusive back transport. Consequently, these salts become stagnant in the region just adjacent to the membrane surface. This event leads to other negative effects such as increase of osmotic pressure as well as formation of fouling or cake which both eventually will lower water flux [63] and reduce the lifetime of the membrane [64].

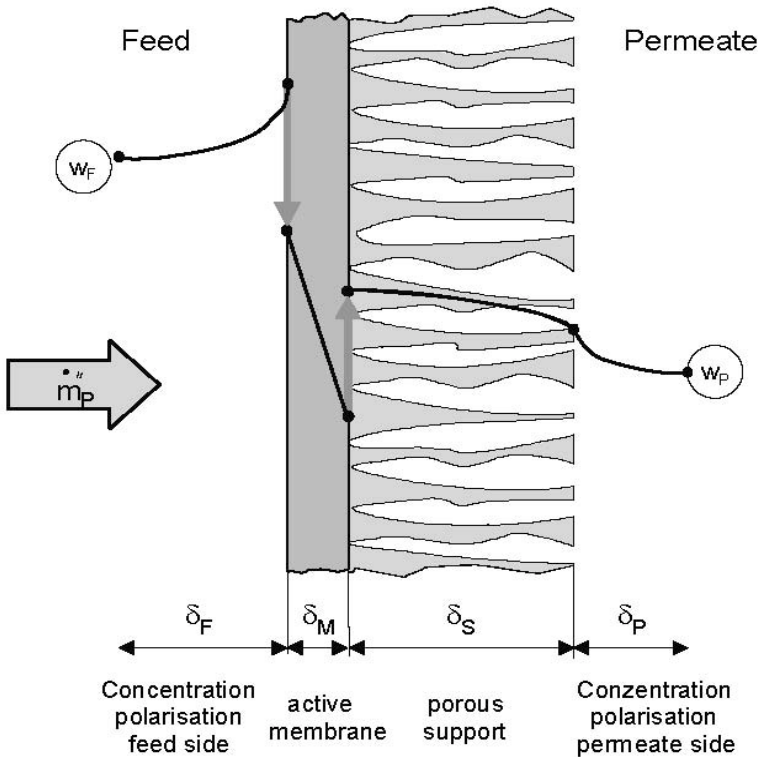

Figure 1.17. Concentration Polarization [63]

Concentration polarization occurs not only in feed side but also in permeate side but permeate side concentration polarization can be neglected [63]. However concentration polarization brings many disadvantages in terms of membrane performance, it is a reversible process and it can be easily controlled by means of velocity adjustment, pulsation, ultrasound or an electric field. Nowadays, almost all membranes are packed in a spiral wound module. This kind of modules has the flow direction of feed perpendicular to that of permeate. This system has been developed with the aim of combating concentration polarization which in turn also reducing fouling tendency. Forces produced by these feed systems sheared liquid near the surface of the membrane and thus removed trapped particles and solutes [65].

1.4.1.1. GEL POLARIZATION MODEL.

The simplest approach to get better understanding of concentration polarization is perhaps by making use of boundary layer model for cross flow system [66]. In this model, it is assumed that a thin layer of unmixed fluid with thickness δ exists between the membrane surface and the well-mixed bulk solution while V is the axial bulk velocity. From mass balance in the boundary layer, the concentration profile can be obtained as follows:

$$\frac{c_m - c_p}{c_b - c_p} = \exp\left(\frac{J_w \delta}{D_i}\right) \qquad (1)$$

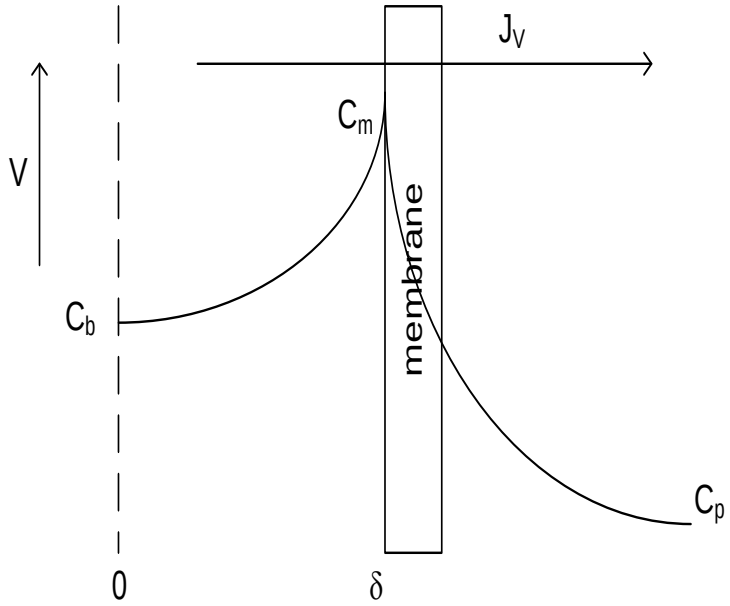

Figure 1.18. Schematic Diagram of Concentration Polarization

Where C_m is concentration of salt at membrane surface, C_b is concentration of it at bulk solution, and C_p is concentration of it at permeate side. J_w is solvent flux, which is water flux in this case. Diffusivity coefficient in that equation varies by concentration however; average diffusivity coefficient can always be used for simplicity. In many literatures, this equation is reported as a function of mass transfer coefficient (k) since boundary layer thickness is basically a measure between diffusivity and mass transfer coefficient. Hence, the above equation can also be expressed as follows:

$$\frac{c_m - c_p}{c_b - c_p} = \exp\left(\frac{J_w}{k}\right) \tag{2}$$

Chilton-Colburn analogy can be used to estimate solute back transport (k) [67, 68] . Correlation between salt rejection and flux can be formulated as follows

$$\ln\left[\frac{1-R_o}{R_o}\right] = \frac{J_w}{k} + \ln\left[\frac{1-R_a}{R_a}\right] \tag{3}$$

with observed rejection (R_o) is formulated as

$$R_O = \left[1 - \frac{C_p}{C_b}\right] \tag{4}$$

While actual rejection (R_a) is expressed as

$$R_a = \left[1 - \frac{C_p}{C_m}\right] \tag{5}$$

1.4.1.2. <u>COMBINED SOLUTION-DIFFUSION MODEL/FILM THEORY MODEL.</u>

The governing equations for water and salt flux in solution diffusion model are given respectively as follows

$$J_w = A(\Delta p - \Delta \pi) \tag{6}$$

$$J_s = \frac{D_{sm} K}{\delta}\left(C_b - C_p\right) \tag{7}$$

J_w and J_s refers to water flux and salt flux, respectively. In this model, correlation between salt rejection and water flux is formulated as follows

$$\ln\left(\frac{1-R_o}{R_o}\right) = \frac{J_w}{k} + \ln\left(\frac{D_{sm} K}{\delta J_w}\right) \tag{8}$$

By supplying R_o against. J_w data, taken at different pressures but at a constant feed rate and constant feed concentration for each set, the parameter (D_{sm} K/δ) and the mass transfer coefficient, k, can be estimated numerically [69].

1.4.1.3. COMBINED SPIEGLER-KEDEM/FILM THEORY MODEL.

Similar to previous section, film theory model can also be combined with spiegler-kedem theory. The governing equation for rejection is expressed as

$$\frac{R_a}{1-R_a} = \frac{\sigma}{1-\sigma}\left(1 - \exp\left(-\frac{J_w(1-\sigma)}{\omega}\right)\right) \tag{9}$$

Hence, the relation between salt rejection and water flux becomes

$$\ln\left(\frac{1-R_o}{R_o}\right) = \frac{J_w}{k} + \ln\left(\frac{1-\sigma}{\sigma\left(1 - \exp\left(-\frac{J_w(1-\sigma)}{\omega}\right)\right)}\right) \tag{10}$$

Once again, by using a nonlinear parameter estimation method by supplying the data of R_o against J_w taken at different pressures but at constant feed rate and constant feed concentration for each set, we can estimate the membrane parameters σ and ω and the mass transfer coefficient, k, simultaneously [69].

1.4.2. SOLUTION DIFFUSION MODEL (SDM)

1.4.2.1. TRADITIONAL SOLUTION DIFFUSION MODEL.

Liquid transport through dense or nonporous membranes was considered by very simple approach and thought to be similar to gas transport. However obviously, there are some marked differences between the gas transport and liquid transport through these membranes. For instance, the affinity of liquids and polymers is much greater than that between gases and polymers. Thus, it was proposed that transfer of ions and water through the polymeric membranes occurs via a solution diffusion mechanism because of dissolution of permeates in the membrane materials. Those ions and water that can associate with membrane material through hydrogen bonding will combine with it and are transported by diffusion [70]. With this hypothesis, ions and water dissolve in membrane material and diffuse through it because of the existence of a concentration gradient. This premise has also clarified distinction between SDM and PFM where in PFM there is no such interaction between permeates and the membrane material. The interaction, in fact, has been proved by recent investigations as discussed in later part of this paper.

The transport in either porous or nonporous membrane comprises of two flow types namely diffusive flow (v) and convective flow (u). In fact, the diffusion also generates an electric field and will act as another driving force called as diffusion potential [71]. For simplicity, the flux generated by this driving force is neglected. Aside from that, convective flow term can also be neglected and diffusive flow will remain. Thus flux can be simply formulated as follows:

$$J_w = v_{wm} C_{wm} \tag{11}$$

ν_w is known as velocity in diffusive flow. When the membrane pores become so small, the velocity will be strongly affected by friction between solute or solvent with pore walls. Thus ν_w obviously will be linearly proportional with the driving force and inversely proportional to the friction force. It is also known that transport of matter from one side to another side will occur if there is chemical potential gradient, which takes also concentration, pressure, temperature, and electrical potential into account [72]. Then by making use of Stoke-Enstein equation that shows clearly the relation among the diffusivity coefficient, temperature and permeates size, one can easily obtain the well-known Nerst-Planck equation:

$$J_w = \frac{D_{im} C_{wm}}{RT} \frac{d\mu_{wm}}{dx} \tag{12}$$

As known from traditional thermodynamics chemical potential can be formulated as

$$\mu_w = \mu_w^0 + RT \ln a_w + V_w \left(p_w - p_w^0 \right) \tag{13}$$

If there is no pressure gradient inside the membrane and there is always thermodynamic equilibrium in either interface, Equation (2) can be modified into

$$J_w = \frac{D_{wm} K_w C_{wf}}{l} \left(1 - \exp\left(\frac{-\bar{V_w} \left(\Delta P - \Delta \pi \right)}{RT} \right) \right) \tag{14}$$

Typical operating condition in RO membrane leads to simplification of term $V_i(\Delta P - \Delta \pi)/RT$. Therefore, we will get

$$J_w = \frac{D_{wm} K_w C_{wf}}{l} \left(\frac{-\bar{V_w} \left(\Delta P - \Delta \pi \right)}{RT} \right) \tag{15}$$

We can simplify equation (5) into

$$J_w = \alpha_w(\Delta P - \Delta\pi) \tag{16}$$

α is known as permeability which is based on our derivation will be a function of diffusivity, solubility, temperature, and concentration. This equation is also similar to what Merten obtained however here is more informative than his equation since we can clearly see what parameter that can affect the flux of permeate.

We can also derive relation for salt flux in the same manner as that for solvent flux as follows

$$J_s = \frac{D_{sm}K_s}{l}(C_{sf} - C_{sp}) = \alpha_s(C_{sf} - C_{sp}) \cong \alpha_s C_{sf} \tag{17}$$

The classic theory considers the transport of solute and solvent to be completely independent without any effect of one on the other when, in general, they may be couple by either frictional or convective effects. This effect is so-called coupling effect. Huge literature on irreversible thermodynamics outlines formalism for describing such effects. Paul reformulated traditional solution diffusion model by means of Ternary Maxwell-Stefan equations and end up with similar results as explained above [73]. With this reformulation, he can show the effect of coupling on flux where the movement of one species will affect on that of the other.

$$J_w = -(1 - w_s)\frac{\rho D_{wm}}{w_m}\frac{dw_w}{dx} - w_w\frac{\rho D_{sm}}{w_m}\frac{dw_s}{dx} \tag{18}$$

$$J_s = -w_s\frac{\rho D_{wm}}{w_m}\frac{dw_w}{dx} - (1 - w_s)\frac{\rho D_{sm}}{w_m}\frac{dw_s}{dx} \tag{19}$$

w refers to weight fraction and $w_m = 1 - w_w - w_s$.

Further, if one looks specifically at salt transport from interface of membrane and water to permeate side, the transport might have two distinct possibilities. First, neutral ion-pairs that are formed at the concentration-polarization zone get partitioned into the membrane phase and then diffuse as ion pairs to the low pressure side. Secondly, individual ions (not ion pairs) get partitioned into membrane phase and then migrate through the membrane active layer in a manner that the negative charge of an anion is balanced by the positive charge of an accompanying cation. Experimental observations done by Mukherjee showed electrolyte transport is in agreement with the second approach for any case of 1-1, 2-1, 1-2, or 2-2 electrolytes [74].

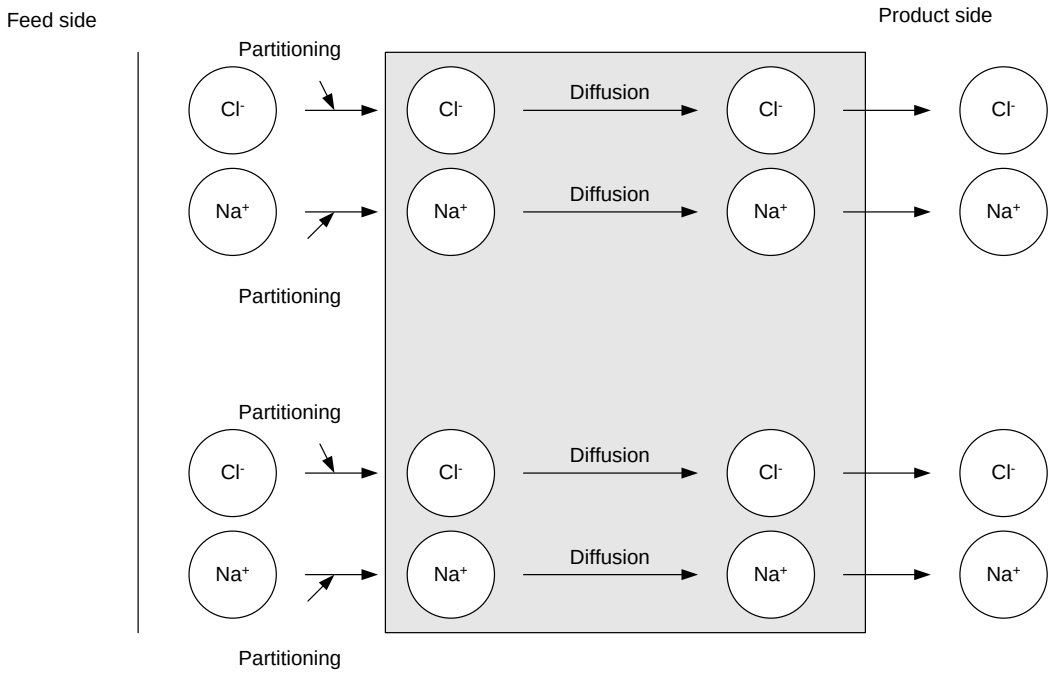

Figure 1.19. Coupled transport of individual ions through the membrane (adapted from [74])

1.4.2.2. SOLUTION-DIFFUSION-IMPERFECTION MODEL.

The traditional solution diffusion model was derived mainly by assuming the membrane has perfect nonporous structure that will not allow water and solute transferred by hydrodynamics flow. In fact, this assumption is not always true since defects, pinholes, or larger pores will always present in membrane at some extent. Thus, people came up with an idea of including pore flow model in traditional solution diffusion model. The early work in this field was done by Sherwood and his co-workers [75].

Several assumptions postulated for this model are similar to traditional solution diffusion model such as transport starts from dissolution of water and solute into the water-swollen polymer matrix at the upstream membrane surface, diffusion across the membrane is as a result of the gradient of chemical potential or concentration and finally desorption from the downstream membrane surface. The difference between the two is the upstream solution also passes through open channels or pores convectively with negligible change in solute concentration due to diffusion in the liquid. The selectivity between water and solute then must be determined by diffusional transport. Therefore, it is important to note that pore flow must be a small fraction of the total flux if the selectivities required for practical desalination are to be achieved. Water and salt flux are given as follows:

$$J_w = k_w(\Delta P - \Delta\pi) + k_p M_w \Delta P C_w \quad (20)$$

$$J_s = k_s(c_w - c_p) + k_p M_s \Delta P C_s \quad (21)$$

k_w, k_s , and k_p are membrane coefficients for diffusion of water, salt and pore flow.

The first term on the right hand side of both equations accounts for diffusional transport same as traditional solution diffusion model, while the second term accounts for

pore flow transport. Thus the first term accounts for perfect regions in matrix while the second one accounts for imperfect regions.

The same hydrostatic pressure difference in both terms is not appropriate, as the pressure drop in pore flow should be more significant than that in diffusive flow. The use of the same hydrostatic pressure in both regions is justified only if the volume flows across regions with different properties are substantially interdependent or on the other words, lateral volume flows are large enough to level tangential pressure differences [76].

In this model, salt rejection is formulated as follows:

$$R = \left[1 + \left(\frac{k_s}{k_w}\right)\left(\frac{1}{\Delta P - \Delta\pi}\right) + \left(\frac{k_p}{k_w}\right)\left(\frac{\Delta P}{\Delta p - \Delta\pi}\right)\right] \quad (22)$$

However this model seems to be more realistic, the concentration and pressure dependence of three coefficient limit the application to design estimation [77].

1.4.2.3. EXTENDED SOLUTION DIFFUSION MODEL.

Traditional solution-diffusion model requires rejection at infinity is equal to 1 under all circumstances. Thus, this model cannot explain negative solute rejection that sometimes happens in specific system for example phenol or organic solutes. However, negative solute rejection has not been found for salt solution. It might be beyond the scope of this paper to discuss this model, but it is still worth to see how this model differs from the traditional one. This negative solute rejection was first time pointed out by Burghoff *et al* [78].

It was known that traditional solution diffusion model neglects applied pressure difference across the membrane. This applied pressure difference can not be neglected particularly if partial molar volume of solute is high enough. The solute and solvent flux

are still independent of each other, exactly the same assumption as traditional model. Thus, by including applied pressure difference, the equation for water and solute flux can be expressed as follows:

$$J_w = l_{wp}(\Delta P - \Delta\pi) \tag{23}$$

$$J_s = \frac{D_{sm}K_s}{l}\left(C_{sf} - C_{sp}\right) + l_{sp}\Delta P \tag{24}$$

l_{wp} and l_{sp} are called as phenomenological coefficient. Rejection can be formulated as follows:

$$\frac{1}{R}\left[1 - \frac{l_{sp}}{C_{sf}l_{wp}}\left(1 - \frac{\Delta\pi}{\Delta P}\right)\right] = 1 + \frac{K_s D_{sm}}{l_{wp}(\Delta P - \Delta\pi)} \tag{25}$$

Since in reverse osmosis, applied pressure is much higher then osmotic pressure, it is clear from equation 25, rejection can be negative only if $\left(l_{sp}/C_{sf}l_{wp}\right) > 1$ that occurs whenever the pressure induced solute permeation velocity is higher than the pressure induced water permeation velocity.

1.4.3. IRREVERSIBLE THERMODYNAMICS MODEL (ITM)

As mentioned earlier that ITM has limitations particularly with respect to the nature of the membrane and the separation mechanism though it has also strong point especially with respect to the coupling of driving force or fluxes. Dissipation function in which the rate of entropy generated is taken into account to maintain the driving force in RO, can be expressed as follows

$$\phi = T\frac{dS}{dt} = \sum J_i X_i \tag{26}$$

Where

$$J_i = \sum L_{ij} X_j = \sum L_{ij} \frac{d\mu_j}{dx} \tag{27}$$

Through equation 27, one can see how the effect of coupling included in this model. L is known as phenomenological coefficient. The dissipation function for RO process can be expressed as follows

$$\phi = \left(J_w V_w + J_s V_s\right)\Delta P + \left(\frac{J_s}{C_s} - J_w V_w\right)\Delta\pi = J_v \Delta P + J_d \Delta\pi \tag{28}$$

Subscripts w stands for water, s for salt. J_v is summation of convective flux while J_d is that of diffusive flux. The corresponding phenomenological equations as

$$J_v = L_{11}\Delta P + L_{12}\Delta\pi \tag{29}$$

$$J_d = L_{21}\Delta P + L_{22}\Delta\pi \tag{30}$$

Water flux can be modified as follows

$$J_v \approx J_w = L_p\left(\Delta P - \sigma\Delta\pi\right) \tag{31}$$

Where

$$\sigma = -\frac{L_{12}}{L_{11}} \tag{32}$$

σ is commonly called as reflection coefficient. It has a value between 0 and 1. $\sigma = 1$ means the membrane is ideal and no solute transport, $\sigma < 1$ means membrane is not completely semipermeable, while $\sigma = 0$ means no selectivity [79, 80] Convective flux (J_v) can be used as approximation for water flux since salt flux can be neglected.

While salt transport can be obtained by similar fashion as water transport and expressed as follows:

$$J_s = \overline{C_s}(1-\sigma)J_v + \omega\Delta\pi \quad (33)$$

ω is called as solute permeability. Both reflection coefficient and solute permeability can be found experimentally at various solute concentrations by using equation 34.

$$\frac{J_s}{\Delta c} = \omega + (1-\sigma)J_v\frac{\bar{c}}{\Delta c} \quad (34)$$

The observed rejections can be explained from Spiegler, Kedem,Katchalsky (SKK) theory and expressed as follows [79, 80]

$$R = \frac{\sigma(1-F)}{1-\sigma F} \quad (35)$$

Where F is defined as

$$F = \exp\left(-\frac{(1-\sigma)}{\omega}J_\upsilon\right) \quad (36)$$

1.5. LITERATURE REVIEW And RESEARCH OBJECTIVES

1.5.1. LITERATURE REVIEW

1.5.1.1. CHAPTER THREE.

It was mentioned in sub-chapter 1.3.3.1 that SA-LbL offers several advantages over d-LbL. The most remarkable advantages of SA-LbL are high layering quality, higher mechanical strength, and short processing time. Char and his coworkers are the first research group introducing spin coating into layer by layer assembly [48]. Since then several fundamental works have been published for SA-LbL. One of SA-LbL film characteristics that distinguish it from other LbL assembly is its internal structure. It is

well known that d-LbL generates highly interpenetrated layer because of long deposition time while SA-LbL produce highly ordered internal structure due to short deposition time. Char *et al* has shown this characteristic using mixture of PAH/PSS and PAH/CdS (for the rest of this dissertation, polyelectrolyte that is mentioned first is also the first polyelectrolyte deposited onto the support) analyzed using X-Ray reflectivity [48]. Tsukruk *et al* has also proved the orderliness of SA-LbL film using neutron reflectivity [52]. However, the degree of orderliness can be drastically changed from highly ordered to more interdiffused simply by adding certain salts.

The orderliness of internal structure is mainly due to fast adsorption process caused by spinning. During the course of spinning, polyelectrolyte chains can be quickly frozen on the top of previously adsorbed layer because of fast solvent evaporation. They do not have enough time to diffuse further into the existing polyelectrolyte layers [48]. The fast solvent removal also causes sudden increase in deposited polyelectrolyte concentration that ultimately boosts up the adsorption rate significantly. Thus more polyelectrolyte chains can be adsorbed and it results in thicker film compared to d-LbL deposited at the same number of bilayer [48, 49].

It has also been observed that SA-LbL film grow linearly due to better surface coverage caused by fast water removal [48, 50, 52, 81-83]. This phenomenon occurs because water molecules present in the assembly generally screen the electrostatic interaction by blocking polyelectrolytes from getting adsorbed onto previous adsorbed layer. However, for few polyelectrolyte systems the growth rate may change because of substrate effect [50, 81].

We have seen that spin has an important role in SA-LbL. All the above mentioned characteristics are mainly caused by spinning effect. However the spin speed itself is an important parameter in determining the growth rate or the thickness of LbL film. The experiment has shown that the growth rate is inversely proportional to the spin speed. This is caused by the deposition time become shorter as the spin speed is increased and it leads to less amount of adsorbed polyelectrolyte [50, 82, 83].

Concentration also has significant impact on PEM growth. The experimental works showed the higher the concentration the faster the growth rate [49, 82]. This increase in growth rate is because higher driving force for the adsorption as the concentration is increased. Thus at the same spin speed, more polyelectrolytes can be adsorbed.

In addition, molecular weight of polyelectrolyte can also affect the growth rate. In general, the bilayer thickness of PEM film is inversely proportional to the logarithm of molecular weight [83]. The polyelectrolyte chains tend to adsorb onto an oppositely charged surface in a strongly extended conformation and then spread out to occupy more area on the surface as the molecular weight increases. The higher the molecular weight, the larger the area a polyion chain occupies and leads to a further thinning of the film [83].

1.5.1.2. CHAPTER FOUR.

It is noticed that most of the works done in this area are related to nanofiltration (NF) membrane rather than RO one as can be seen later on in this sub-chapter. Though both are slightly different in terms of membrane transport characteristic, at least, one should be able to obtain some useful information from those works particularly the characteristic of

PEM membranes towards sodium chloride. It is also important to know that almost all PEM NF membrane reported below were tested under multi salt solution which is containing at least two types of salts containing monovalent ions such as NaCl (1-1 salt) and divalent ions such as Na_2SO_4 (1-2 salt), $MgSO_4$ (2-2 salt), $MgCl_2$ (2 -1 salt), etc. Typically, lower NaCl rejection is obtained in this case rather than that in single salt test due to coupling effect.

Tieke and his co-worker were the first researchers reporting the use of dip-LbL to prepare NF membrane. They studied permeation performance of several polyelectrolyte pairs as can be seen in Table 1.1 by using home made-dead end permeation cell. All polyelectrolytes pairs were deposited onto PAN / PET with pore size of 20-200 nm. Permeability of NaCl and $MgCl_2$ through PEM was then investigated at feed salt concentration of 5850 ppm (0.1 M). Their experiment showed that as the number of bilayer is increased the permeability of both salts decreases and the decrease is more significant for divalent ion/salt. The experiment also revealed that polyelectrolyte pairs that have high ion pair per number of carbon atom such as PAH/PVS show lowest ion permeability. Lower ion permeability is indirectly indicating higher salt rejection [84].

Table 1.1. Polyelectrolyte Pairs Investigated in Tieke and Krasemaan work [84]

Polycation	Polyanion
PEI	PVS
PAH	PVS
PEI	PSS
PAH	Dextran – DEX
PAH	PSS
CHI	PSS
P4VP	PSS
PDADMAC	PSS

In 2001, Bruening and his coworker reported the fabrication of PAA/PAH on porous alumina support. In this work, they compared permeation performance of cross-linking PAA/PAH to non-cross linking PAA/PAH membrane. Unfortunately, no information was mentioned about operating condition of the permeation test however it seems within the range of nanofiltration application. The main result was cross link of 5 bilayers of PAA/PAH film at 115 ^{0}C for 2 hours can reduce the Cl^- flux by 50%. The reduction is believed due to reduced pore size as part of carboxylate group of PAA and ammonium group of PAH is converted into amide bond. Other interesting finding is that the donnan exclusion at the most outer layer is a primary factor behind the rejection of ions. This result based on the fact that changing outer most layer from positive charge into negative charge by depositing one more additional layer only can reduce Cl^- flux as much as 15%. This theory seems more accurate than previous theory mentioned by Tieke *et al* [84] especially in the case of dip-LbL. It is generally accepted that 50% of charge of any layer will be compensated by 50% of charges of previously adsorbed layer while the rest 50%

of charges will be compensated by subsequent layer. With this basis, even if any, the uncompensated charges will be quite less and donnan exclusion will be very low [85].

Tieke and his coworker reported similar work to their previous work for poly(vinyl amine) (PVAm) and PVS in 2003. This pair has higher ion pair per number of carbon atom than PAH/PVS. The 60 bilayers of PAH/PVS film deposited on PAN/PET membrane shows 84 % and 93.5% of NaCl rejection at operating pressure of 5 bar and 40 bar, respectively. However, they tested the membrane at very low salt concentration which was less than 600 ppm. This is obviously quite far from typical RO condition. Other result that needs to be improved is the water flux that was very low i.e. 3.75 $L/m^2.h^{-1}$. This work is the first work showing the application of LbL membrane under reverse osmosis condition [86].

In 2003, Bruening and his coworker prepared multilayer thin film consisting of PAH/PSS for NF application. Their work showed 5 bilayers of PSS/PAH coated on porous alumina support can reject 43% of salt solution containing 1000 ppm NaCl. The water flux was about 58.3 $L/m^2.h$ at pressure of 4.8 bar. The membrane was tested using home-made cross-flow permeation cell [87]. In 2004, they prepared similar PEM thin film as previous one consisting of PSS/PDADMAC. It was found that 5 bilayers of PSS/PDADMAC deposited from 0.1 M NaCl on porous alumina support shows NaCl rejection of 21% and water flux of 137.5 $L/m^2.h$ at pressure of 4.8 bar. Membrane was tested at feed solution containing of 575 ppm NaCl also using home-made cross flow permeation cell [88].

In 2004, Deratani and his coworkers prepared PEM thin film consisting of CHI/Alginate-(ALG) for NF application. PEM was coated on cellulose acetate (CA) membrane with pore size ranging from 0.44 nm to 1.37 nm depending up on the annealing temperature of CA during the casting process, for example, CA membrane heated at 80^{o}C has pore size of 0.44 nm. All membranes were tested by using dead end permeation cell at feed solution containing 2000 ppm NaCl and 2000 ppm $MgSO_4$ and operating pressure up to 12 bar. Uncoated CA membrane shows 85% NaCl rejection while coated CA membrane with 25 bilayers of CHI/ALG shows lower NaCl rejection i.e. 75%. The same trend was also found for other CA membranes which have larger pore size. According the authors this phenomenon happened because the swelling of CHI/ALG film increases the chance of salt to stay longer in the surface of the membrane and causes concentration polarization [89].

In 2005, Bruening and Malaisamy prepared PEM membrane which was the same as previous work i.e. PSS/PDADMAC for NF application. This time, they deposited PSS/PDADMAC onto poly(ether sulfone) - PES with different molecular weight cut-off. PES with 50 kDa molecular weight cut-off showed the best permeation performance. It was found that after 18 hour equilibration period, 4 bilayers of PSS/PDADMAC showed water flux of 35.8 L/m^2.h and NaCl rejection of -8%. Permeation test was run at pressure of 4.8 bar and feed solution concentration of 1000 ppm. Negative Cl^- rejection occurs because the experiment was done under couple effect i.e. more than one type of salt in feed solution, for instance NaCl and Na_2SO_4 thus transport of Na^+ from Na_2SO_4 drags Cl^- across the membrane to maintain electrical neutrality [90].

In 2006, Bruening and his coworkers optimized several PEM membranes such as PAA/PAH, PAA/PDADMAC, PSS/PAH, and PSS/PDADMAC. Like their previous works, those membranes were also prepared via dip-LbL assembly. Of these four systems, 4.5 bilayers of PAA/PAH showed the best performance in terms of Cl^- rejection which was about 12.9 %. PAA/PAH was deposited at the same pH of 7 and obtained water flux was 7.08 L/m^2.h. On the other hand, 4.5 bilayer of PSS/PAH deposited at the same pH of 4 showed the best performance in terms of water flux which was 91.7 L/m^2.h but poor Cl^- rejection which was -8.7%. All polyelectrolyte systems were deposited on porous alumina support and tested at feed solution containing of 1000 ppm NaCl and 1000 ppm of Na_2SO_4 and home made cross flow permeation cell was run at pressure of 4.8 bar [91].

In 2007, Once again, Bruening *et al* prepared PSS/PAH and PSS/PDADMAC film through dip-LbL assembly for NF application. This time the membranes were tested at feed containing mixture of NaCl and NaF, at the same operating condition as previous study except feed solution containing very low salt concentration i.e. 58.4 ppm NaCl and 42 ppm NaF. Under this very low salt concentration, it is obvious the membrane in this work apparently showed much better performance compared to those of previous work, for instance, PSS/PAH membrane has chloride rejection of 16.2 % and water flux of 195.8 L/m^2.h while PSS/PDADMAC membrane has chloride rejection of 9.5% and water flux of 145.8 L/m^2.h. Aside from less concentration polarization effect, the use NaF rather than Na_2SO_4 reduces the coupling effect. It is known that size of fluoride ions is smaller than sulfate ions therefore some fluoride can pass through the membrane to partly

compensate sodium ions in order to maintain electroneutrality. This indeed decreases the amount of chloride ions to partly compensate sodium ions therefore no negative chloride rejection is obtained in this work [92]. Bruening et al also tested PSS/PDADMAC membranes for different salt mixture that was NaCl (58.4 ppm) and NaH_2PO_4 (120 ppm). The experimental result showed salt rejection of chloride varied depends of the pH of feed solution while water flux remained relatively constant. This happened because the amount of active species of NaH_2PO_4 in water changed as the pH of the solution was changed for instance NaH_2PO_4 could present in form of HPO_4^{2-} , $H_2PO_4^-$ depending upon the pH. These ionic species had different hydrated ionic radii thus their respective rejection rates were different and since the test was done in a mixed salt solution, there was indeed a coupling effect that altered Cl^- rejection [93].

In 2008, Pavasant et al fabricated PEM membrane consisting of CHI/SA and CHI/PSS on electrospun CA nanofibers by using dip-LbL assembly. Unlike other forementioned works, they tested the membrane in single salt solution i.e. NaCl by using dead-end permeation cell. It was found that 25 bilayers of CHI/SA membrane has water flux of 40 L/m^2.h and salt rejection of 14% while CHI/PSS one has water flux of 50 L/m^2.h and salt rejection of 10% [94].

In 2008, Xu et al prepared PEM membrane via dynamic LbL assembly. They employed PAH, PSS and PSS co- maleic acid (PSSMA) for the active layer while PAN was used as substrate. In the case of dynamic LbL assembly, the polyelectrolyte is deposited by passing it through the substrate instead of dipping the substrate in it. With this approach, deposition occurs much faster than the conventional dip-LbL. However, this seems to be true only for first several layers because as the number of layer increases

the permeability of polyelectrolyte solution decreases significantly. They tested the membrane by using cross-flow permeation cell for feed concentration of 1000 ppm (NaCl) and pressure of 8 bar. The experimental result shows that $(PAH/PSS)_2$PAH/PSSMA membrane prepared via dynamic LbL has water flux of 47 L/m^2h and salt rejection of 32.4 %. The same membrane prepared via dip-LbL showed water flux of 48.3 $L/m^2.h$ and salt rejection of 31%. This indicated that dynamic LbL resulted in tighter film than dip-LbL. Other interesting result was increasing number of layer up to 4 i.e. $(PAH/PSS)_4$PAH/PSSMA resulted in somewhat increase of rejection up to 36.1 % but quite significant decrease of water flux that was 31 $L/m^2.h$ [95].

It is concluded from the above literature review that almost all works were done for NF application while only very few works were done for RO application [86, 89, 94]. From those works, PEM membrane seems quite promising as NF membrane while using it as RO membrane is still challenging task. This is because RO membrane is used at not only high pressure but also at high salt concentration. We have seen that even as such lower salt concentration for example below 100 ppm of NaCl, PEM NF membrane has rather low salt rejection and the rejection is more even lower if salt concentration is increased.

The most successful work in terms of salt rejection was done by Tieke et al [86] however it took almost 1.5 hours to deposit only single bilayer. Thus the process itself is very time consuming and practically can not be applied in large scale. Aside from that, the membrane showed quite low water flux which is far from typical flux of RO membrane. Not to mention low salt concentration test arises curiosity about the stability and the performance of this membrane if it is tested at more extreme condition i.e. high

concentration. The work that was done by Xu et al [95] by using dynamic LbL gave us information about stability of PEM membrane wherein they tested the membrane for 140 hours with very stable water flux and salt rejection. Unfortunately, dynamic LbL which was claimed to be faster than dip-LbL can be applied only for the first few layers because as the number of bilayer is increased the permeability of any solution trough the existing layer significantly decreases.

1.5.1.3. CHAPTER FIVE.

Early work on dip-LbL separation membrane proposed that the ions are rejected due to the Donnan exclusion principle where each layer will be repel the ions carrying the same charge as the layer itself [84]. Other workers propose that Donnan exclusion is only operative in the outermost layer instead of contribution from each charged layer. These worker argue that charge compensation between adjacent layers can occur intrinsically or extrinsically except for the outermost layer and thus may not contribute in the Donnan exclusion [96, 97]. Recently it is also proposed that some LbL membranes behave like glassy polymer and the rejection and permeation in such membranes is better characterized by the solution diffusion principle (see sub-chapter 1.4) rather than the Donnan exclusion principle [98]. It is thus obvious that transport mechanism in LbL assembled polyelectrolyte membranes is still not clearly understood and further work is needed to fully understand transport mechanism in these membranes.

Few fundamental researches have indeed been conducted to study the effect of several parameters such as external salt concentration and temperature on the permeation characteristic of LbL film [99, 100]. However effect of those parameters at elevated pressure has not been investigated yet.

1.5.1.4. CHAPTER SIX.

In the last decade, term nanotechnology has become very popular and it has been applied in many fields. Nanotechnology has produced entirely new class of functional materials whose application of them in desalination needs exploration. People have used some of nanomaterials for fabricating separation membrane. For example, Holt *et al* fabricated pure CNT membranes with all CNTs are vertically aligned. This membrane showed superior flux and was able to separate 2 nm gold particles from water [101]. Matsuura et al used montmorillonite to fabricate clay membrane. This membrane was able to reject sodium ions up to 50 % and has flux of 0.35 L/m^2.h operated at pressure of 30 bar and feed salt concentration of 5850 ppm [102]. Dong *et al* employed MFI zeolite crystal to fabricate zeolite membrane through hydrothermal synthesis. This membrane was able to reject sodium ions up to 76.7 % and has flux of 0.112 L/m^2.h operated at pressure of 20 bar and feed salt concentration of 5850 ppm [103].

Those successful pure inorganic membranes have opened up the possibility to incorporate such nanomaterials in membrane which is known as mixed matrix membrane (MMM). People have developed MMM for gas separation, pervaporation, ion-exchange, and fuel cell applications by employing , nanoclays, zeolite or carbon molecular sieve particles dispersed within relatively thick membrane films [104-108].

New concept of embedding nanomaterials in TFC membrane was introduced by Jeong et al [109]. They embedded zeolite A nanocrystals into the active layer of TFC membrane. This membrane was able to increase the flux from 9.37 L/m^2.h to 16.96 L/m^2.h and maintain the rejection at 93% operated at pressure of 12.4 bar and feed salt

concentration of 2000 ppm. Min et al did the similar work but for nanofiltration polyamide membrane by incorporating titanium dioxide nanoparticles [110].

The use of nanoclays in TFC desalination membrane has not been explored yet meanwhile it has been successfully used for gas separation membranes as mentioned earlier [107, 108]. These materials are comparable to zeolite nanocrystals in terms of properties such as hydrophilicity and surface charge thus introducing nanoclays is expected to enhance hydrophilicity, surface charge and mechanical strength of the membrane. There have been many works done for introducing nanoclays in PA membranes however the purpose of those works is to enhance a barrier property which is indeed not suitable for RO application. There were also very few works reported the decrease of barrier properties due to embedded nanoclays [111]. This is obviously an encouraging result which motivates us to work further with this material.

1.5.2. OBJECTIVES

1.5.2.1. MAIN OBJECTIVE.

It is concluded from the above discussed literature review that SA-LbL has many remarkable properties and advantages compared to d-LbL or Sr-LbL yet the application of this kind of assembly in separation film or membrane such as gas separation, nano filtration or reverse osmosis has not been explored yet. Meanwhile the same application has been studied quite a lot for d-LbL. Therefore, the main objective of this work is to develop thin film composite membrane for RO application using SA-LbL assembly.

1.5.2.2. PARTICULAR OBJECTIVES.

Several fundamental works in SA-LbL have been done including effect of number of bilayer, spin speed, concentration, ionic strength and molecular weight on film characteristic. Having said that, it is noticed that pH has not been investigated yet whereas this parameter is extremely important particularly if weak polyelectrolytes are used in the assembly. Hence, I devote chapter three to discuss the investigation of the effect of pH on SA-LbL film. Two most well studied polyelectrolytes i.e. poly(acrylic acid) (PAA) and poly(allylamine hydrochloride) PAH are choosen [42, 112-114] for this purpose. Aside from that, this study is also important as a base line for fabrication of SA-LbL film on polymeric as can be seen in the subsequent chapters.

Departing from the base line study in chapter three; it is then important to study the application of SA-LbL to fabricate thin film composite membrane for water desalination. I then selected four polyelectrolyte pairs i.e. PAH/PAA, PEI/PAA, PDAC/PVS, and PAH/PVS. PAH and PAA are the most well studied polyelectrolyte and have been used extensively in dip-LbL. Both are weak polyelectrolytes meaning their degree of ionization depends up on the pH [42, 113]. PEI is also weak polyelectrolytes and cannot even reach fully ionized condition i.e. maximum degree of ionization is about 80% [115] but it has higher number of pair/carbon atom compared to PAH [84]. PDAC and PVS are strong polyelectrolytes that fully ionized over all pH range. I dedicate chapter four for this study.

The studies mentioned in sub chapter 1.5.1.3 were conducted at atmospheric pressure while effect of those parameters at elevated pressure has not been investigated yet. The

stability of polyelectrolyte multilayer membrane is also another important issue to be answered. Whether such membrane remain stable or does not when it is exposed to salt solution with high pressure and high cross-flow velocity in the case of separation membrane such as NF or RO needs to be investigated. Based on these facts, I then investigate the long term stability of the deposited film and the permeation characteristic of SA-LbL assembled PAH/PAA membrane as a function pressure, temperature, and feed salt concentration using a cross flow permeation test cell as can be seen in chapter five. Chapter six is the last experimental chapter in this dissertation devoted to the development of IP PA membrane by introducing nanoclay to enhance its performance.

CHAPTER TWO

MATERIALS AND METHODS

2.1. MATERIALS

2.1.1. POLY (ACRYLIC ACID) SODIUM SALT (PAA).

PAA has formula of $(C_3H_3NaO_2)_n$ and it is also named sodium prop-2-enoate according to IUPAC. PAA with molecular weight of 5,100 g/mol was obtained from Sigma-Aldrich. Molecular weight of repeating unit is 94.04449 g/mol. PAA used in this work was received in white powder form with impurities of 8-14 % water and has density of 0.55 g/mL at 25°C. When it is dissolved in water, the pH of PAA solution is ranging from 6 to 9.This material is categorized as hydrophilic polymers. PAA is anionic polymers due to carbonyl functional group attach to its backbone (see Figure 2.1). PAA is also water soluble sequesters metal ions and hydrolytically and thermally stable. It is mainly used as scale inhibitor, builder in detergents, aid in soap and detergent processing and control of water hardness, polyelectrolyte for SAMS (Self-Assembled Monolayers) [116], disposable diapers, thickening agent, and antiseptic chlorhexidine gluconate deactivator [117].

2.1.2. POLY (VINYL SULFATE) POTASSIUM SALT (PVS).

PAA has formula of $(C_2H_3KO_4S)_n$ and it is also named potassium ethenyl sulfate according to IUPAC. PVS with molecular weight of 170,000 g/mol was obtained from Sigma-Aldrich. Molecular weight of repeating unit is 162.2061 g/mol. This materials is

also sort of hydrophilic polymers and soluble in water. It is an anionic polymer due to SO_3OK group looses its potassium ions and becomes SO_4^- (see Figure 2.1). PVS is available in form of yellow or light brown powder. This material is commonly used for biomedical application [118].

2.1.3. POLY (ALLYL AMINE HYDROCHLORIDE) (PAH).

PAH has formula of $(NH_2CH_2CHCH_2)_n (HCl)_n$ and it is also named prop-2-en-1-amine hydrochloride according to IUPAC. PAH with molecular weight of 120,000-180,000 g/mol was obtained from Polyscience. Molecular weight of repeating unit is 93.55532 g/mol. This cationic material is also hydrophilic and very soluble in water. It is usually used make redox hydrogel-modified electrodes for measuring enzyme responses [119]. The most prominent use of this polyelectrolyte is in the field of cell encapsulation.

2.1.4. POLY (DIALLYLDIMETHYL AMMONIUM CHLORIDE (PDAC).

PDAC has formula of $([(CH_3)_2N(CH_2CH=CH_2)_2]Cl)_n$. PDAC with molecular weight of 100,000 g/mol and concentration of 35 wt% in water were obtained from Sigma-Aldrich. Molecular weight of repeating unit is 126.2188 g/mol. PDAC used in this work has density of 1.09 g/mL and viscocity of 100-200 cP at 25 °C [120]. This cationic and hydrophilic materials is usually used in waste water treatment as a primary organic coagulant which neutralizes negatively charged colloidal material and reduces sludge volume compared with inorganic coagulants. It is also used for for controlling disturbing substances in the papermaking process, as a flocculant to improve soap separation process in the evaporation plant of kraft pulp mills [121].

2.1.5. POLY (ETHYLENE IMINE) (PEI).

PEI has formula of $(C_2H_5N)_n$ and it is also named aziridine according to IUPAC. PEI with molecular weight of 70,000 g/mol (30% solution in water) was obtained from polyscience. Molecular weight of repeating unit is 43.0678 g/mol This PEI is highly branched polyamine with high charge density. It is a liquid polymers and soluble in water at all molecular weights, also soluble in lower alcohols, glycols, and THF. Branched PEI contains primary, secondary, and tertiary amine groups in approximately 25/50/25 ratio. It has density of 1.029-1.038 g/mL and viscosity of 400-900 cps [122].

This cationic and hydrophilic materials is usually used in the cell culture of weakly anchoring cells to increase attachment. PEI was the second polymeric transfection agent discovered, after poly-l-lysine. PEI condenses DNA into positively charged particles, which bind to anionic cell surface residues and are brought into the cell via endocytosis. Branched PEI has also been used for CO_2 capture, frequently impregnated over porous materials [123].

2.1.6. POLYSULFONE (PSF).

PSF has formula of $(C_6H_4C(CH_3)_2C_6H_4OC_6H_4SO_2C_6H_4O)_n$. PSF used as support in this work is in form of flat sheet ultrafiltration (UF) membrane manufactured by GE Osmonics except for TFC polyamide membrane in which hand made PSF supports were used. UF PSF membrane is rated with 30 kDa and is reported to have water flux of 552.5 L/m^2.hr at 50 psi [124]. PSF belongs to family of thermoplastic polymers. These polymers are known for their toughness and stability at high temperatures.

Its resistance to high temperatures gives it a role of a flame retardant, without compromising its strength that usually results from addition of flame retardants.

Polysulfone is also known for its reproducible properties and controllable size of pores down to 40 nanometres. Thus it can be used in applications like hemodialysis, waste water recovery, food and beverage processing, and gas separation. PSF is also widely used material of filter cartridges since it shows extremely high flow rates at very low differential pressures when compared with Nylon or polypropylene media. Additionally filter cartridges made from polysulfone can be sterilized with in line steam or in the autoclave without loss of integrity up to 50 times. Its application is also found in electronic industry such as capacitors. It is even also used as the primary component of the gold-plated Lunar Extravehicular Visor Assembly, the iconic gold-film visor portion of the Apollo space-suits worn by Apollo astronauts during their lunar excursions [125].

2.1.7. SILICON WAFER.

P-Doped [100] silicon wafers (University wafers, USA) with thickness 625 μm were used as substrate for few baseline studies. This silicon wafer is generally not 100% pure silicon, but is instead formed with an initial impurity doping concentration between 10^{13} and 10^{16} per cm^3 of phosphorous which is added to the melt and defines the wafer as either bulk n-type or p-type. Silicon wafer is usually used in microdevice and integrated circuit [126].

2.1.8. METHYL PHENELENE DIAMINE (MPD).

MPD has formula of $CH_3NHC_6\ H_4NH_2$ and it is also named as N-methylbenzene-1,2-diamine according to IUPAC. it is one of the monomers used in polyamide preparation using interfacial polymerization. It is a water soluble monomer having molecular weight of 122.168 g/mol, density of 1.09 g/mL, m.p amd b.p of 22^O C and 123.5^O C respectively.

2.1.9. TRIMESOYL CHLORIDE (TMC).

TMC has formula of $C_6H_3(COCl_3)$ and it is also named as benzene-1,3,5-tri carbonyl chloride according to IUPAC. It is one of the monomers used in polyamide preparation using interfacial polymerization. It has molecular weight of 265.48 g/mol, density of 1.487 g/mL, m.p and b.p of 35^{O} C and 180^{O} C respectively.

Polycation

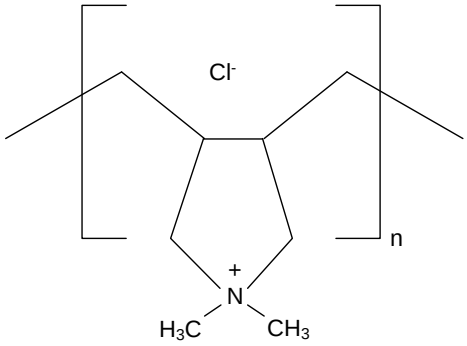

PDAC

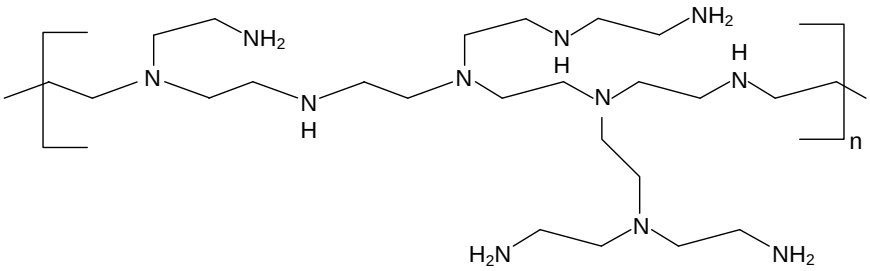

PEI

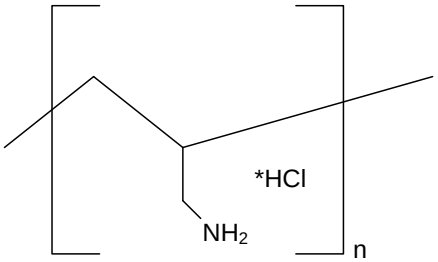

PAH

Polyanion

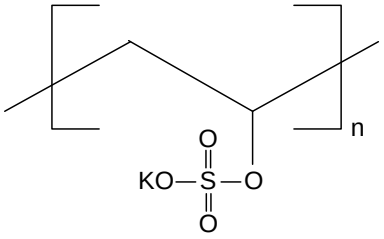

PVS

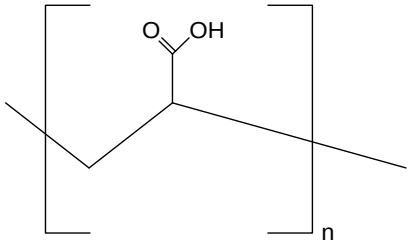

PAA

Support

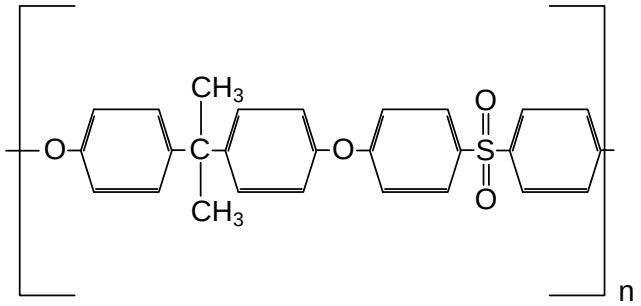

PSF

Monomers

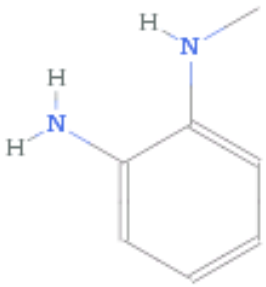

MPD

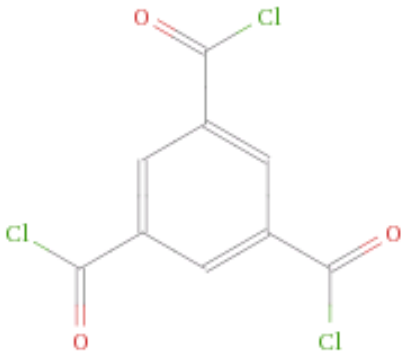

TMC

Figure 2.1. Molecular structure of organic materials used in this work

2.1.10. MONTMORILLONITE (MNT).

Montmorillonite is a 2-to-1 layered smectite clay mineral with a sandwich structure. Individual platelet thicknesses are just one nanometer (one-billionth of a meter), but surface dimensions are generally 300 to more than 600 nanometers, resulting in an unusually high aspect ratio. Naturally occurring montmorillonite is hydrophilic. The properties of this clay can be seen in Table **2.2**.

2.1.11. CLOISITE 15-A (CS-15A).

CS-15A is natural montmorillonite modified with a quarternary ammonium salt with concentration of 125 meq/100 g clay. It is an additive for plastic and rubber to improve various physical properties such as reinforcement, synergistic flame retardant and barrier. The properties of this clay can be seen in Table 2.3.

Table 2.2. Physical Properties of MNT

Physical Properties	**Comment**
Density	2.8 g/cm3
Particle size	≤ 2 μm (10%) ; ≤ 10 μm (50%); ≤ 25 μm (90%).
Moisture content	≤ 9%
XRD d-Spacing	1.55 nm

Table 2.3. Physical Properties of CS-15 A

Physical Properties	**Comment**
Density	1.66 g/cm3
Particle size	≤ 2 μm (10%) ; ≤ 6 μm (50%); ≤ 13 μm (90%).
Moisture content	≤ 2%
XRD d-Spacing	3.15 nm

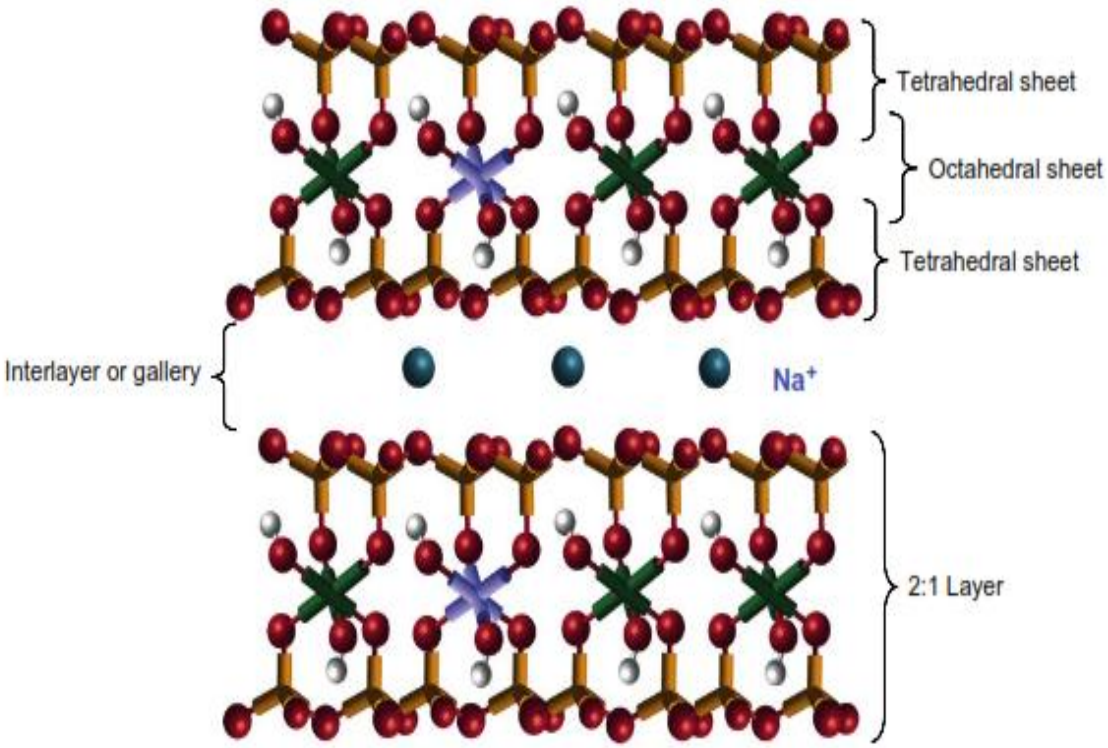

Figure 2.2. Montmorillonite Structure (Adapted from [127])

2.2. METHODS

2.2.1. THIN FILM COMPOSITE (TFC) LAYER BY LAYER MEMBRANE PREPARATION.

The SA-LbL deposition technique involved sequential deposition of dilute polyelectrolyte solutions with drying and rinsing between each deposition step. Ultra filtration polysulfone membrane was pretreated by using UV at wavelength of 256 nm for 40 seconds to increase surface charge and hydrophilicity following the procedure that was described at somewhere else [128]. After this pretreatment, PDAC was then deposited on spinning PSF or silicon wafer support. Spin grower^{TM} (Absolute Nano Inc., see appendix A for detail description) was used to build multilayer film. The deposition was done exactly when the speed reach the desired spin speed to eliminate the effect of ramp speed during the deposition [129]. PDAC was deposited at a rate of 0.4 mL/sec for 7 sec and the film was subsequently spin-dried for another 20 sec. The rather dry film was then rinsed with DI water at a rate of 0.4 mL/sec for 14 sec to remove weakly bound polyelectrolyte then again followed by spin-drying for 20 sec. PVS was deposited afterwards with similar manner to PDAC deposition. Complete cycle (PDAC/PVS) was repeated until prescribed number of layer achieved. PAH/PVS, PEI/PAA, and PAH/PAA films were also deposited in similar way to PDAC/PVS film.

Figure 2.3. SpinGrower

2.2.2. THIN FILM COMPOSITE POLYAMIDE MEMBRANE PREPARATION.

2.2.2.1. SUPPORT PREPARATION.

Polysulfone was chosen to make the porous substrate membrane on which a polyamide thin film is formed by in-situ polymerization. The support is prepared as follows: 16 wt% of polysulfone and 3 wt% of polyvinyl pyrrolidone are dissolved in N-Methylpyrrolidone. The solution is stirred for several hours until polymers are completely dissolved. The solution is then spread via knife-edge over a polyester non-woven fabric taped to a glass plate. Then the glass plate is immediately immersed in bath of 18 uw laboratory deionized water maintained at 20 ^{O}C. After several minutes, the non-woven support fabric, together with the polysulfone membrane is separated from the glass plate. The membrane is then washed thoroughly with deionized water and sotred in a refrigerator at 5^{O}C before use.

2.2.2.2. POLYAMIDE THIN LAYER PREPARATION.

A support membrane (PSF + nonwoven fabric) taped to a glass plate is immersed in an aqueous solution containing 2 wt% of MPD for approximately 30 min. The excess MPD solution is blotted from the membrane surface before the membrane is immersed in a solution of 0.1 wt% TMC in n hexane. After the TMC solution is drained by holding the membrane vertically, the membrane is kept at room temperature. During this period in-situ polymerization takes place. The resulting membrane is rinsed with an aqueous solution of 0.2 wt% sodium carbonate before being stored in deionized water. The membrane is heated in an air circulated oven at 105OC for 90 s to facilitate the in-situ

polymerization for the heat treatment. The resulting membrane is again rinsed with an aqueous solution of 0.2 wt% sodium carbonate.

The incorporation of nanoclays in polyamide layer is done by dispersing certain amount of nanoclays (0.005 – 0.04 wt%) in TMC-hexane solution. The mixture is then ultrasonicated for 1 h prior to immersion of the PSF membrane in TMC-hexane solution. The rest is the same as interfacial polymerization without nanoclays. Two types of nanoclays are used in this work i.e. Cloisite-15 A (CS) and montmorillonite (MNT). The two nanoclays have been extensively used to improve barrier properties of polyamide.

2.2.3. CHARACTERIZATION.

2.2.3.1. ATOMIC FORCE MICROSCOPE (AFM).

Veeco Metrology Nanoscope IV Scanned Probe Microscope Controller with Dimension 3100 SPM is used to study the surface topography of SA-LbL film on silicon wafers. Tapping mode using RTESP tip (Veeco) with spring constant of 20-80 N/m is used for scanning the surface topography of the samples. Meanwhile, contact mode PicoSPM LE (Agilent Corp.) was used to study the surface morphology of the SA-LbL films on polysulfone ultrafiltration membrane. AFM scanning probes with spring constant of 0.02-0.77 N/m was employed during the characterization. Surface roughness and morphology was taken for sample size of 20 μm by 20 μm and RMS surface roughness reported in this work is average value of three different locations.

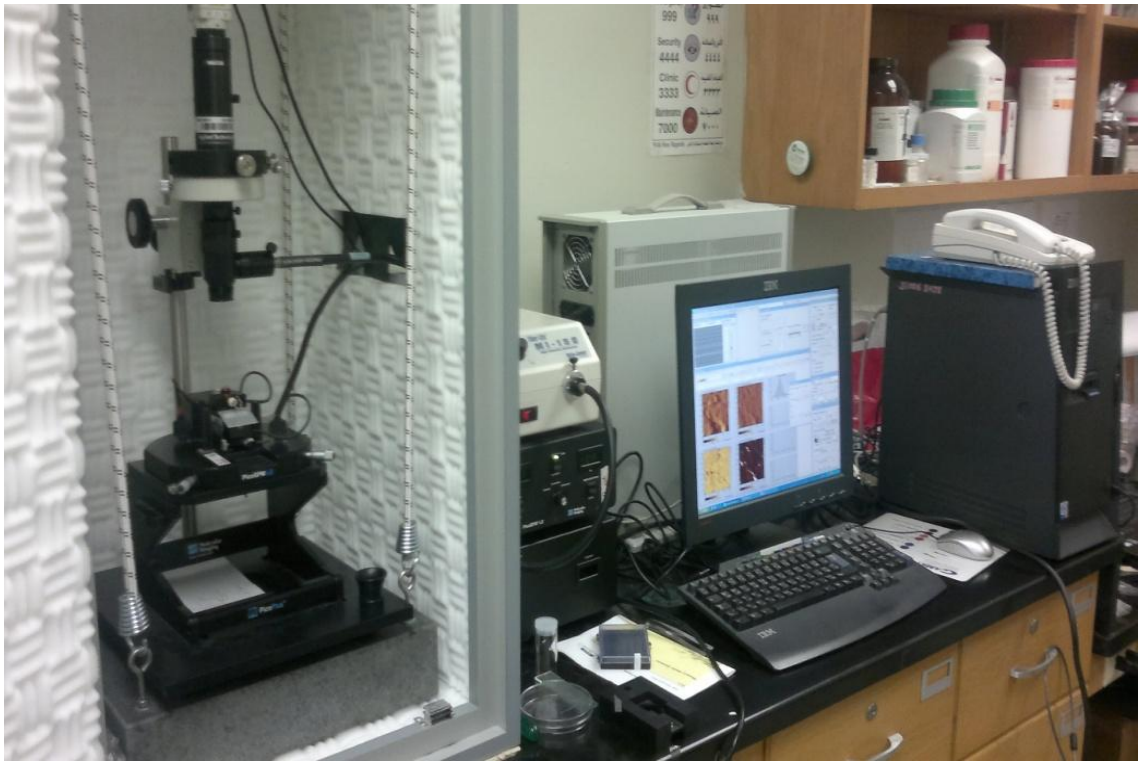

Figure 2.4. Contact mode PicoSPM LE (Agilent Corp.)

2.2.3.2. ELLIPSOMETER.

The measurement of film thickness on silicon wafers was carried out at ambient temperature by using 3-Wavelength Variable Angle Ellipsometer (Gaertner Scientific) operating at a wavelength of 633 nm with incident angle of 70^{O}. Refractive index of 1.49 was used through all measurements. The film growth behaviour was investigated from the first layer deposited up on the silicon wafer. The growth then was observed by measuring total thickness after depositing subsequent polyelectrolyte on previously adsorbed layer. This measurement was repeated until prescribed number of layers achieved. The values that are reported in this paper are average of measurements from 5 different spots. The measurements for average incremental thicknesses (either bilayer thickness or monolayer thickness) were taken after deposition of 12 layers. Thickness measurement was always done immediately after layer deposition and it was followed by subsequent layer deposition and so on. Therefore the thickness data provided in this work are basically the thickness of relatively wet film since the spin process only remove excess water from the surface film.

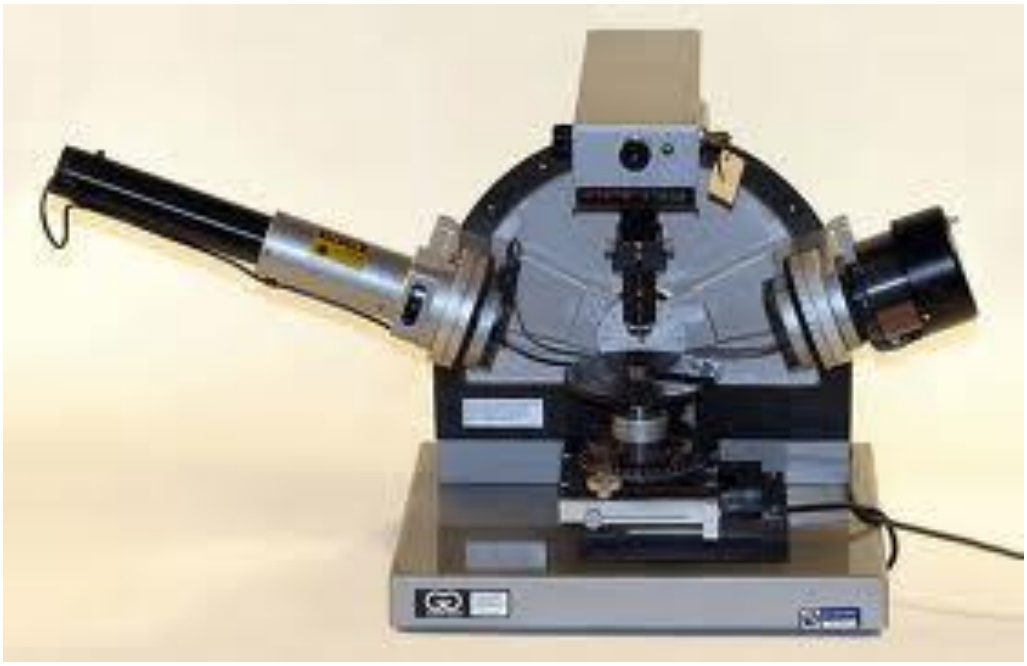

Figure 2.5. Ellipsometer 3-Wavelength Variable Angle Ellipsometer (Gaertner Scientific)

2.2.3.3. PROFILOMETER.

Surface Profilometer (KLA Tencor P-16) with 2 μm radius diamond tipped stylus was used to measure the surface roughness at scan speed of 20 μm/sec, scan rate of 200 Hz, length of measurement of 500 μm and applied force of 0.5 mg. Surface roughness measurement was performed on 4 different locations and was done only for SA-LbL films on silicon wafer.

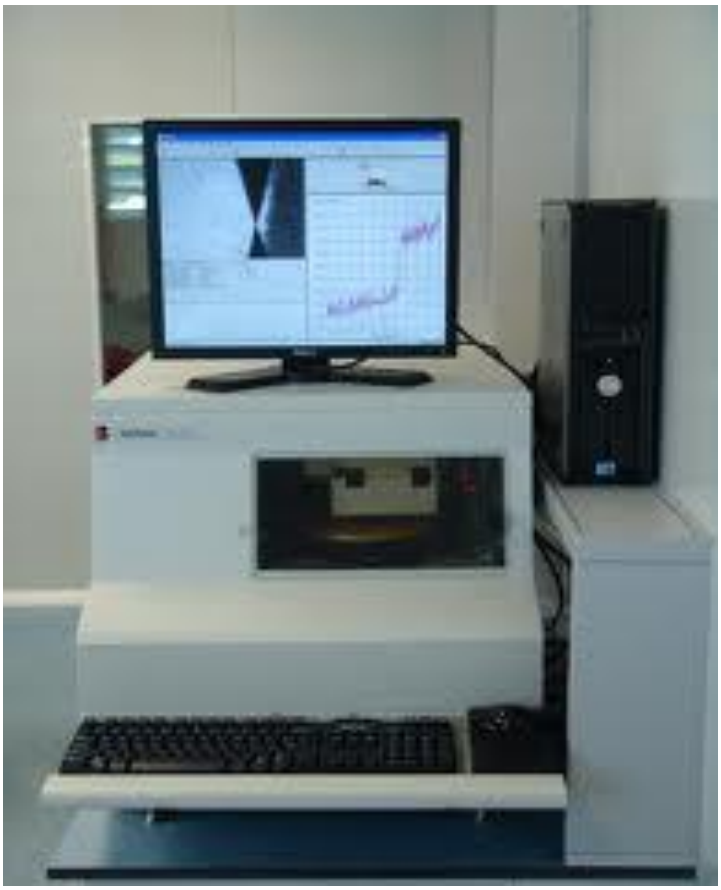

Figure 2.6. Surface Profilometer (KLA Tencor P-16)

2.2.3.4. TRANSMISSION ELECTRON MICROSCOPE (TEM).

TEM (Tecnai T12) was used to study the structure of SA-LbL Membrane. Prior to TEM characterization, small piece of cross section of SA-LbL membrane sample was embedded in epoxy. This embedded sample was then trimmed and sliced using trimmer and microtome in order to obtain about 80 nm thick sample. The ultrathin sample was characterized using the TEM.

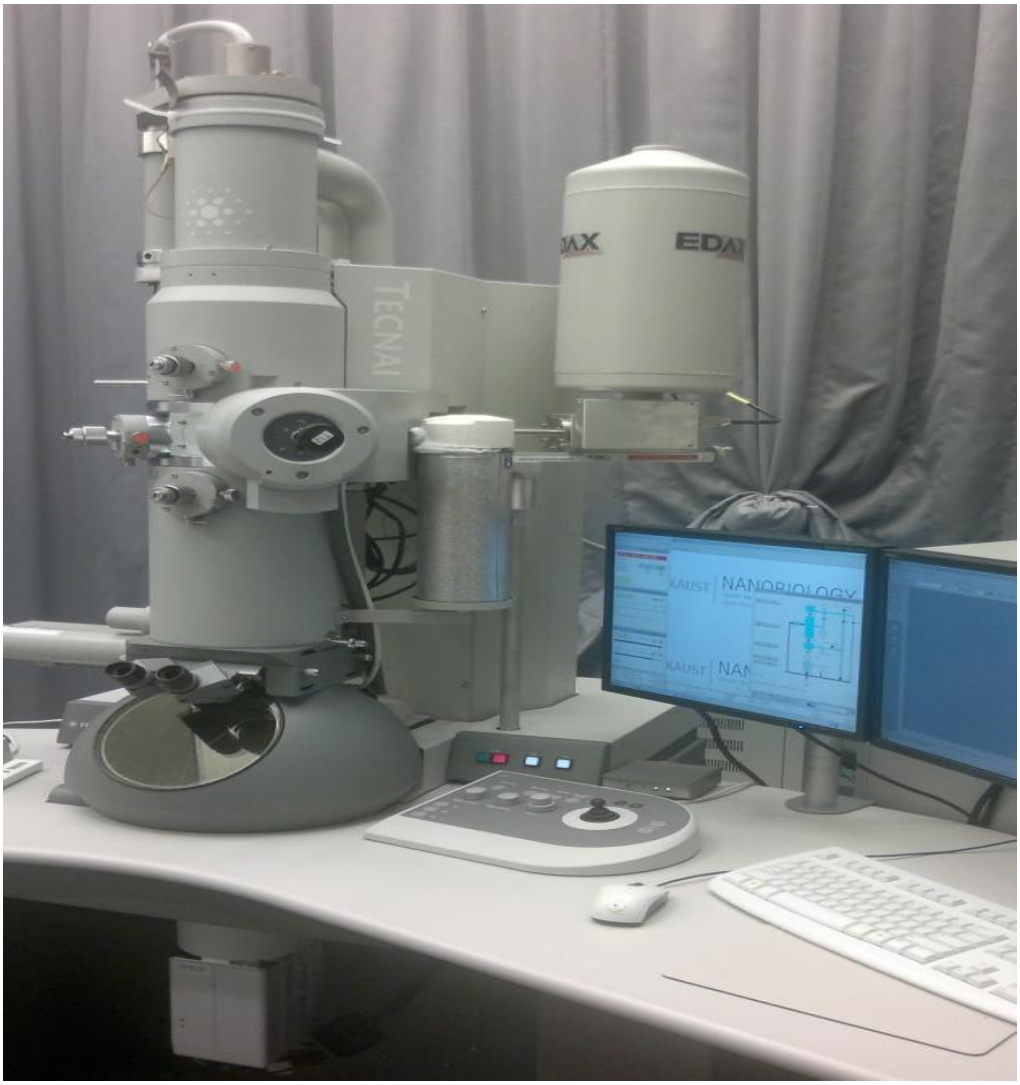

Figure 2.**7.** Transmission Electron Microscope - Tecnai T12

2.2.3.5. X-RAY DIFFRACTION (XRD).

The crystalline structure and nanoclays was evaluated by powder X-ray diffraction, XRD (Bruker AXS D8 diffractometer using Cu K_ radiation). This characterization is used to study the intercalation degree of nanoclays in PA film.

Figure 2.8. Bruker AXS D8 diffractometer

2.2.3.6. CONTACT ANGLE (CA).

Sessile drop contact angle measurement was carried out by using DM-501 (Kyowa Interface Science Co.) to mainly examine the hydrophilicity or wettability of SA-LbL membrane. DI water as much as 2 μL was dropped on the surface of the membrane and the angle formed from the tangent of water droplet curvature (liquid-gas interface) with the solid surface (liquid-solid interface) was then calculated (see Figure 2.9). All CA data reported in this work are average of 10 measurements.

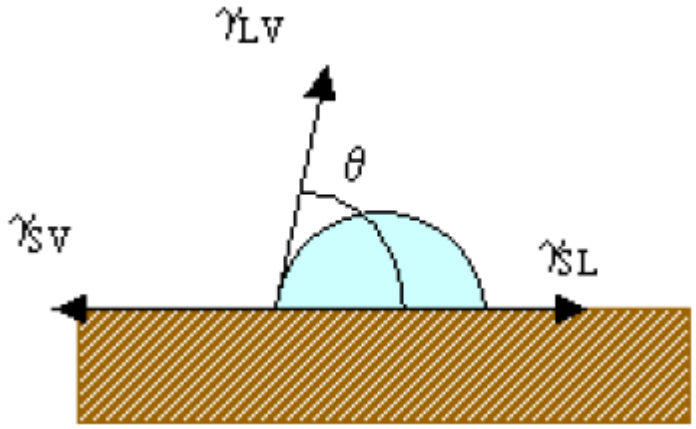

Figure 2.9. Schematic Diagram of Contact Angle Measurement.

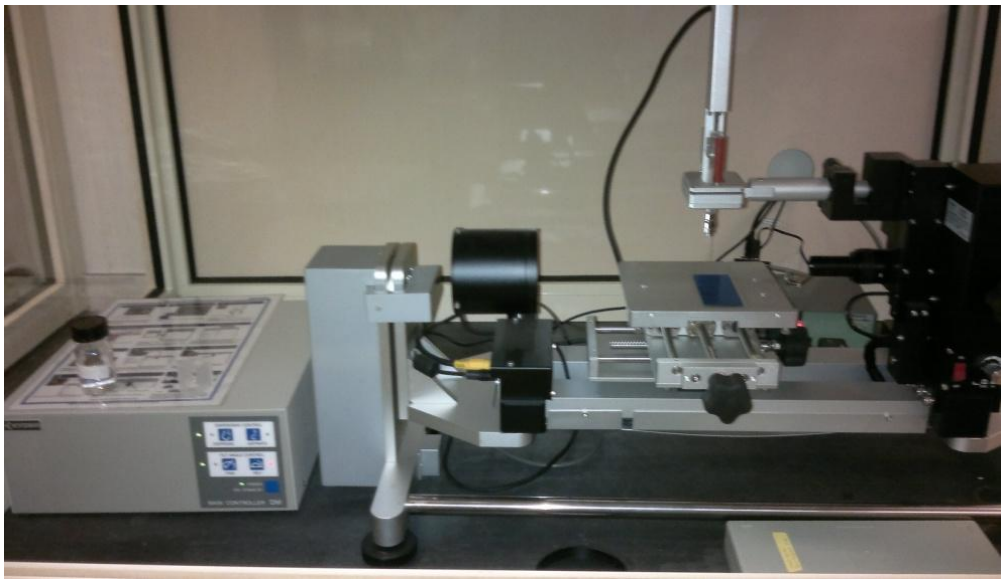

Figure 2.10. Contact Angle DM-501 (Kyowa Interface Science)

2.2.3.7. FOURIER TRANSFORM INFRA RED (FTIR).

In infrared spectroscopy, IR radiation is passed through a sample. Some of the infrared radiation is absorbed by the sample and some of it is passed through (transmitted). The resulting spectrum represents the molecular absorption and transmission, creating a molecular fingerprint of the sample. Like a fingerprint, no two unique molecular structures produce the same infrared spectrum. This makes infrared spectroscopy useful for several types of analysis.

The iTR-FTIR Nicolet 6700 Model (Thermo scientific) was used to investigate functional groups of polyelectrolyte multilayer film and the support. This type of FTIR is also known as Attenuated Total Reflectance (ATR) FTIR which allows the measurement without further sample preparation. ATR uses a property of total internal reflection resulting in an evanescent wave. A beam of infrared light is passed through the ATR crystal in such a way that it reflects at least once off the internal surface in contact with the sample. This reflection forms the evanescent wave which extends into the sample. The penetration depth into the sample is typically between 0.5 and 2 micrometres, with the exact value being determined by the wavelength of light, the angle of incidence and the indices of refraction for the ATR crystal and the medium being probed [130].

Figure 2.11**.** iTR-FTIR Nicolet 6700 Model (Thermo scientific)

2.2.4. MEMBRANE TESTING.

TFC SA-LbL and PA membrane with active membrane surface area of 42 cm^2 was tested by using CF042 (Sterlitech Corp.) cross flow permeation cell (see appendix A for detail description). Feed water consisting of 2000 ppm of sodium chloride was pumped through the SA-LbL membrane at pressure of 40 bar and temperature of $25^{O}C$. Permeate flow rate and conductivity measurement were repeatedly taken for every 1 hour after the permeation cell condition reached steady state.

The membrane testing described in chapter five is done slightly different from the above procedure. Here, Membrane testing includes two type of test i.e. membrane stability and effect of various parameters on membrane performance. When membrane stability test was conducted, all parameters such as salt concentration of feed water, pH, pressure, and temperature were kept constant. By default, salt concentration of feed solution was 2000 ppm, pressure across the membrane was maintained at 40 bar, temperature was kept at $25^{o}C$, and pH of feed water was hold at 6. Here, the membrane was tested for 40 hours and the measurement of water flux and conductivity of permeate solution was done for certain time interval for instance for every 2 hours.

When the effect of various parameters on membrane performance was investigated the studied parameter was varied while other parameters were kept constant at the abovementioned default values. For example, salt concentration of feed solution was varied from 2000 ppm to 35000 ppm when the effect of salt concentration was studied. Similarly, the pressure was varied from 30 bar to 60 bar with 10 bar increment and temperature was changed from $25^{o}C$ to $45^{o}C$ with $10^{o}C$ increment when those

corresponding parameters were investigated. Water flux and salt conductivity for both feed and permeate solution were measured at specific time for instance every 1 hour after the membrane was conditioned for 50 hours.

Figure 2.12. Permeation Cell (CF042 Sterlitech)

CHAPTER THREE

FABRICATION OF HIGHLY ORDERED MULTILAYER FILM VIA SPIN ASSISTED LAYER BY LAYER ASSEMBLY

3.1. RESULT AND DISCUSSION

Spin assisted Layer by Layer (SA-LBL) assembly was used to fabricate bi-polar thin films consisting of PAH/PAA on silicon wafer as well as on commercial polysulfone ultra filtration membranes. Following the findings of Rubner and coworkers who fabricated the PAH/PAA thin films via Dip-LbL technique, we chose to investigate the bilayer thickness as a function of assembly pH, which was varied systematically from 3.5 to 9 for each polyion solution. It is clearly shown in Figure 3.1 that by simply adjusting the pH, it is possible to construct rather thick bilayers (100 Å) or typically thin bilayers (30 Å) similar to Rubner's report on weak polyelectrolyte films [42]. It can be seen that in general, the thinnest films were achieved when the pH of PAH solution is kept low, at 3.5 in this work. In contrast, thinner films were obtained when the pH of PAA solution was maintained at higher values, thus the thinnest films were formed at low pH for PAH and high pH for PAA, as anticipated.

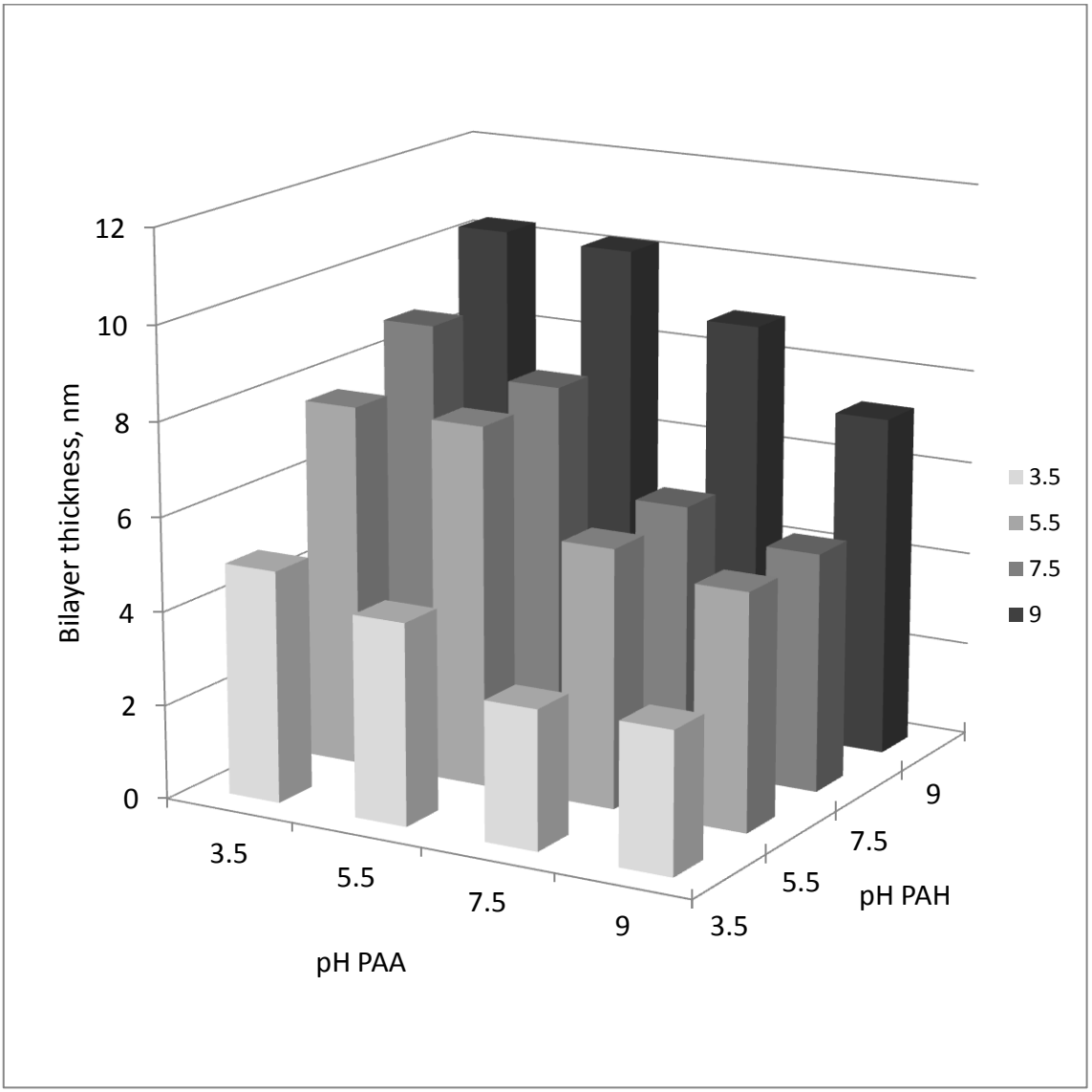

Figure 3.1. Average incremental thickness contributed by PAH/PAA as a function of solution pH.

The regularity of the thickness trends in Figure 3.1 is caused by the change in degree of ionization of the weak polyacid (PAA) and polybase (PAH) with pH. Similar film thickness dependencies on pH have been observed by Rubner and other researchers, typically directly associated with the pKa of the corresponding polyions in solution. PAA, with a pKa of 5.5 to 6.5 [131], becomes fully charged or fully ionized at pH values above 6.5 while in contrary, PAH has a pKa of approximately 9.0 [131]. In both cases, polyelectrolytes can exhibit broad pKa transitions that span a few pH units due to the fact that the effective pKa shifts as the backbone becomes more and more charged due to polyvalent electrostatic effects. The thickness of each individual layer is determined by the charge density of the adsorbing polyelectrolyte chains and that of the previously adsorbed layer [113]. In general, the charges of the previously adsorbed layer should be neutralized by the charges of the adsorbing layer. However, the amount of adsorbing polyelectrolyte required to compensate the previously adsorbed layer is not the only contributor to film thickness. The polymer chain conformation of the previously adsorbed layer and the contour of the underlying surface are some other significant factors, which also determine the film thickness.

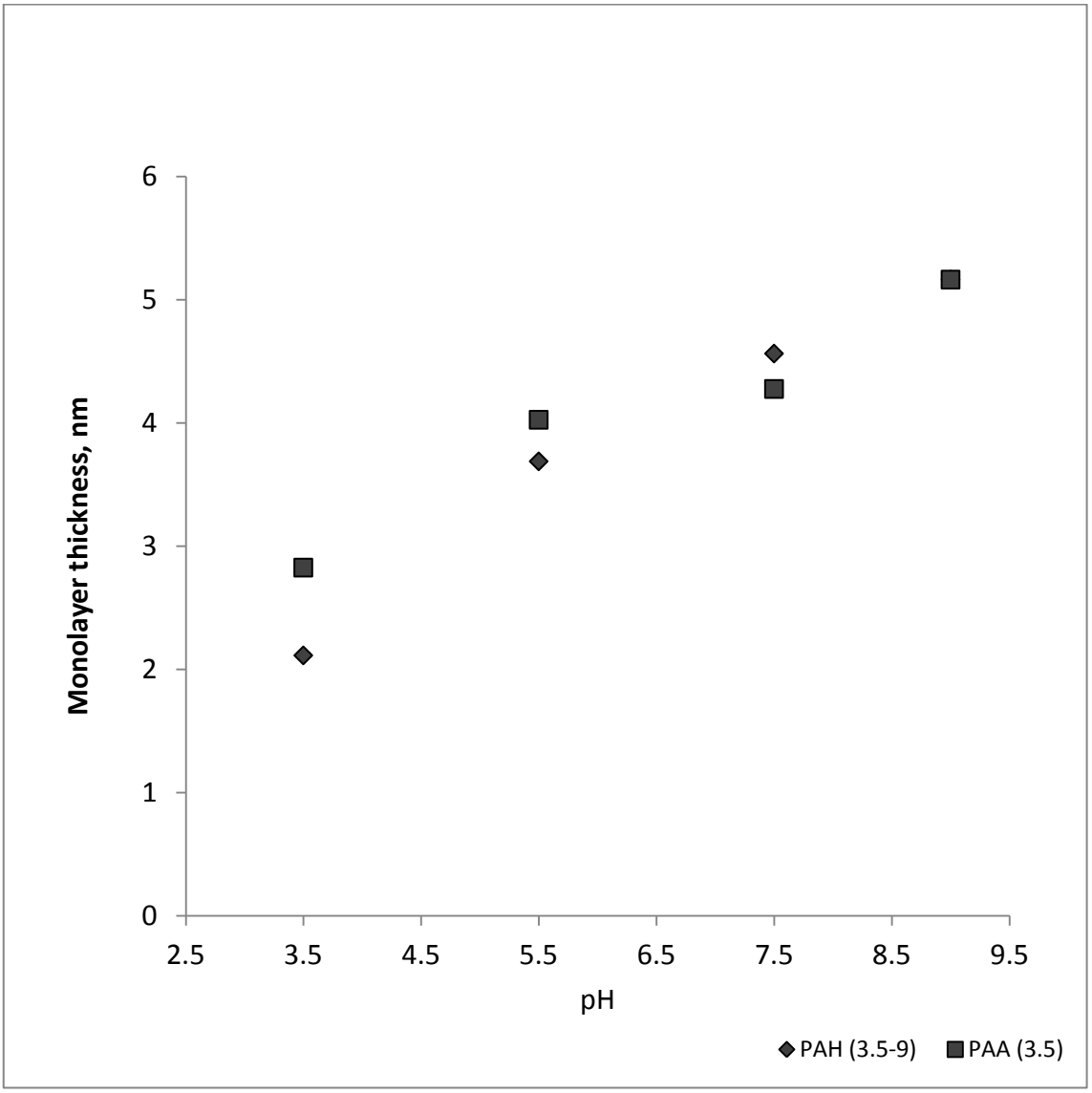
Monolayer thickness, nm
6
5
4
3
2
1
0
2.5
3.5
4.5
5.5
6.5
7.5
8.5
9.5
pH
PAH (3.5-9)
PAA (3.5)

(a)

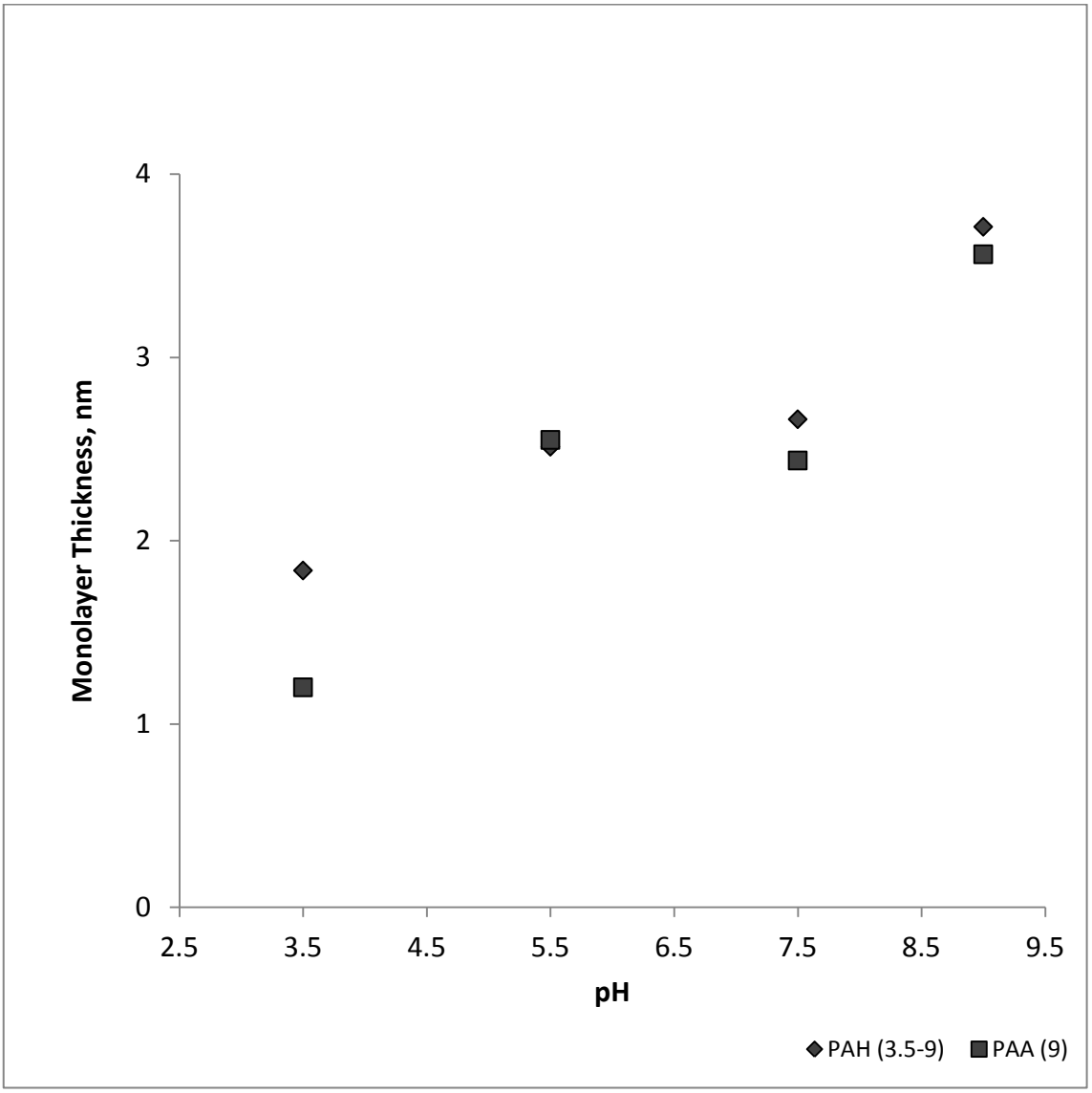

(b)

Figure 3.2. Average monolayer thickness contributed by PAH and PAA adsorbed layer as a function of solution pH while pH of PAA is kept constant at each figure: (a) PAA pH of 3.5 (b) PAA pH of 9.

To further understand the film growth behavior, monolayer thickness of the adsorbed PAH and PAA is plotted as shown in Figure 3.2. In this figure, the pH of PAA was kept constant either at 3.5 or at 9, while the pH of PAH was varied from 3.5 to 9. It can be clearly seen that PAH thickness increases as pH is increased. This is expected because as PAH becomes less charged, more PAH is required to compensate the underlying surface charge of previously adsorbed layer, and the conformation of these PAH chains on the surface also becomes loopier and more extended with lower degrees of ionization, as previously reported. It is noteworthy to observe that the PAA thickness also increased with PAH pH increase, even though its pH was kept constant during deposition. In Figure 3.2, we can also clearly see that the PAA thickness profile, whether in its fully charged (PAA pH of 9) or poorly charged state (PAA pH of 3.5) exhibits the identical pattern as the PAH thickness profile. This is strong evidence that the conformational state of the previously adsorbed layer is strongly affecting the thickness of the subsequently adsorbing layer. Similar observations have been made for dip-LbL systems, in that increased thickness of the underlying layer allows access to more adsorption sites for the next polyelectrolyte adsorption step. This effect is one that does suggest some role of interpenetration between polyelectrolyte layers, even in spin-assisted LbL assembly. This interpenetration is also supported by contact angle measurement from which CA of 20^{o}C was obtained as PAA as the outermost layer. It was reported that pure PAA has CA of 5^{o}C while pure PAH has CA of 55^{o}C [42, 113]. If the polyelectrolytes are completely interpenetrated each other, CA of 30^{o}C should be obtained. Meanwhile in our case here, the CA suggests more PAA exposed to the surface rather than PAH. This means in the

case of SA-LbL, interpenetrating between PAA and PAH with PAA do exists at less extent than d-LbL.

It is known that at low pH, PAA is poorly charged and it was generally anticipated that the PAA adsorbed layer should be thicker than the PAH film because PAH is fully charged under these conditions. This phenomenon can actually be seen Figure 3.2 (a), however as the pH of PAH increases, and PAH starts losing charges and yields thicker monolayers of both PAA and PAH. These changes occur regardless of whether PAA is presented in a partially (pH of 3.5) or fully charged state (pH of 9), thus suggesting that the effect of the degree of ionization of PAH on the thickness is not the key factor here. Rather, we show that the chain conformation of the previously adsorbed layer strongly affects the thickness of subsequent layer, as previously described by Rubner and others for Dip-LbL systems.

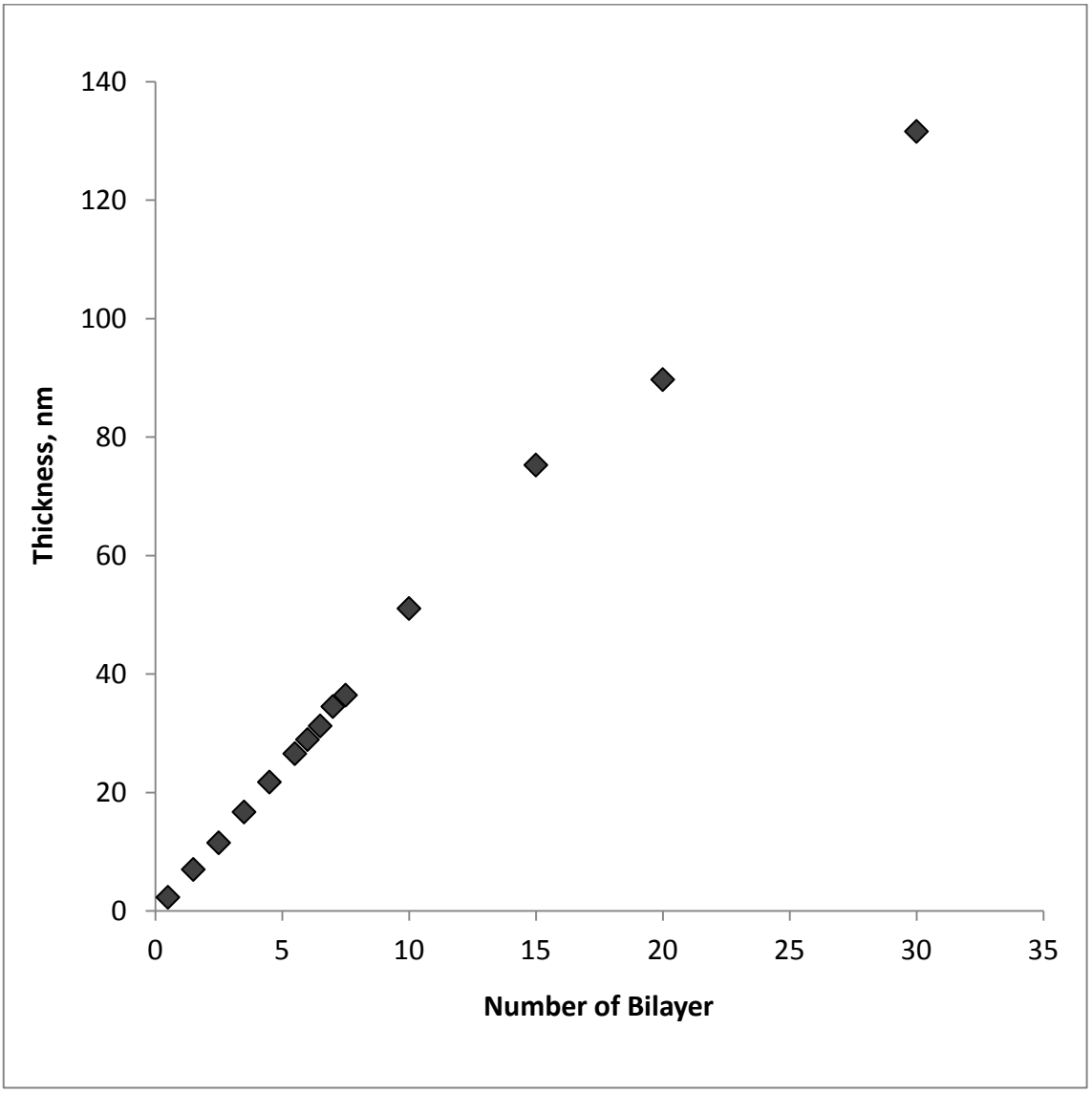

Figure 3.3. PAH/PAA spin assisted LbL film growth behaviour (pH 3.5/3.5).

Figure 3.3 indicates that the SA-LbL film grows linearly from a very early stage in the deposition process, with film building up uniformly even after the first deposition cycle. Typically in d-LbL films, linear growth is achieved following the deposition of the first 3 to 10 bilayers [42], during which full surface coverage must be attained. In dip-LbL, this behavior is attributed to the formation of islands of polyelectrolyte in the first few cycles of adsorption from dilute solution [132, 133]. This induction period is not observed in SA-LbL because of the rapid evaporation of water helped by centrifugal force of spinning process, which leads to a kinetically trapped but uniform layer of polyelectrolyte on the surface. As a result, polyelectrolyte chains are rapidly adsorbed directly onto the surface as they are distributed across the substrate, and they do not have an opportunity to assume equilibrium island configurations as expected in the immersion conditions present in the dip-LbL. Another advantage of the rapid water removal in the spin process is the significant enhancement of the polyelectrolyte concentration at the surface, which in turn enhances the rate of polyelectrolyte adsorption. All of these phenomena are considered major factors to the increased surface coverage at low bilayer numbers and the linear growth observed in the SA LbL process.

It can be seen in Figure 3.4 the presence of the coating becomes more prominent as the number of bilayer increases. The interesting fact is eventhough the morphology becomes more prominent actually the surface rougness decreases significantly from about 4 nm at 5 bilayers to 0.8 nm at 30 bilayers. This indicates the valley and mountain structures in film surface topology diminish due to much better surface coverage as number of bilayer is increased.

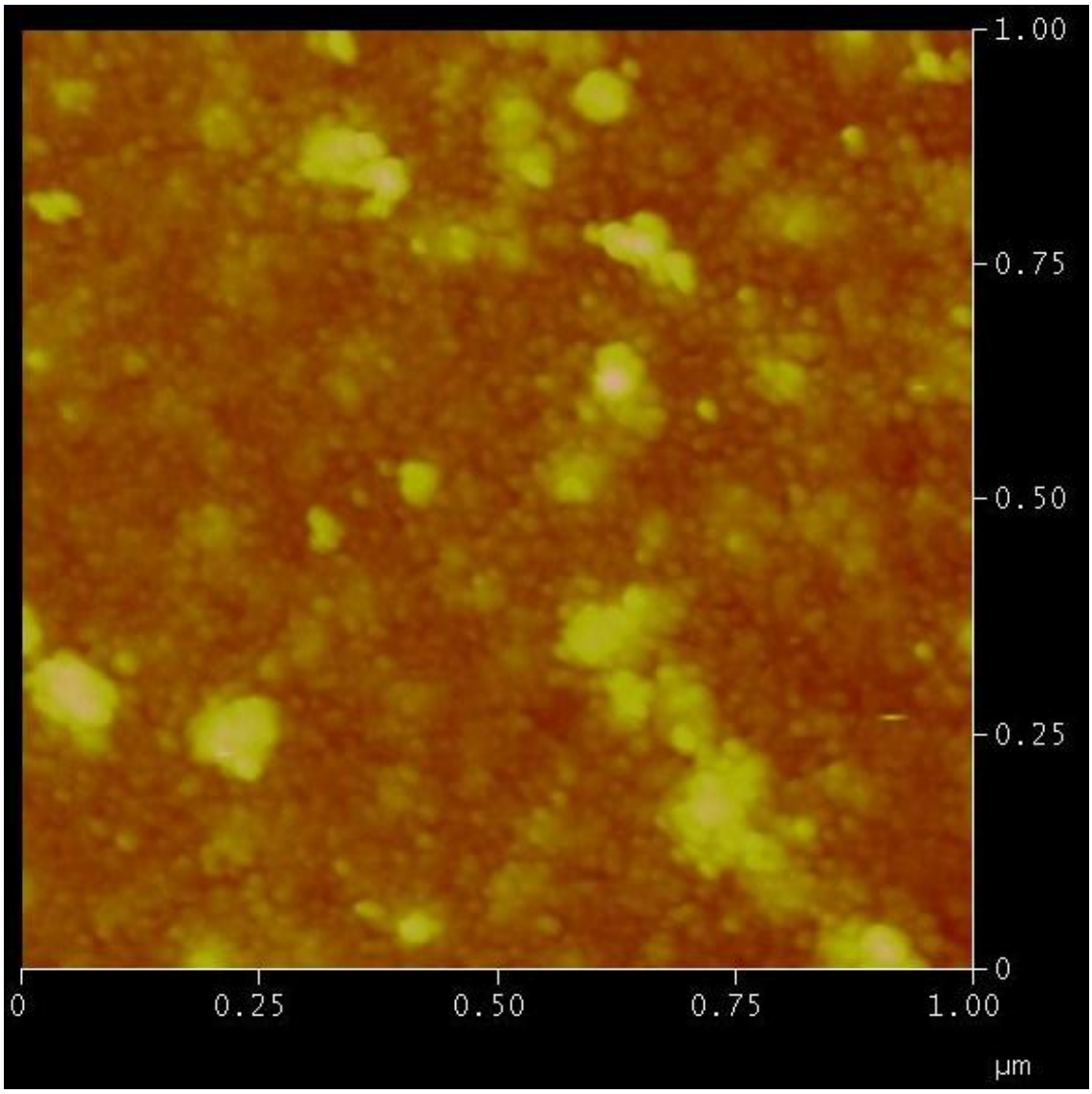

(a)

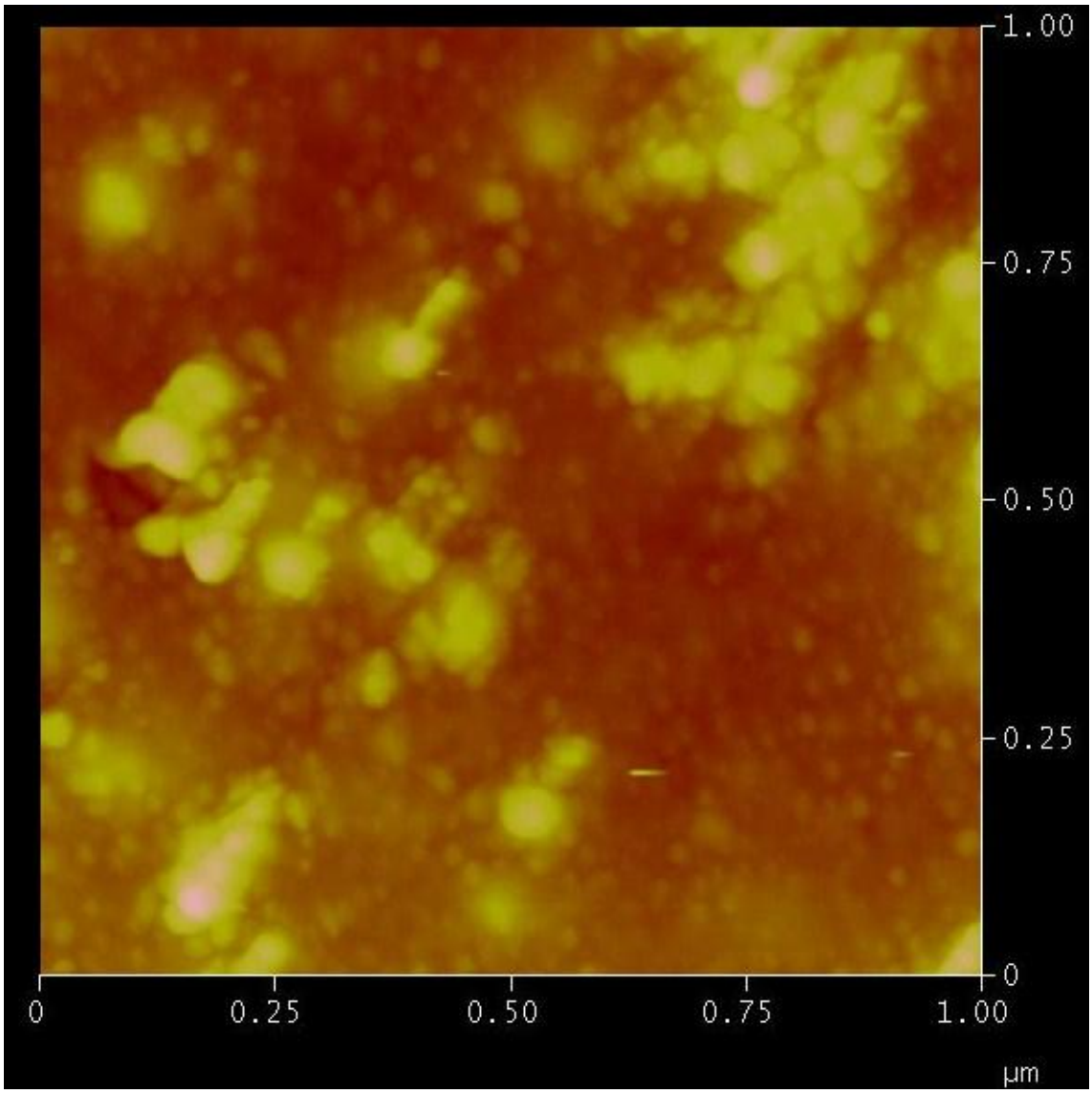

(b)

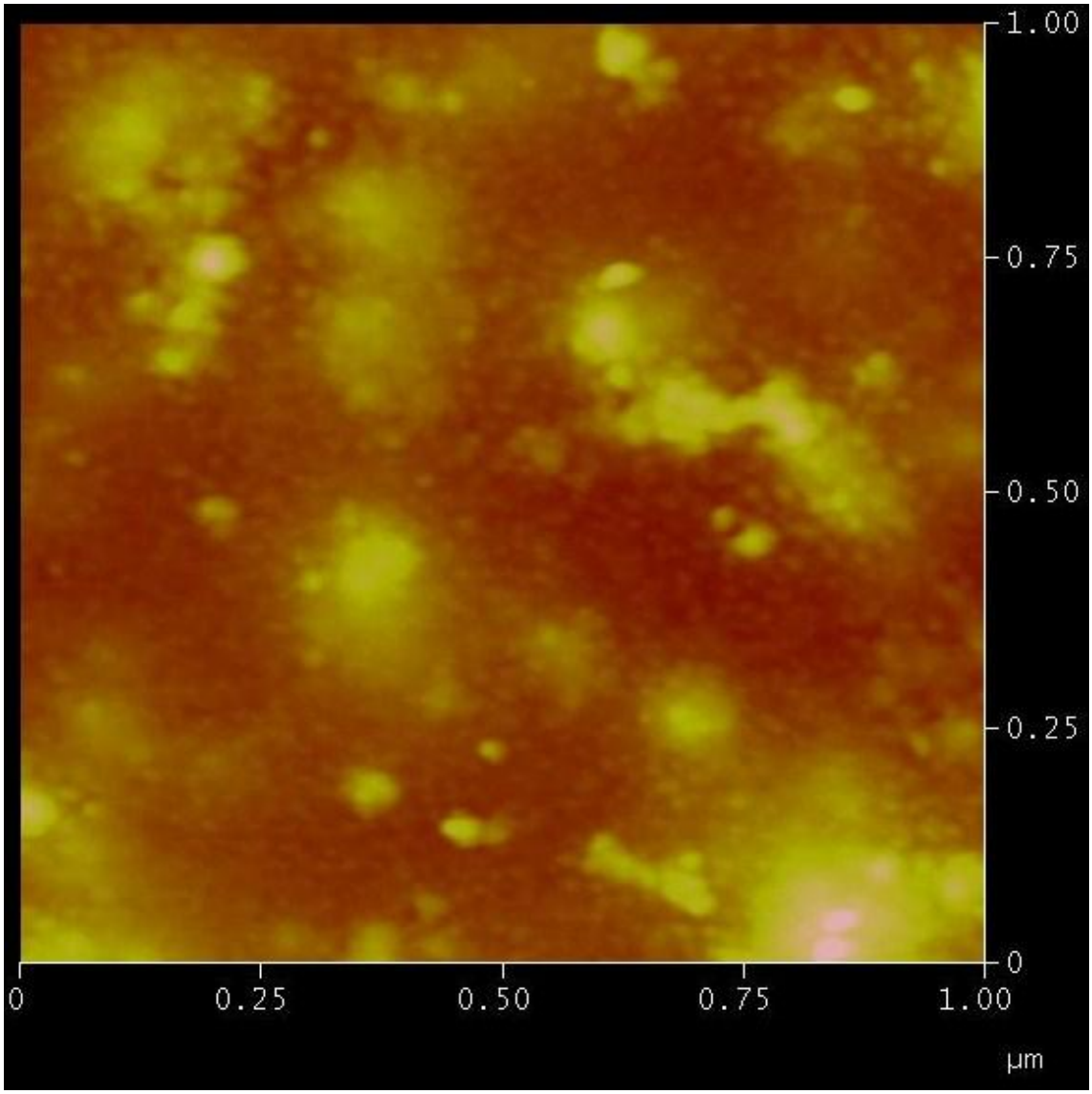

(c)

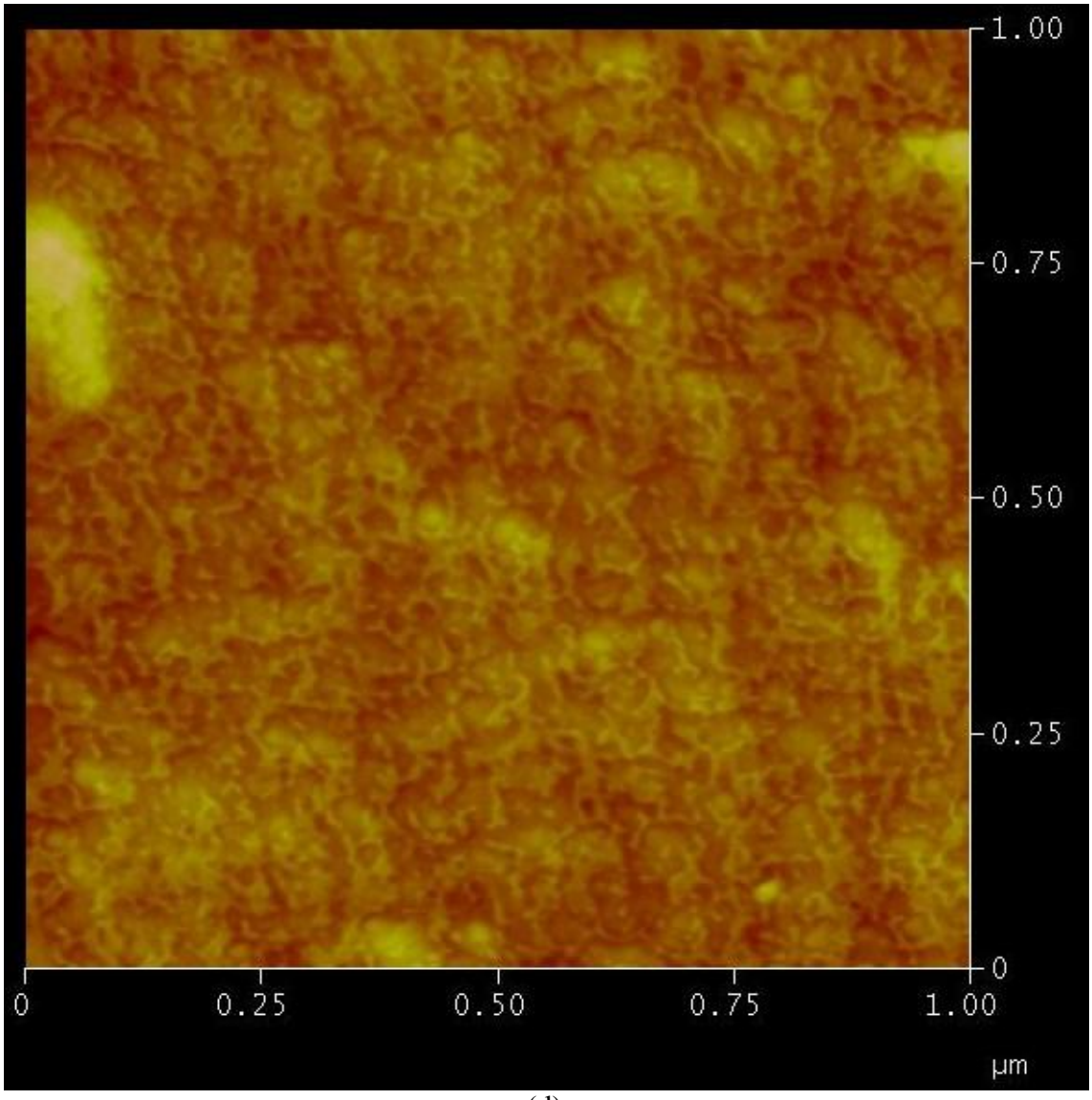

(d)

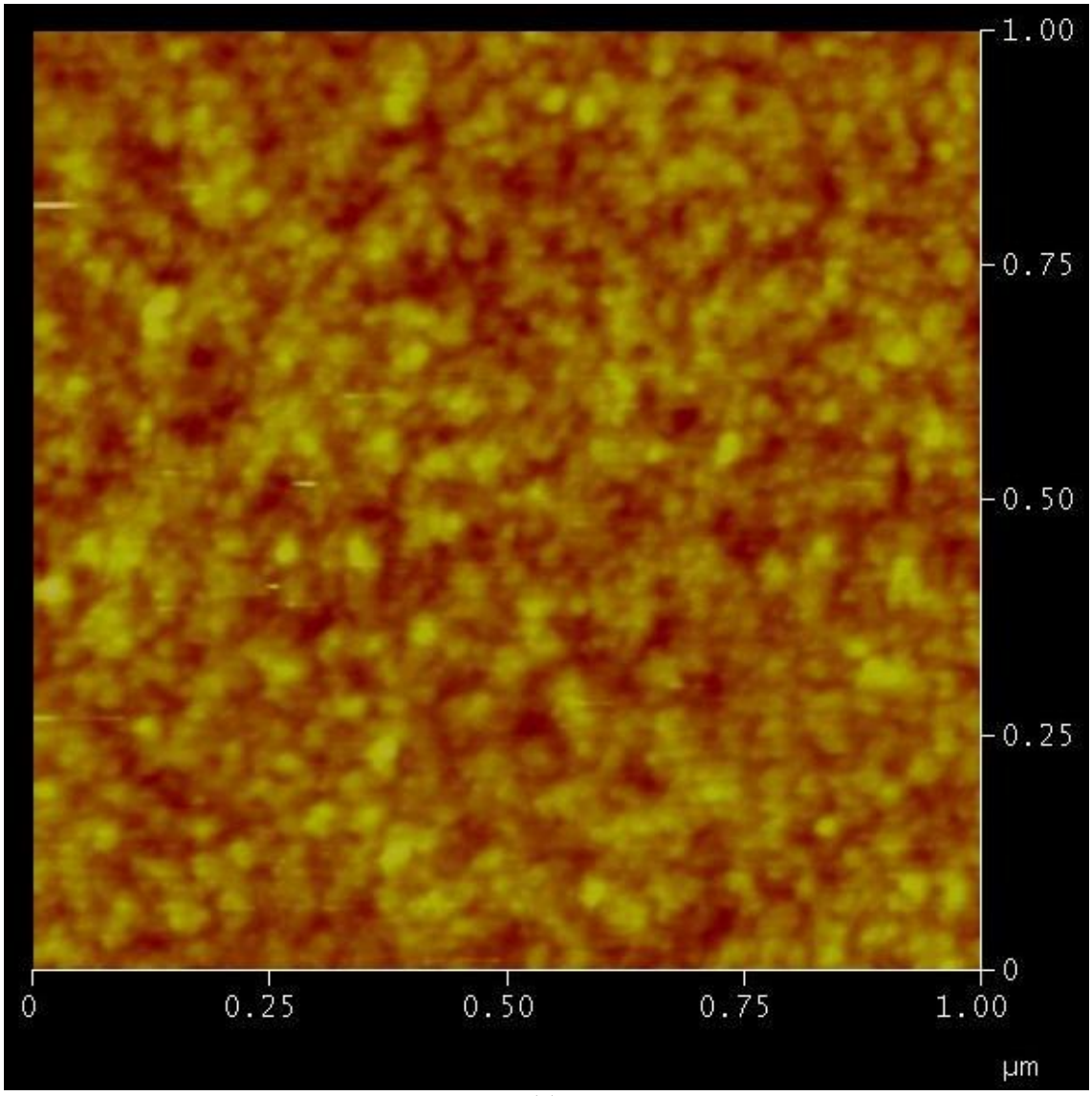

(e)

Figure 3.4. AFM images of PAH/PAA film on silicon wafer at different number of bilayers. (a) 5 bilayer; (b) 10 bilayers; (c) 15 bilayers; (d) 20 bilayers; (e) 30 bilayers.

The impact of spin speed on layer thickness has also been studied extensively as a unique parameter of SA-LbL that can be used to directly control the film thickness [49, 82, 134-139]. It was found that SA-LbL assembled PAH/PAA films exhibit a near linear decrease in multilayer growth with increased spin speed, similar to other reports. As the spin speed increases, mechanical forces applied to the depositing film also increase, thus shorten the polyelectrolyte contact time for adsorption which results in decreasing the amount of adsorbed polyelectrolyte adsorbed, and consequently the thickness also decreases.

Interestingly, increased spin speed not only reduces the thickness but also decreases the surface roughness, as shown in Figure 3.5. Again, the mechanical forces i.e. shear force in this case, play an important role. The higher the spin speed, the higher the shear force which stretches the polymer chains on the substrate during adsorption and leads to smoother surfaces. However, the effect of spin speed on the surface roughness tends to diminish with the increase in the spin speed. This may perhaps be attributed to the fact that at a certain critical spin speed (3000 rpm in our case) the polymer chains get fully stretched and further increase in spin speed only marginally improve the surface roughness of the adsorbed film. This critical speed may vary for different polymer systems because of the difference in key polymer parameters such as molecular weight, chain stiffness, and degree of solvation.

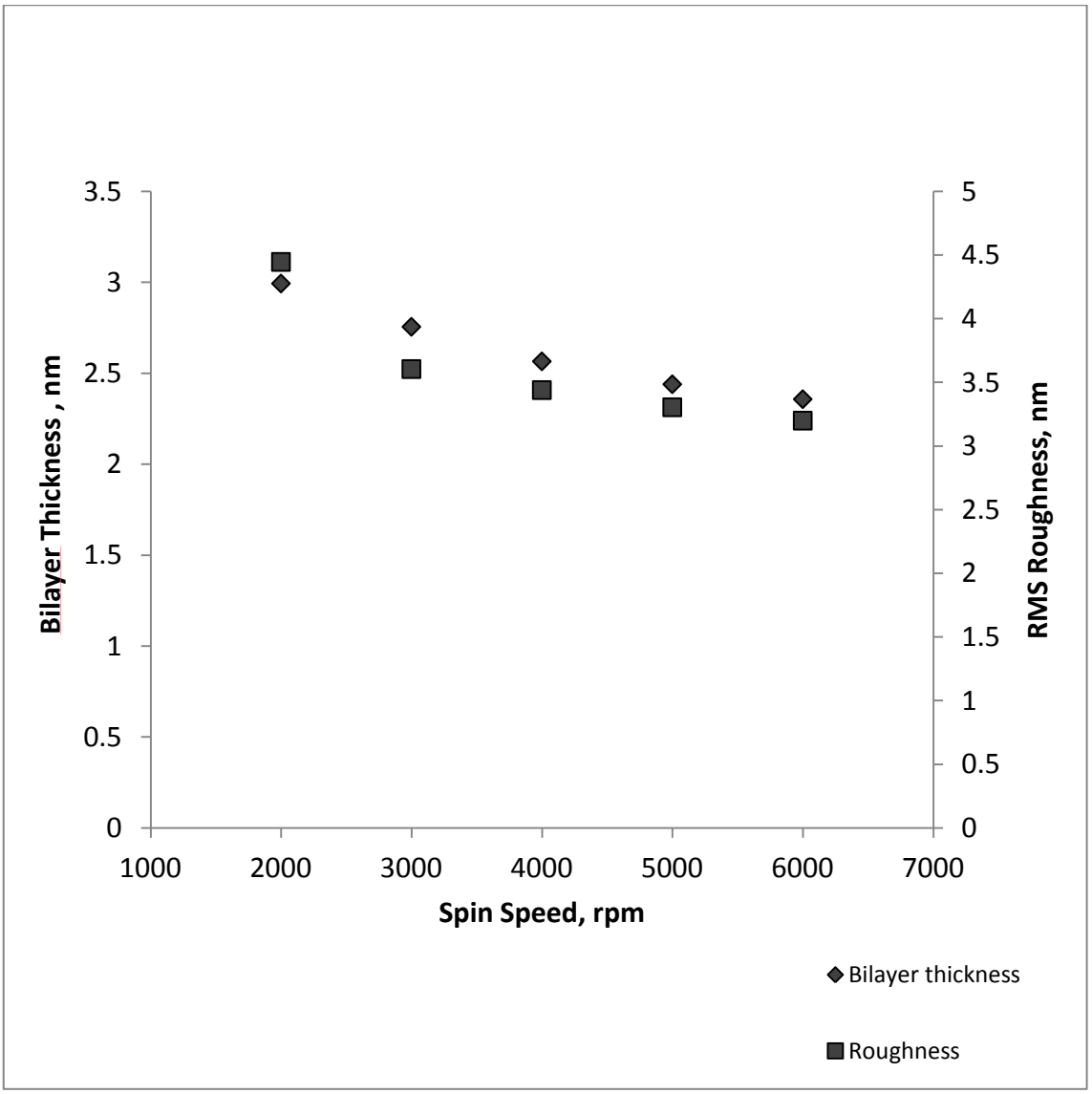

Figure 3.5. Effect of Spin Speed on Bilayer Thickness and surface roughness

Last but not least, in order to study the effect of concentration, we deposited the polyelectrolytes of different molar concentration at constant speed of 3000 rpm. For each concentration level the molar concentration of both PAH and PAA was kept identical. Lee *et al* [139] studied the effect of concentration on layer thickness, however the concentrations that they used in their study were relatively low. In our work, we extend the range of concentration up to 50 mM.

As shown in Figure 3.6, it is obvious that there is a maximal concentration beyond which increasing the concentration does not have significant impact on the film thickness. For instance, increasing the concentration from 5 mM to 10 mM produced a film which is twice as thick as the one formed at 5 mM. Increasing the concentration from 25 mM to 50 mM however produced only a 15% thicker film. This tendency toward reaching an equilibrium amount of polyelectrolyte adsorbtion at high concentration implies that the SA-LbL approach is ultimately governed by equilibrium amounts adsorbed based on electrostatic potential, as anticipated for a true LbL process. The effect is even more significant when coupled with fast water removal during the spinning process. Therefore the thickest layers are formed by using high concentration and maintaining a low to moderate spin speed.

It can also be seen clearly from Figure 3.6 that polyelectrolyte concentration also moderately affects the surface roughness of the film, for instance, increasing polyelectrolyte concentration by ten times, results in about 50% increase in surface roughness.

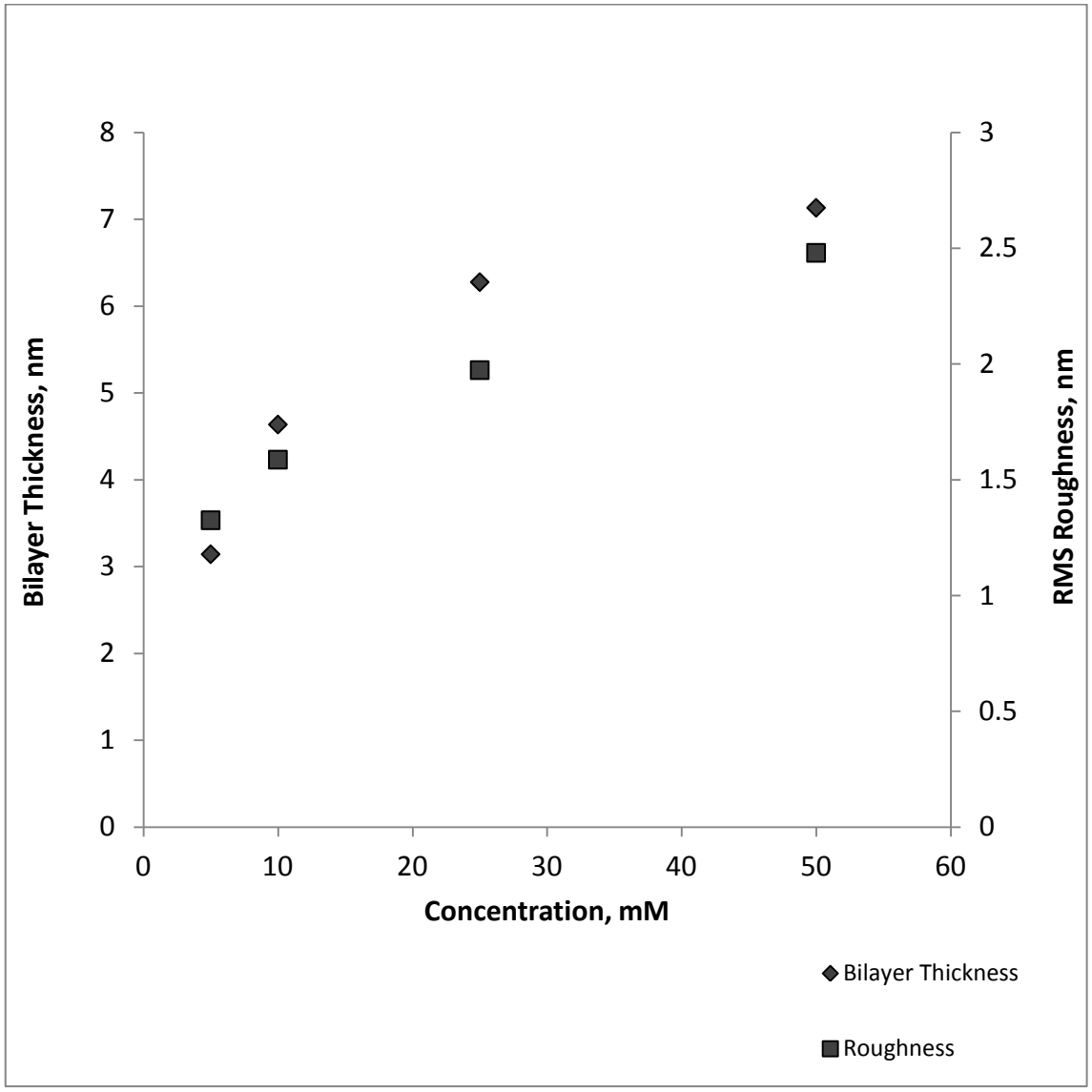

Figure 3.6. Effect of Concentration on Layer Thickness and Surface Roughness

3.2. CONCLUSION

It is demonstrated a convenient, robust and versatile technique to fabricate multilayer film using spin assisted layer by layer assembly. The thickness of the film can be easily controlled by changing the solution pH, varying the number of bilayers, regulating the spin speed and adjusting the solution concentration. This technique also provides a linear film growth within a short time which makes this technique is technologically friendly. So far, we have seen the application of this technique in photolithography, nuclear track, gas sensing, electronic devices, and light emission. The application of it in separation membrane has not been investigated yet and will be discussed thoroughly in the next chapters.

CHAPTER FOUR

POLYELECTROLYTE MULTILAYER FILMS PREPARED THROUGH SPIN-LAYER BY LAYER ASSEMBLY FOR REVERSE OSMOSIS APPLICATION

4.1. RESULT AND DISCUSSION

In this study thin film composite membranes fabricated from various polyelectrolyte systems were investigated. PDAC/PVS membrane has less number of ion pair per carbon atom but it is combination of strong-strong polyelectrolyte which means the system may form less dense film but it will be quite stable for broad pH range. PAH/PVS has higher ion pair per carbon atom and represents weak-strong combination. Meanwhile PEI/PAA and PAH/PAA are combination of weak-weak polyelectrolytes and also have high ion pair per carbon atom but PEI has more branch in its backbone compared to PAH. As is well known, the degree of dissociation of weak polyelectrolyte is mainly determined by its pH. In the case of PAH, it is reported that PAH with pKa of 8.5 starts gaining protons at pH lower than 6 [42, 140]. In this work, pH of 3.5 was selected for PAH and PEI depositions to ensure both polyelectrolytes are in their fully ionized state. PAA is also weak polyelectrolyte with pKa of 6.5 and become fully ionized at pH above 6.5 [42, 98, 141]. Unlike weak polyelectrolyte, charge density of PDAC and PVS remains constant over most of pH range in water. It is reported that PDAC has pKb of 11.8 [142] while PVS has pKa less than 2 [143]. It is also reported that complex formation from PDAC and PVS showed stoichiometric chemistry meaning that all potential ionic bond between the two are most likely formed [144]. The PSF UF membrane is used here as support

because this membrane has also been widely used as support in TFC NF/RO membrane and has been known for its outstanding chemical, thermal, and mechanical stability.

4.1.1. SURFACE MORPHOLOGY AND HYDROPHILICITY

Comparison of surface morphology and surface hydrophilicity before and after coating is one of means that can be utilized to investigate the presence of coating. For instance, Figure 4.1 (a) shows highly porous surface with pore size of few tens of nanometer size, such morphology is common for PSF UF membrane. Meanwhile,Figure 4.1 (b) – (e) show the membrane after deposition of 60 bilayers of PAH/PVS, of PDAC/PVS, of PEI/PAA, and of PAH/PAA, respectively. These all AFM images provide clear evidence that the deposition was successful since the rough and porous PSF substrate surface is seen covered completely with a rather smooth and nonporous film.

AFM image analysis showed that the bare PSF substrate has RMS roughness of 28.18 nm while the surface roughness of $[PAH/PVS]_{60}$, of $[PDAC/PVS]_{60}$, of $[PEI/PAA]_{60}$, and of $[PAH/PAA]_{60}$ membranes showed RMS roughness of 15.35 nm, 13.45 nm, 12.63 nm, and 10.70 nm respectively. In general, SA-LbL assembly can generate extremely smooth surface due to centrifugal force applied during the course of coating. Thus the surface roughness difference from one polyelectrolyte multilayer system to another as mentioned earlier is caused solely by properties of polyelectrolyte such as chain flexibility and charged density. For example, the lower surface roughness of PDAC/PVS film compared to that of PAH/PVS film is related to chain flexibility and charge density. It is known that PDAC is stiffer and has lower charge density than PAH [145] and as such, PDAC can adopt flatter conformation than PAH.

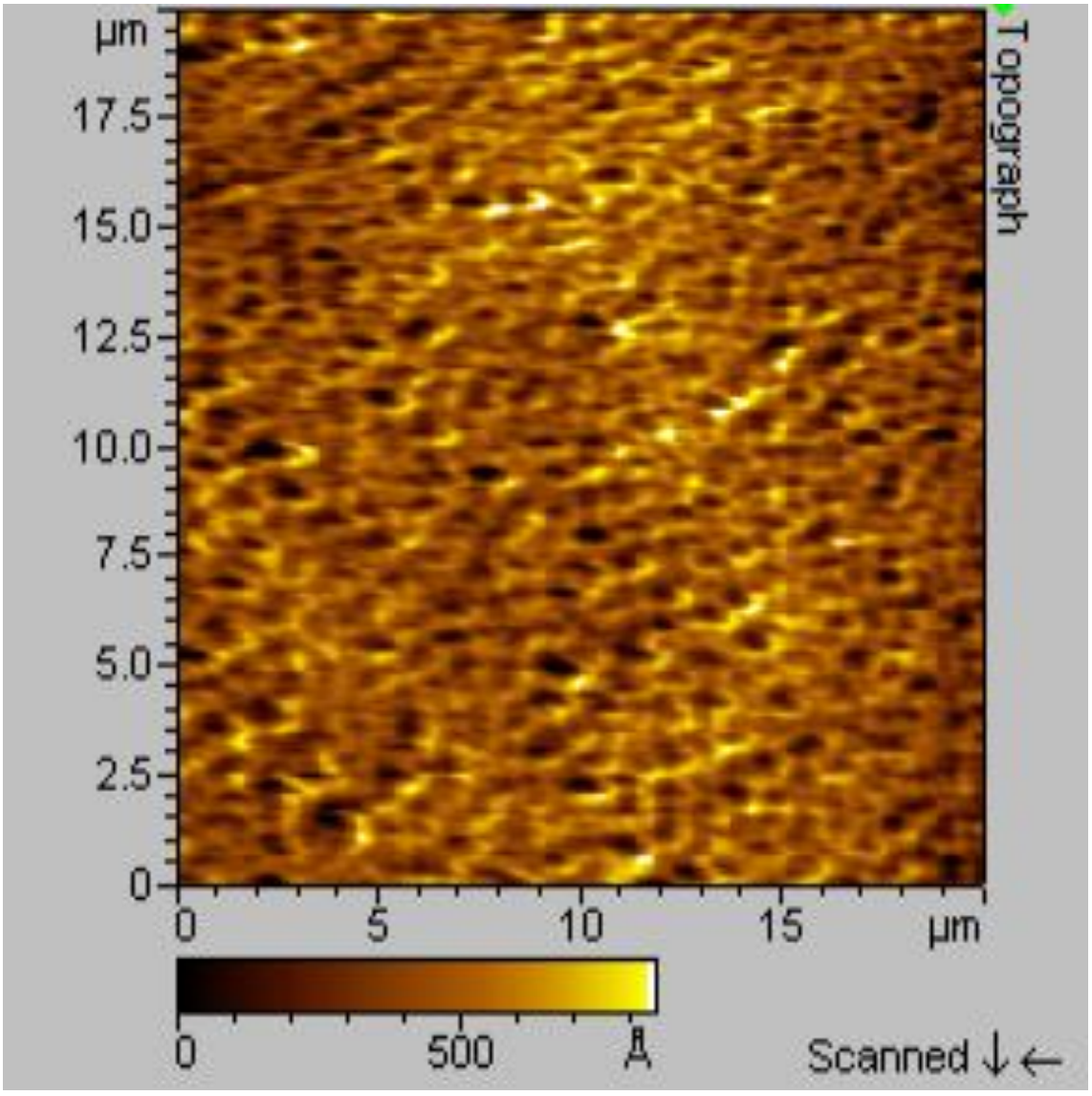
µm
17.5
15.0
12.5
10.0
7.5
5.0
2.5
0
0
5
10
15
µm
0
500
Å
Topograph
Scanned ↓ ←

(a)

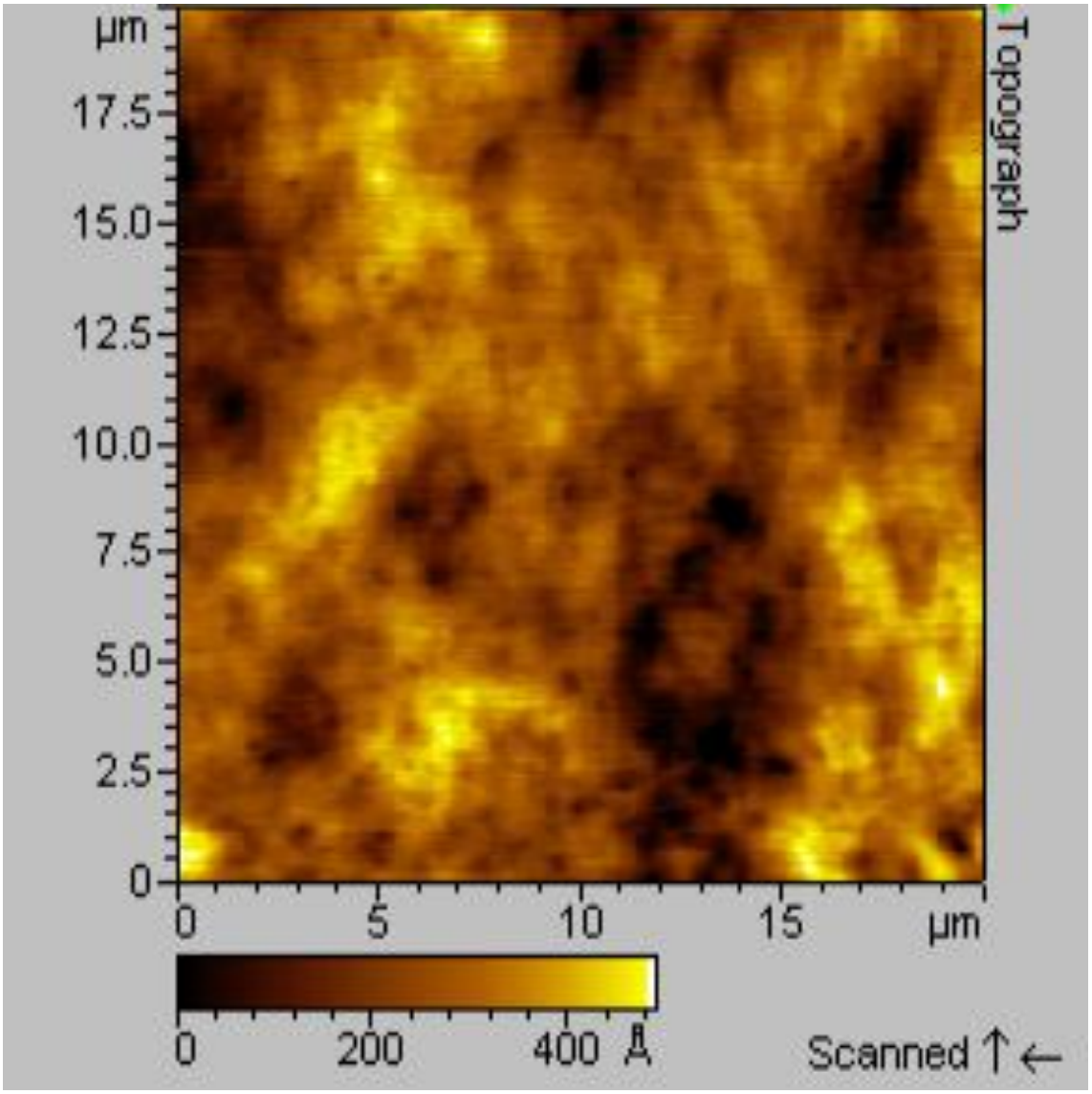
µm
17.5
15.0
12.5
10.0
7.5
5.0
2.5
0
0
5
10
15
µm
0
200
400
Å
Topograph
Scanned

(b)

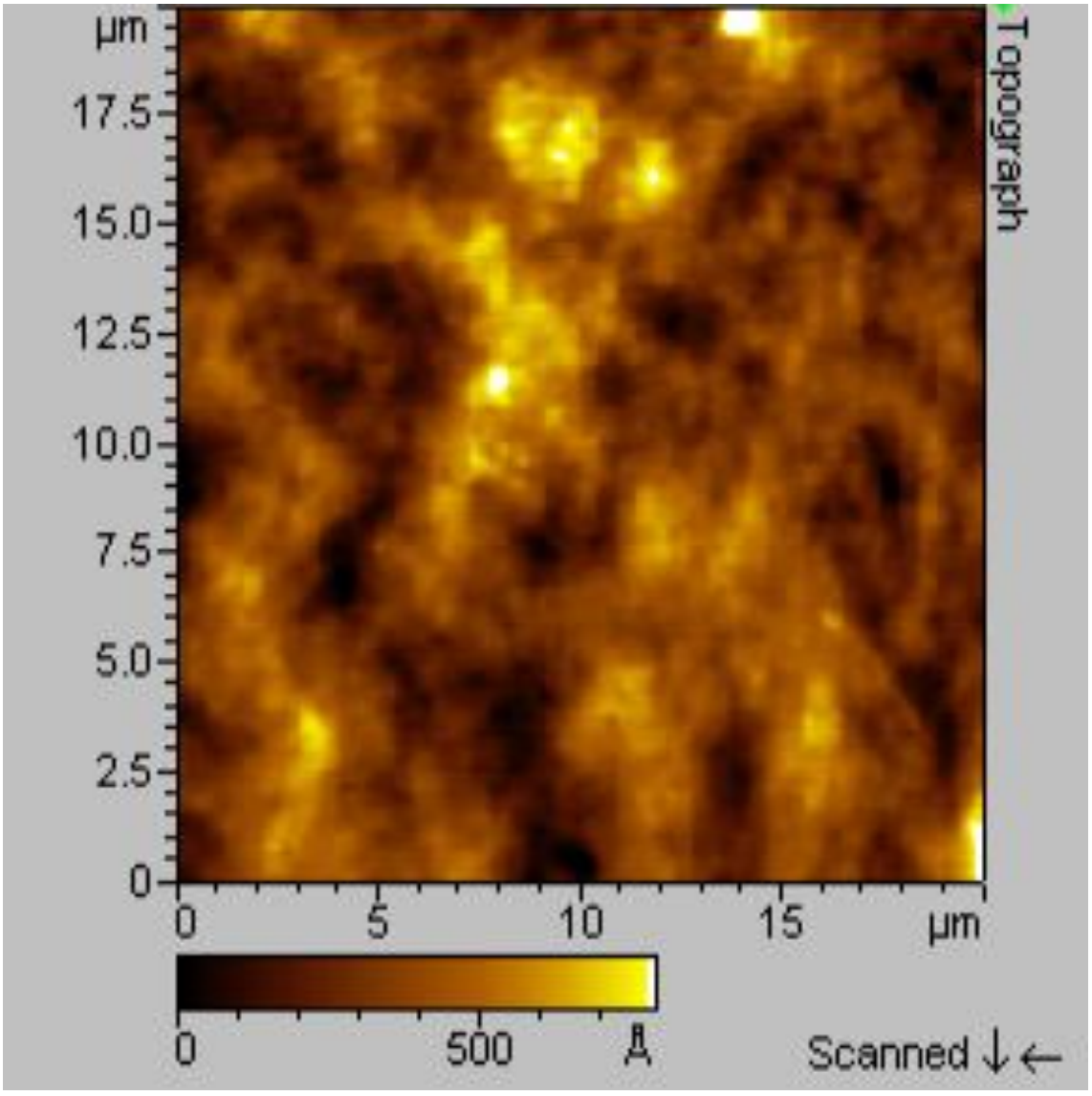
µm
17.5
15.0
12.5
10.0
7.5
5.0
2.5
0
0
5
10
15
µm
0
500
Å
Topograph
Scanned ↓ ←

(c)

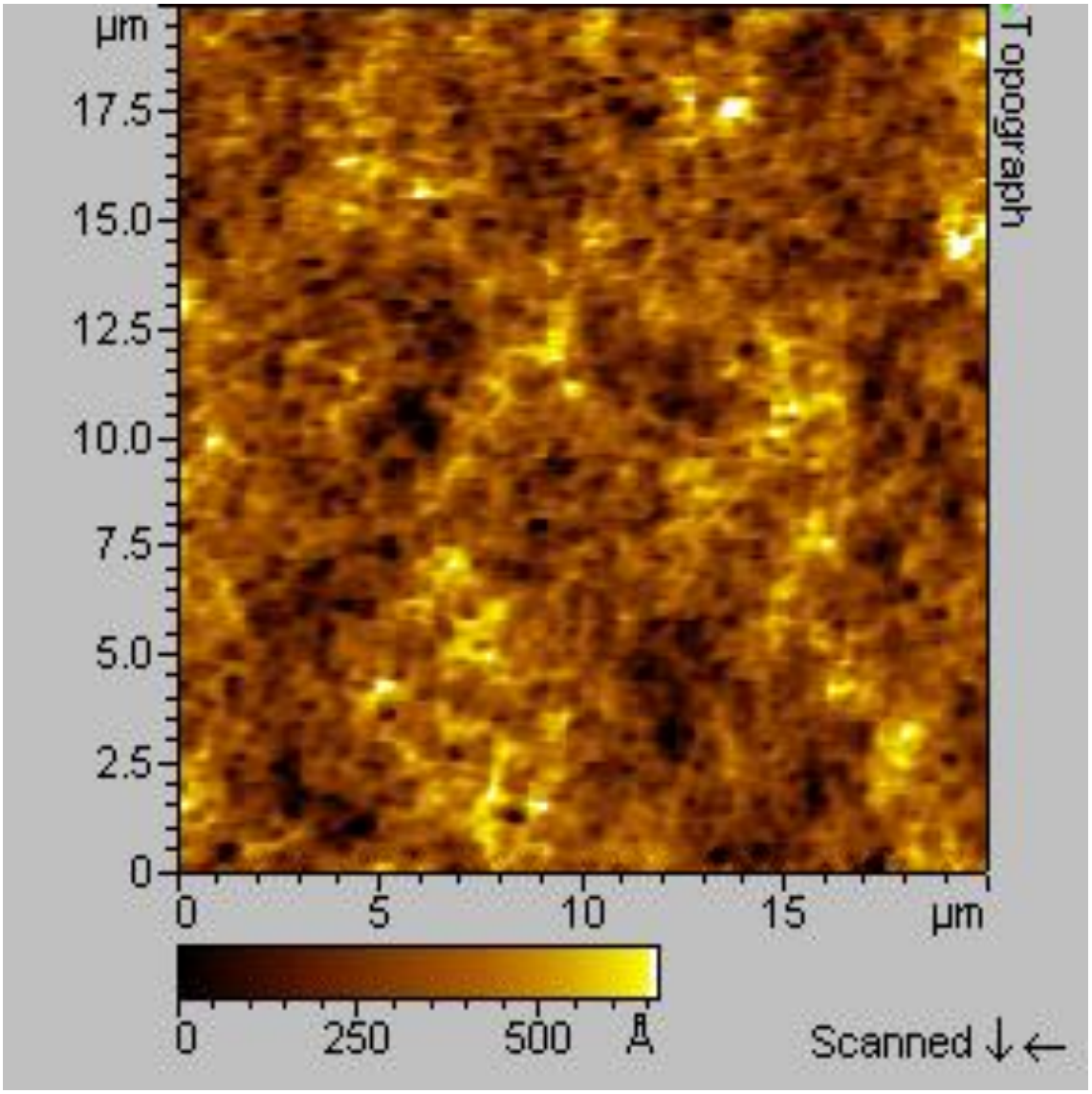
µm
17.5
15.0
12.5
10.0
7.5
5.0
2.5
0
0
5
10
15
µm
0
250
500
Å
Topograph
Scanned ↓ ←

(d)

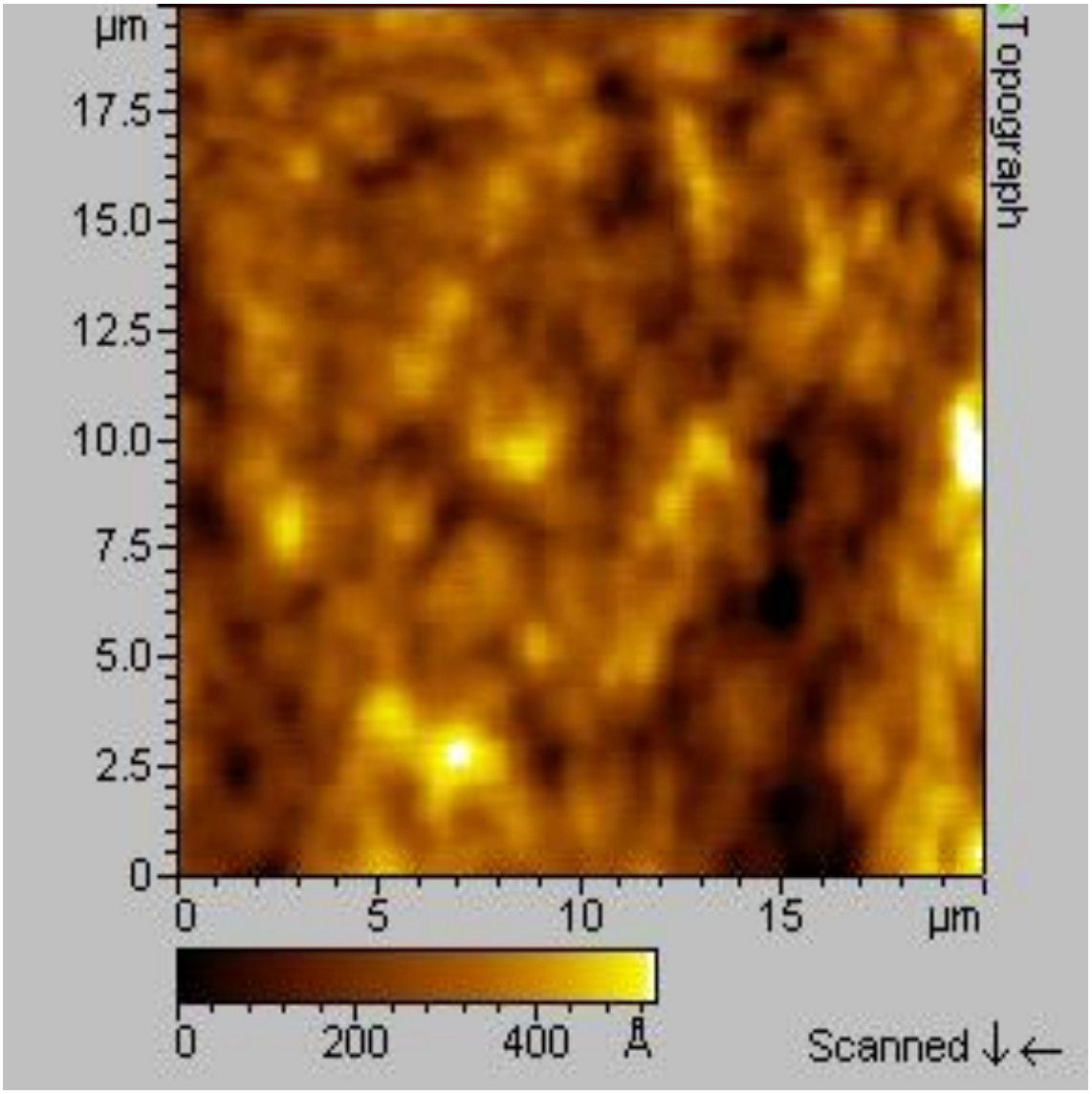

(e)

Figure 4.1. AFM images with scan size of 20 µm x 20 µm: (a) uncoated PSF; (b) $[PDAC/PVS]_{60}$; (c) $[PAH/PVS]_{60}$; (d) $[PEI/PAA]_{60}$; (e) $[PAH/PAA]_{60}$

CA measurements as can be seen in Figure 4.2, indicate that the layer by layer coated membranes are more hydrophilic than that of bare PSF substrate. $[PDAC/PVS]_{60}$, $[PAH/PVS]_{60}$, $[PEI/PAA]_{60}$, and $[PAH/PAA]_{60}$ membrane showed CA of 57.8^{o}, 57.9^{o}, 57.1^{O}, and 35.5^{O} respectively. In comparison the CA of bare PSF is reported to be 80.5^{o}. The change of hydrophilicity is a strong indication of the presence of the film on PSF substrate.

4.1.2. FUNCTIONAL GROUP (FTIR)

The FTIR technique is widely used to study some changes that take place on the polymer surface during a modification process. Unfortunately, this method is too insensitive in many cases because of the large sampling depth of the ATR-FTIR spectroscopy. This sampling depth is usually much greater than the thickness of the modified layer and the absorption bands of introduced functionalities might show very low intensity.Figure 4.3 and Figure 4.4 provide the ATR-FTIR results from the finger print regions of the PEM membrane systems.

As can be seen, the characteristic peak of PSF appears at wavelength of 1151 cm^{-1} and 1323 cm^{-1}. Due to large sampling depth, both PSF characteristic peaks also appear in coated sample but their lower intensity provides evidence of the presence of coating or thin deposited layer on PSF substrate. A weak peak appearing at wavelength of 1385 cm^{-1} shows the sulfate functional group for PVS which does not appear in the spectra of bare PSF, This peak thus provide the proof that PVS was successfully deposited on PSF.

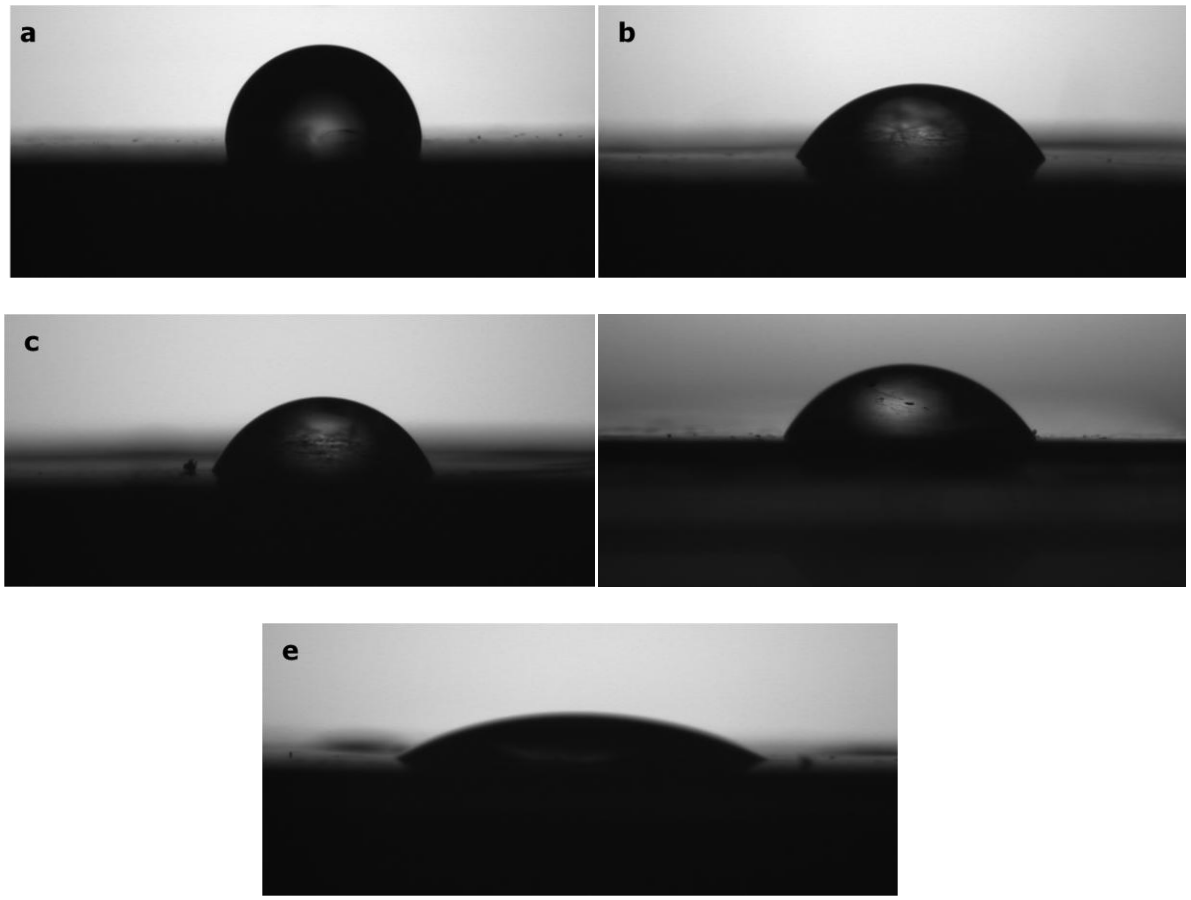

Figure 4.2. Water droplet images for CA measurement of PEM Film on top of PSF Membrane ((a) Bare PSF Substrate; (b) $[PDAC/PVS]_{60}$ membrane; (c) $[PAH/PVS]_{60}$ membrane; (d) $[PEI/PAA]_{60}$ membrane; (e) $[PAH/PAA]_{60}$ membrane)

It can also be seen in Figure 4.3, the characteristic peak initially appear at wavelength of 910 cm^{-1} and 1040 cm^{-1} for PSF spectra diminish and even completely disappear for the other two spectra i.e. PDAC/PVS and PAH PVS. The same case occurs for PEI/PAA and PAH/PAA spectra in Figure 4.4. Those two peaks are assigned for C=C bond and C-O ester respectively. The C=C peak disappears due to chain scission of PSF during UV irradiation [128] whereas C-O ester peak disappear because the IR irradiation can not reach polyester reinforcing web anymore due to the presence of the coating.

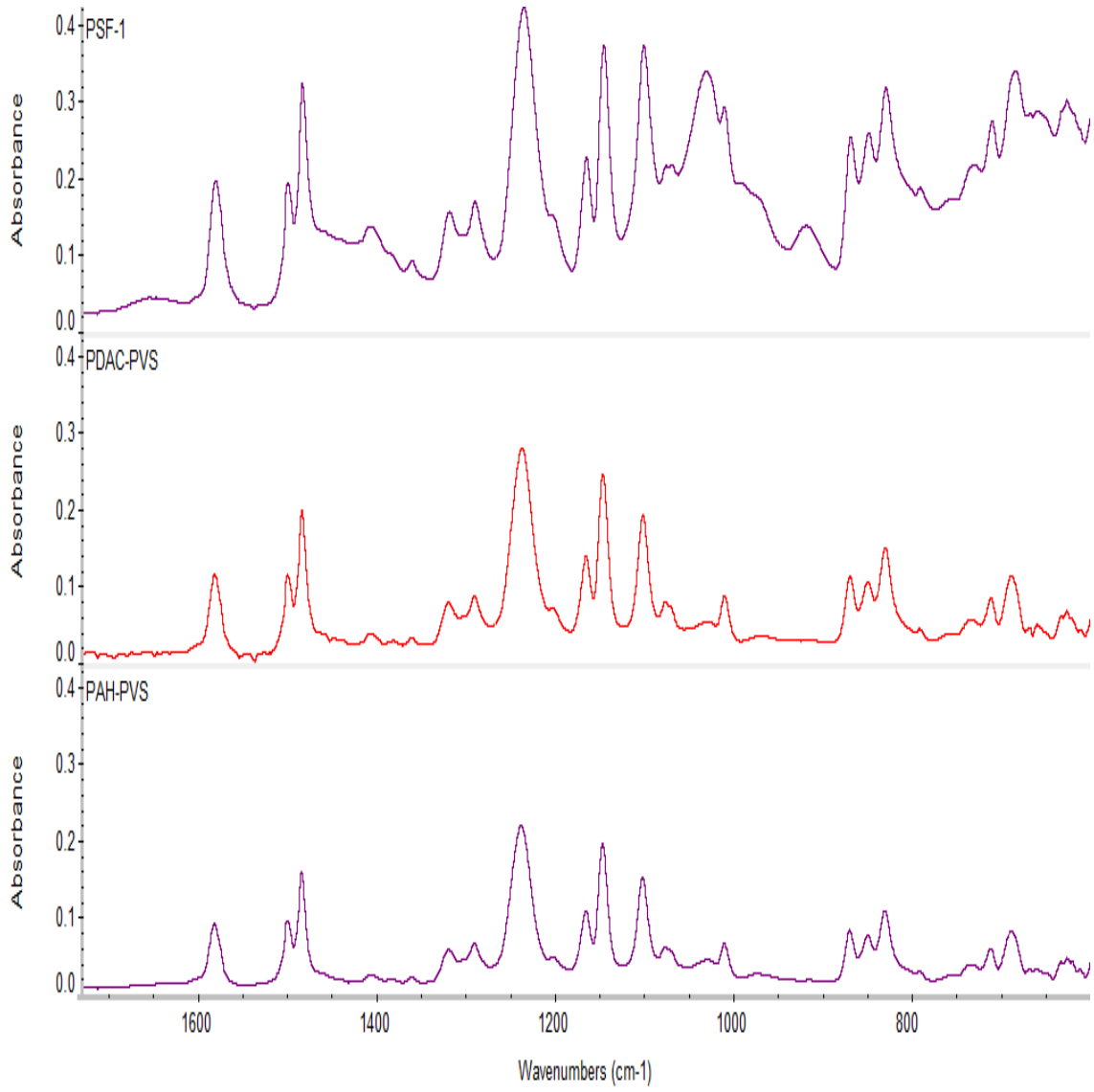

Figure 4.3. FTIR Characteristic peak for bare and coated PSF within finger print region (a. commercial PSF; b. $[PDAC/PVS]_{60}$; c. $[PAH/PVS]_{60}$)

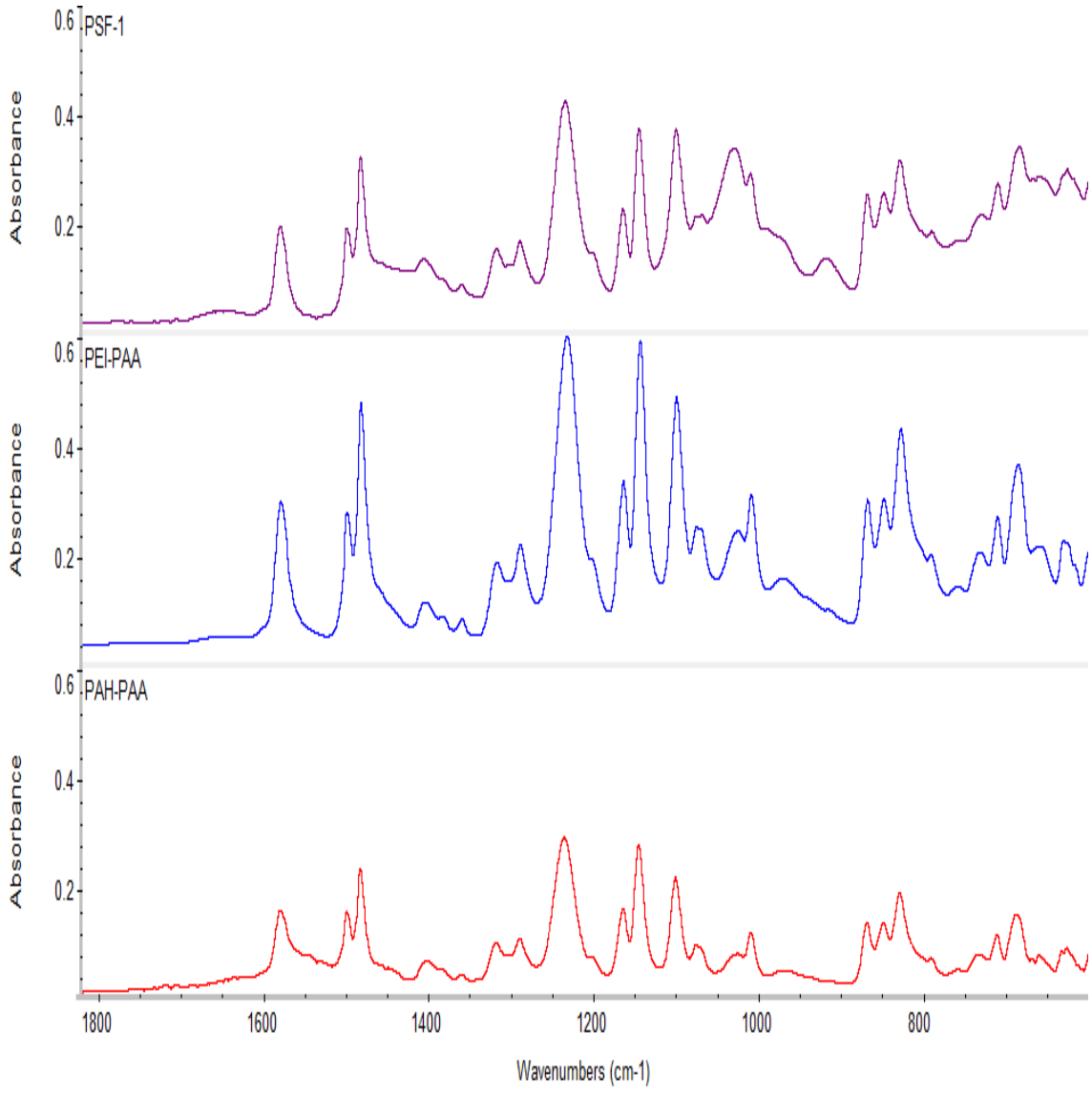

Figure 4.4. FTIR Characteristic peak for bare and coated PSF within finger print region (a. commercial PSF; b. $[PEI/PAA]_{60}$; c. $[PAH/PAA]_{60}$)

4.1.3. PERMEATION TEST

Figure 4.5 provides the results of the permeation test for the [PDAC/PVS], [PAH/PVS], [PEI/PAA], and [PAH/PAA] membranes containing various numbers of bi-layers. As can be seen Figure 4.5, the flux decreases as the number of bi-layers are increased. This is expected because water flux is inversely proportional to the film thickness and with increase in the number of bi-layers the film thickness increases and results in the flux decline. Similarly, as the number of bi-layer increases, the permeability of salt decreases which obviously leads to the decrease of the salt flux. The decrease in salt flux means less amount of salt passes through the membrane and results in higher salt rejection.

Figure 4.5 shows flux order as follow PDAC/PVS >> PAH/PVS > PAH/PAA > PEI/PAA while salt rejection order as follow PDAC/PVS < PEI/PAA < PAH/PVS < PAH/PAA. The trends are the same for both 60 and 120 bilayers. In typical glassy polymeric membrane this phenomenon can be explained based on a concept of structure property relationship. This concept suggests several segments of the polymer chain are also involved in each movement of the diffusing species. Though polyelectrolytes have charged species along their backbone, thermo-chemical properties of polyelectrolytes do not show that they behave differently from glassy polymers [146]. Therefore this concept can also be applied to explain the permeability behaviour of solute or solvent through polyelectrolyte film. Many researchers have been using the concept of fractional free volume (FFV) to relate the permeability of specific molecules with the membrane structure. Experimentally, this can be done by using Positron Annihillation Lifetime

Spectroscopy (PALS) [147-149] while theoretically it can be predicted by using group contribution method by Bondi [150] and modified group contribution by Paul [151].

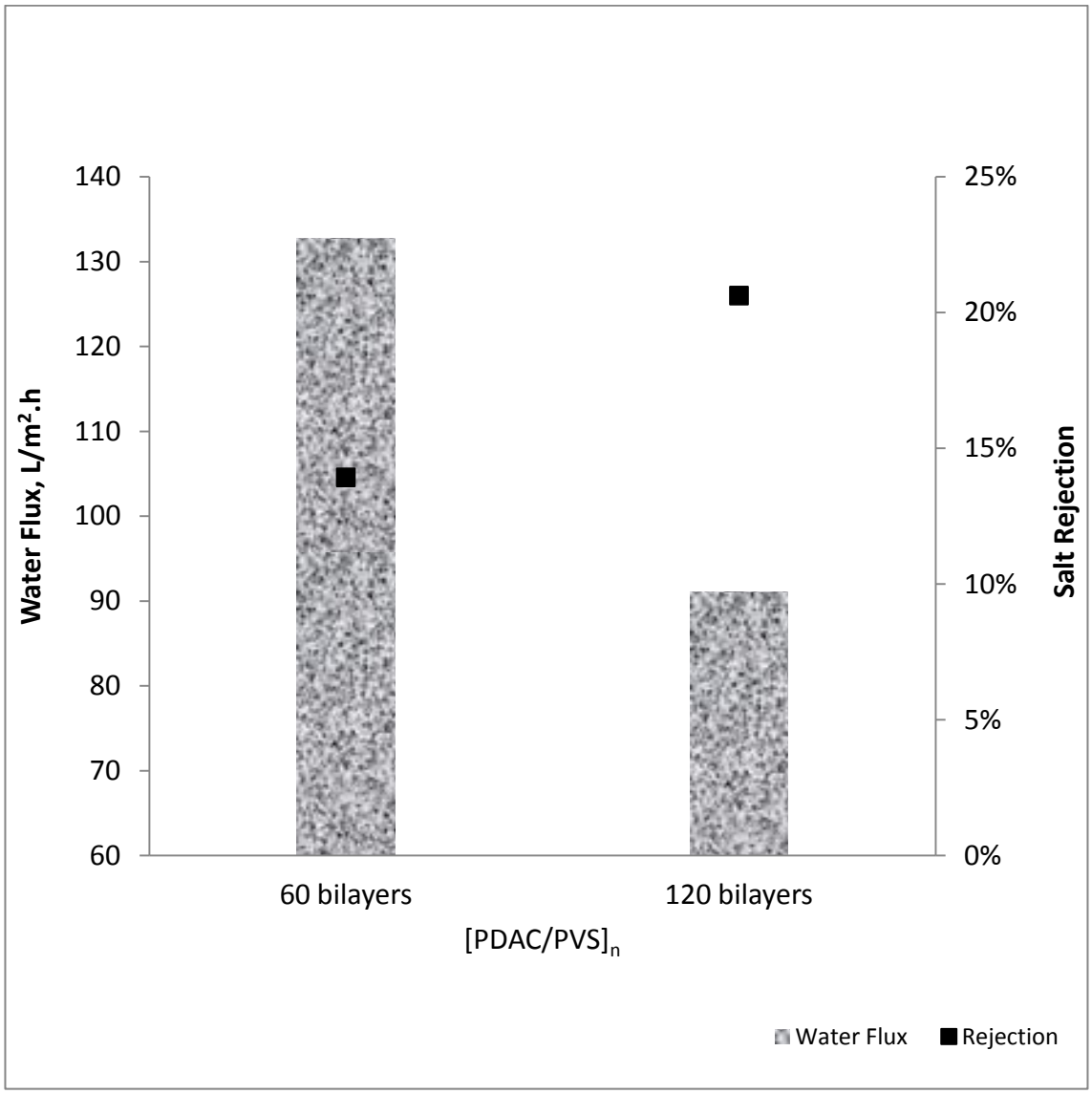

(a)

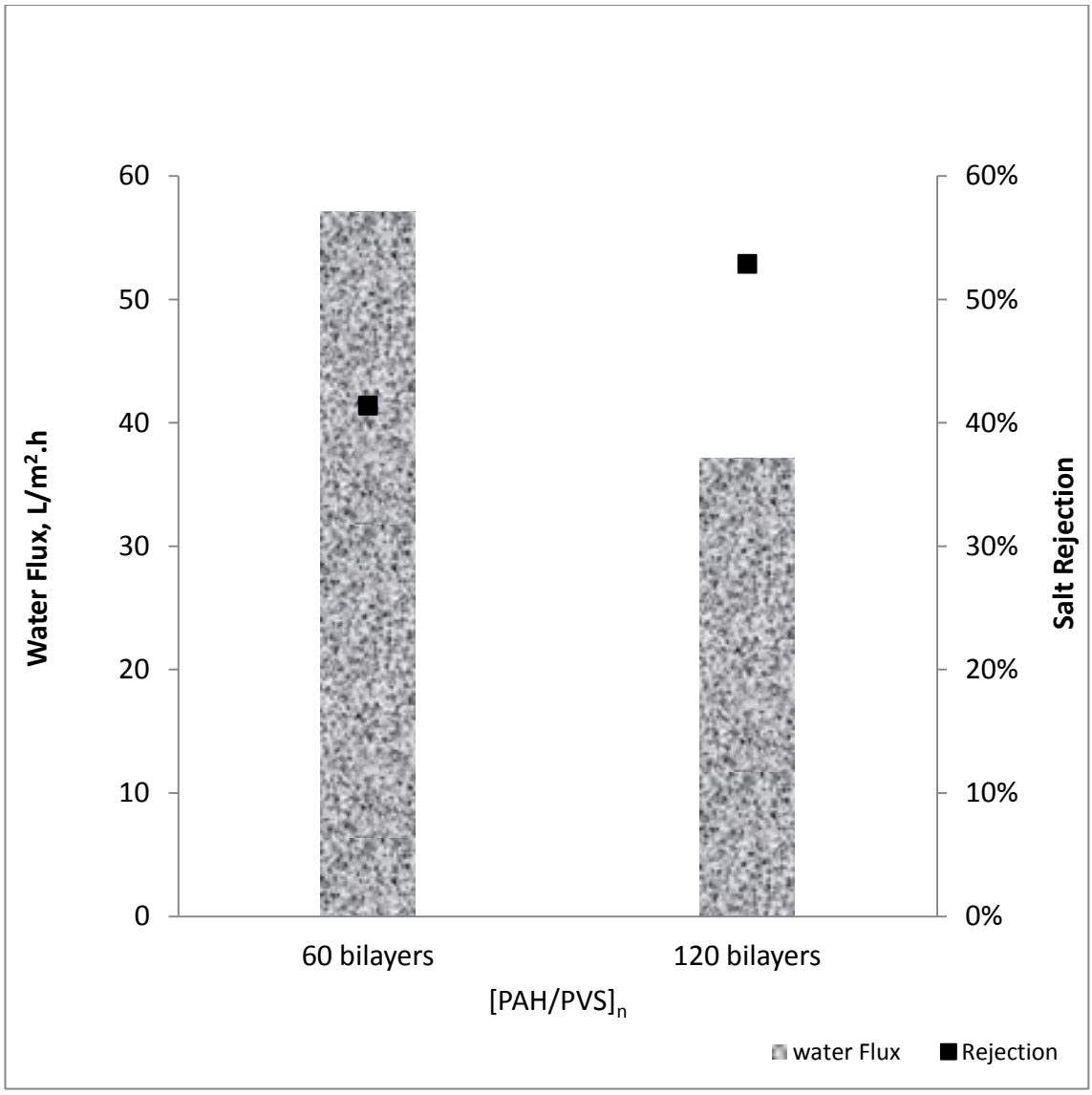
60
50
40
30
20
10
0
60%
50%
40%
30%
20%
10%
0%
Water Flux, L/m².h
Salt Rejection
60 bilayers
120 bilayers
[PAH/PVS]n
water Flux
Rejection

(b)

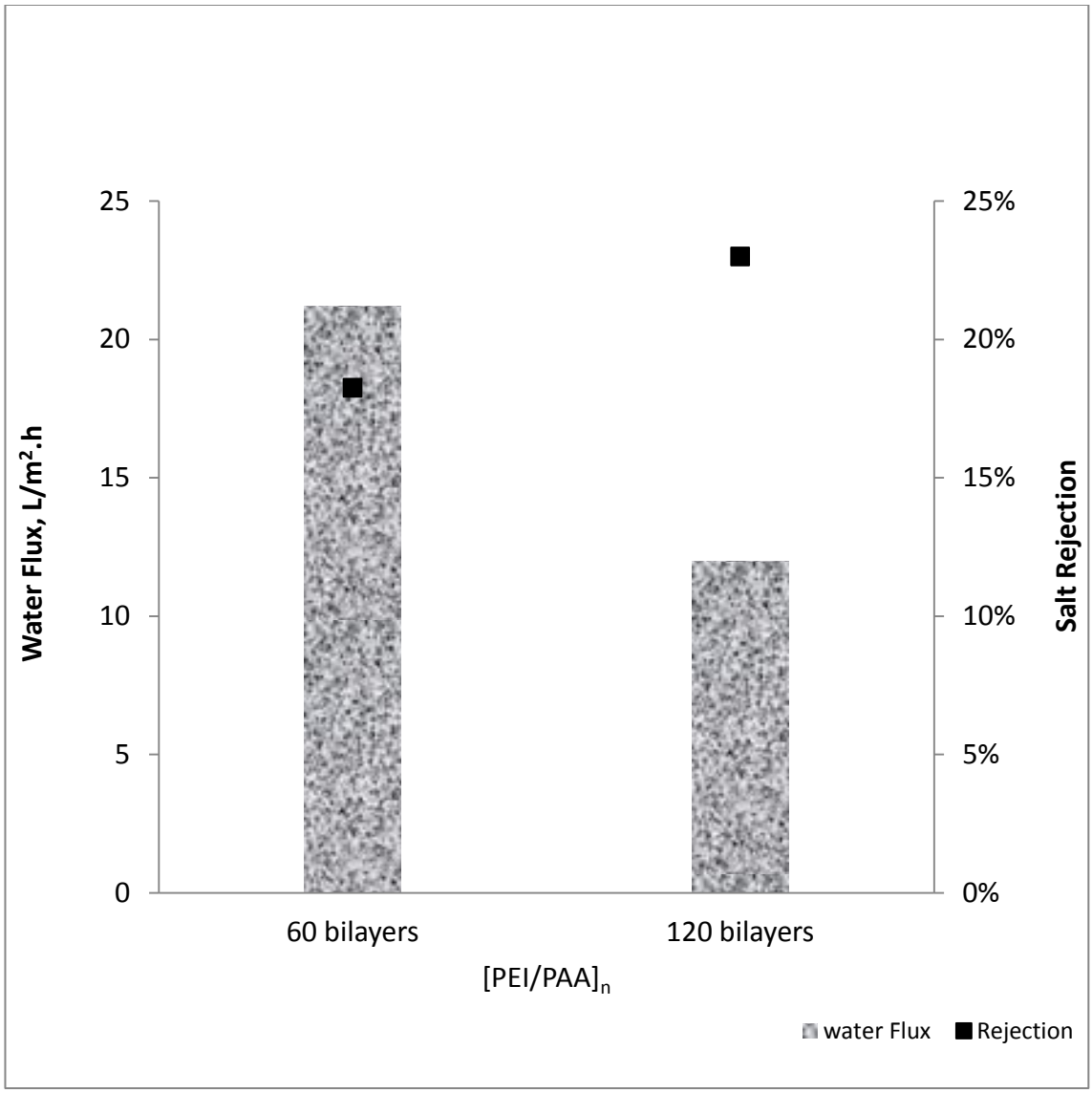
25
20
15
10
5
0
25%
20%
15%
10%
5%
0%
Water Flux, L/m².h
Salt Rejection
60 bilayers
120 bilayers
[PEI/PAA]n
water Flux
Rejection

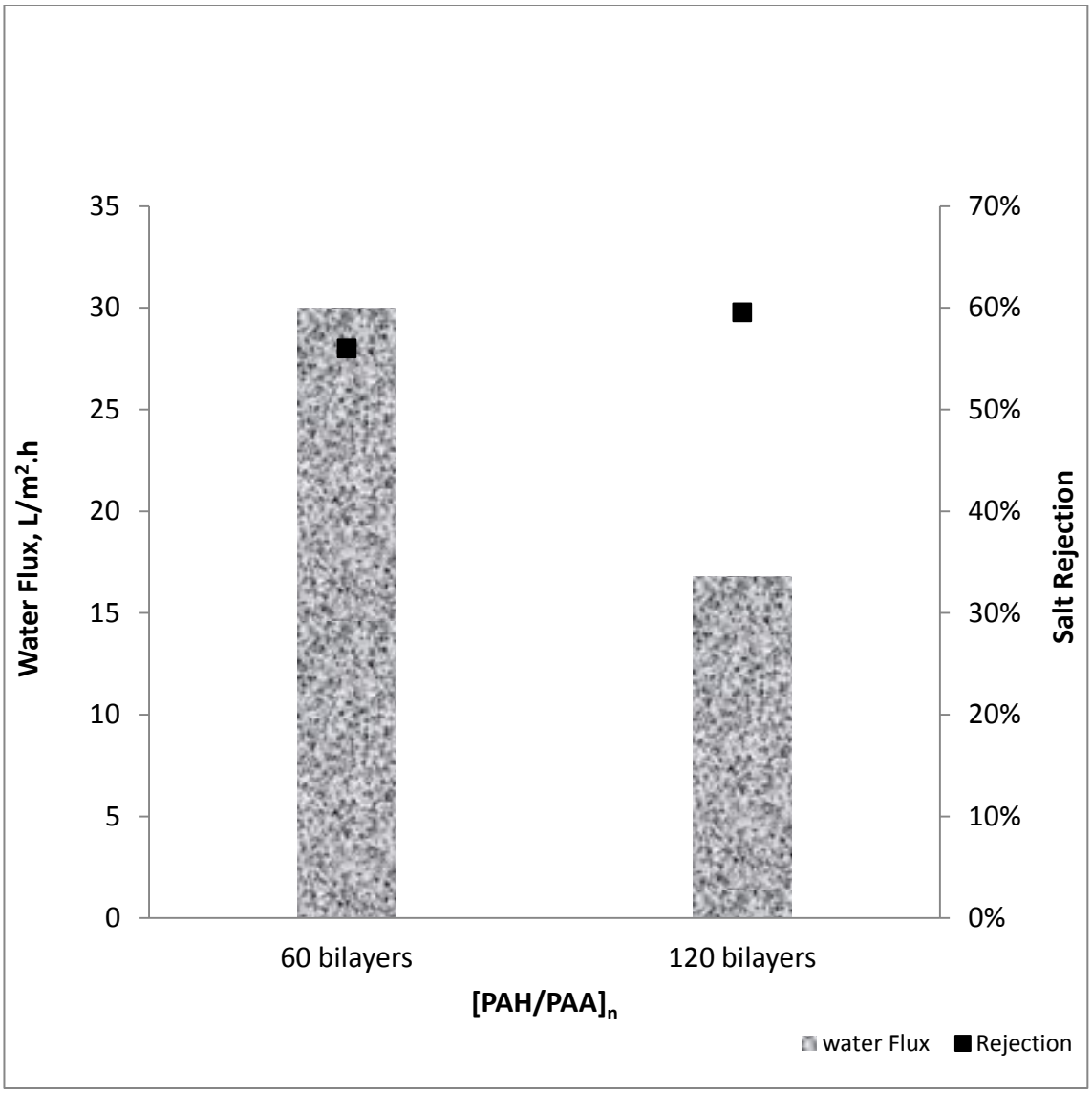

Figure 4.5. Permeation test result for various PEM membrane with different number of bilayer (n = 60 and 120)

The FFV values are typically just few percents of total volume but it is enough to provide space for the polymer chain to rotate. We calculated FFV theoretically for both PAH/PVS and PDAC/PVS. It was found that FFV of PDAC/PVS, PAH/PVS, and PAH/PAA are 0.261, 0.246 and 0.171, respectively. This means the polymer chain of PDAC/PVS can rotate more freely compared to the others hence the permeating molecules i.e. water and salt (NaCl) can move more easily in PDAC/PVS membrane. PEI/PAA has the same functional group as PAH/PAA thus suggests the flux of the two should not much different. This is clearly reflected in the results where PEI/PAA film shows slightly lower flux compared to that of PAH/PAA. This is most likely due to PEI has many branches that may hamper the molecular motion of polyelectrolyte chain. In general, the membrane that shows high flux will result in low salt rejection. This is reflected in the above results except for PEI/PAA. This is because PEI has much more active sites suggested from molecular structure (see chapter two) that actually act as carriers for ion transport across the membrane. This so called facilitated ion transport will be explained in detail in chapter five.

4.2. CONCLUSION

Four polyelectrolyte multilayer systems i.e. PDAC/PVS, PAH/PVS, PEI/PAA and PAH/PAA were successfully deposited as multi-layer thin films via spin assisted layer by layer assembly to create active layers on top of commercial PSF UF membranes. This work establishes that spin assisted layer by layer processing can be successfully used to fabricate thin film composite membranes via the process of depositing alternate nano thin layers on a given support scaffold. The [PDAC/PVS] and [PAH/PVS] thin film membranes fabricated by SA-LbL provide high flux and moderate salt rejection. For

example, [PDAC/PVS]120 membrane showed water flux of about 90 L/m2.h and salt rejection of 21% while [PAH/PVS]120 membrane showed water flux of 37 L/m2.h and salt rejection of 53%. [PAH/PVS] membrane thus performs better than PDAC/PVS membrane in salt rejection of almost two times higher and a reasonable water flux.

CHAPTER FIVE

POLYELECTROLYTE MULTILAYER MEMBRANE STABILITY AND PERMEATION CHARACTERISTICS

5.1. RESULT AND DISCUSSION

Polyelectrolyte multilayer membrane (PEM) consisting of PAH/PAA was prepared via SA-LbL assembly on PSF ultrafiltration membrane as the support. In general, the PAH/PAA membrane is similar to thin film composite membranes in which PAH/PAA acts as the active layer while PSF provides the required mechanical robustness to the composite membrane. Both PAA and PAH are well studied polyelectrolytes and hence their chemical, mechanical, and thermal properties are well documented [42, 112, 113]. PAA and PAH with pKa of 6.5 and 8.5, respectively, are weak polyelectrolytes and thus their ionization degree is strong function of pH. PAA is fully ionized at pH above 6.5 while PAH starts losing its protons if the pH is above 7 [42, 98, 112].

We deposited 60 and 120 bilayers of PAH/PAA on the PSF UF membrane as support layer. Figure 5.1 provide AFM images of the bare and coated membranes. As can be seen from Figure 5.1, the surface morphology of the bare PSF membrane changes significantly from porous and rough surface to rather non porous and much smoother after deposition of PAH/PAA thin films.

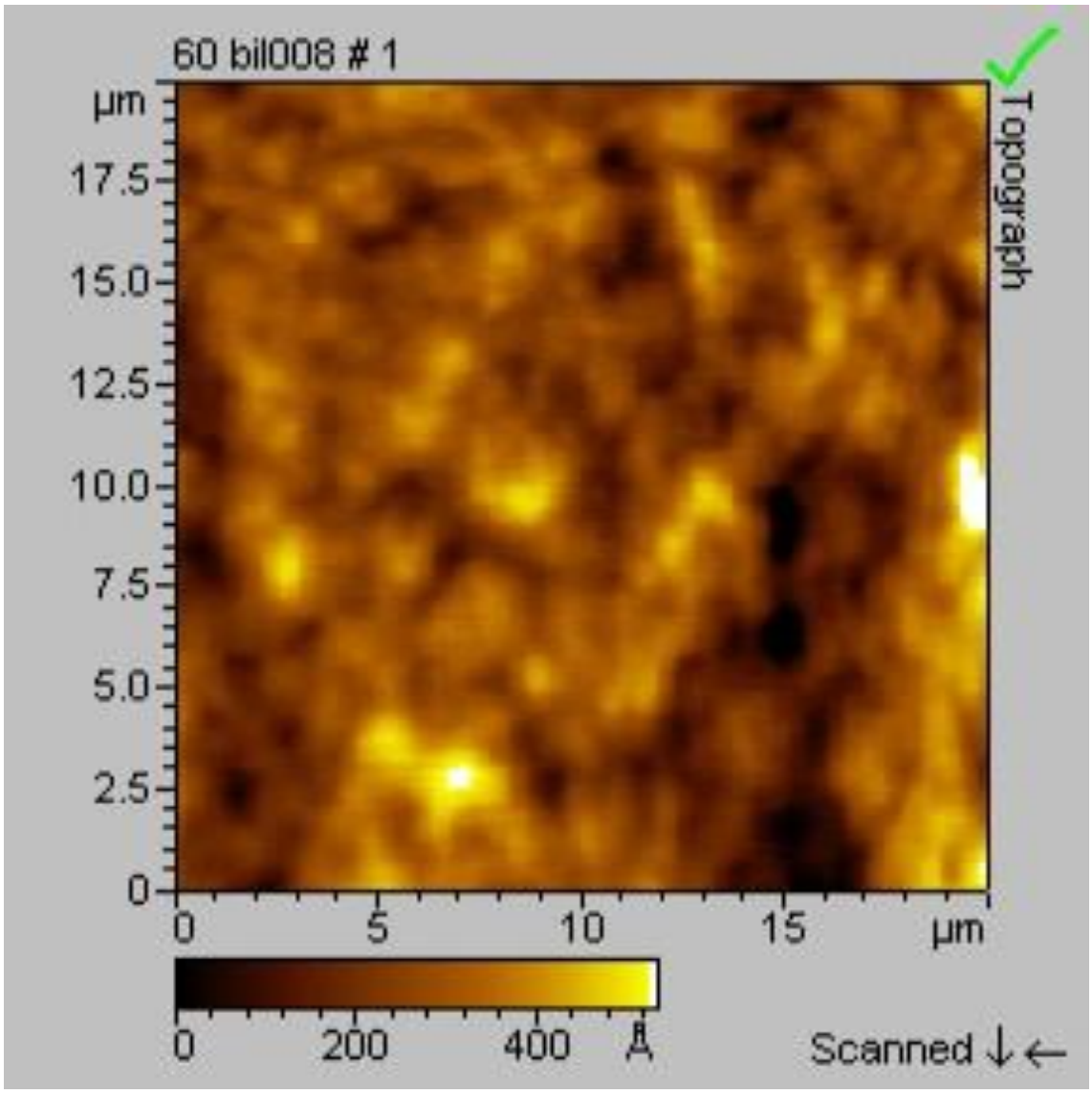
60 bil008 # 1
µm
17.5
15.0
12.5
10.0
7.5
5.0
2.5
0
0
5
10
15
µm
0
200
400
Å
Topograph
Scanned ↓ ←

(a)

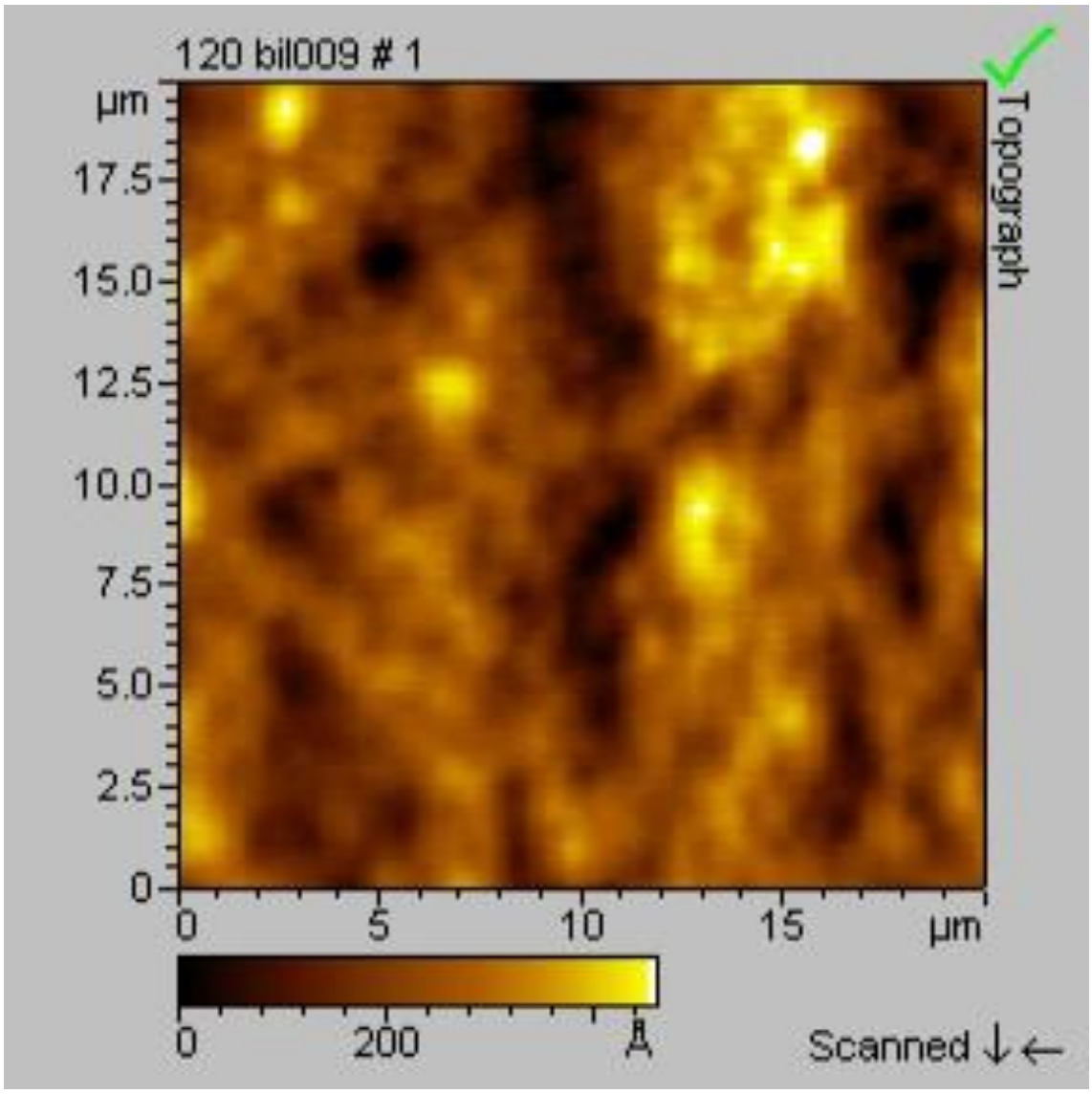
120 bil009 # 1
µm
17.5
15.0
12.5
10.0
7.5
5.0
2.5
0
0
5
10
15
µm
0
200
Å
Topograph
Scanned ↓ ←

(b)

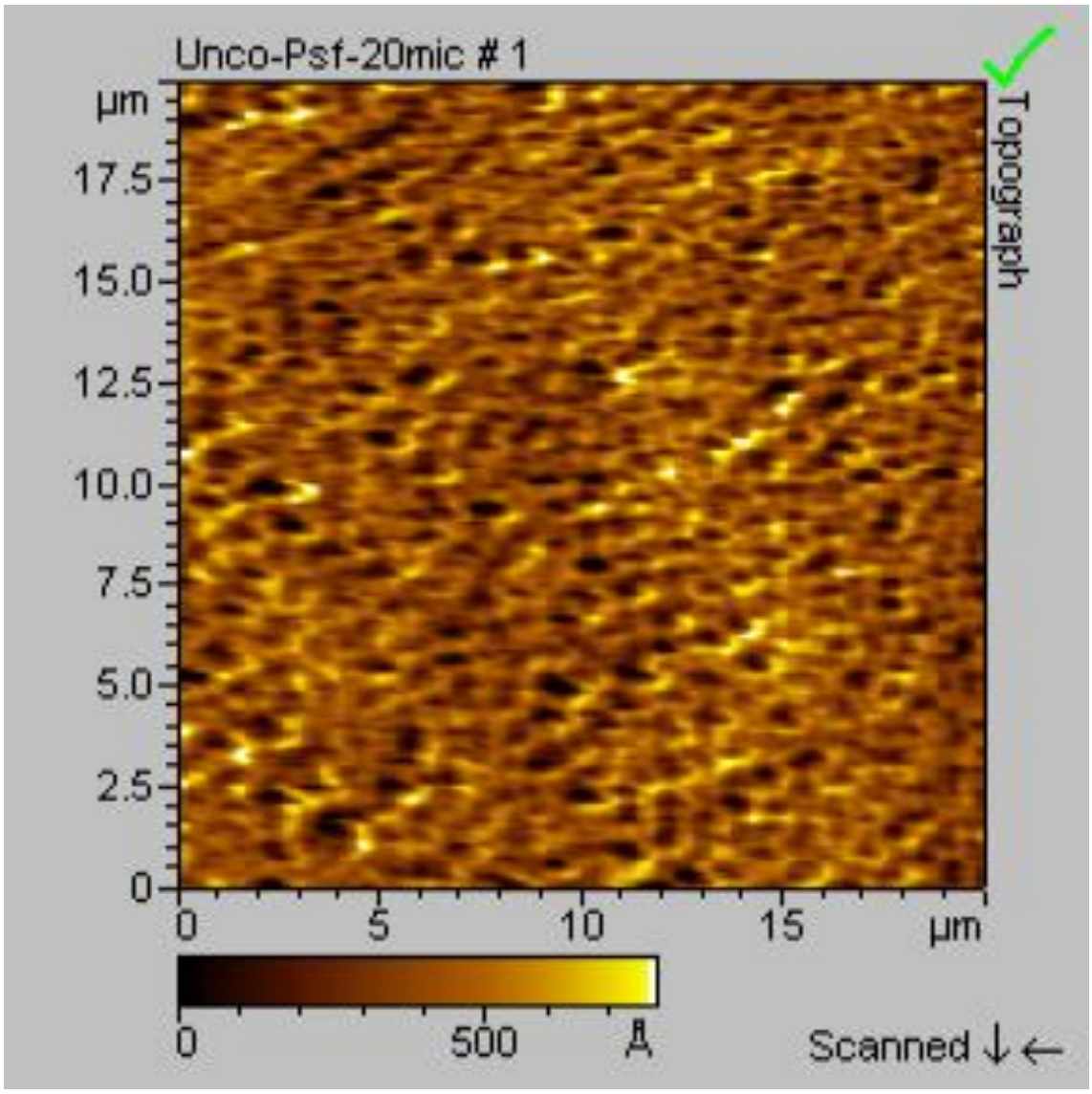

(c)

Figure 5.1. AFM Images of PAH/PAA and bare PSF Membrane (((a) $[PAH/PAA]_{60}$; (b) $[PAH/PAA]_{120}$; (c) Bare PSF)

The effect of coating by SA-LbL assembly is quite similar to other LbL assemblies that generates relatively smooth surface. The surface roughness measurements provided by the AFM indicate that $[PAH/PAA]_{60}$, has an average RMS roughness of 10.7 nm while for $[PAH/PAA]_{120}$, the average RMS roughness was 9.88 nm. These surface roughness values when compared with the surface roughness of 28.18 nm of the bare uncoated PSF-UF support demonstrate that SA-LbL assembly can be used to deposit very smooth and conformal thin films on a given substrate. The low surface roughness of the polyelectrolyte membrane fabricated via SA-LbL has a big advantage over many commercial RO/NF membranes which normally have much rougher surface which makes these membranes susceptible to fouling. For instance, our measurement of surface roughness of two commercial RO membranes i.e. Hydronautics SWC and ESPA provide the values of 133.9 nm and 112.4 nm, respectively, which are significantly rougher than our PAH/PAA membranes.

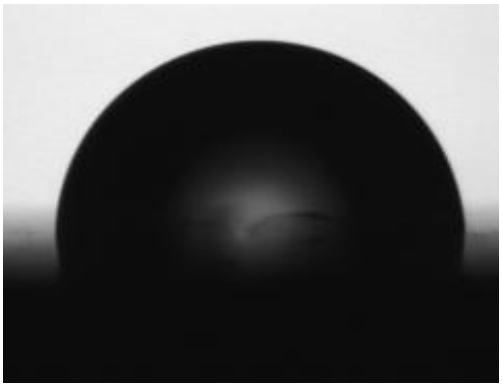

(a)

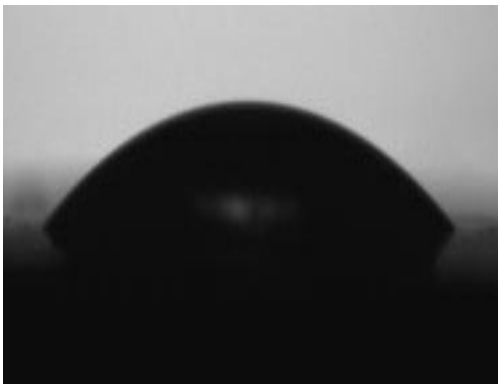

(b)

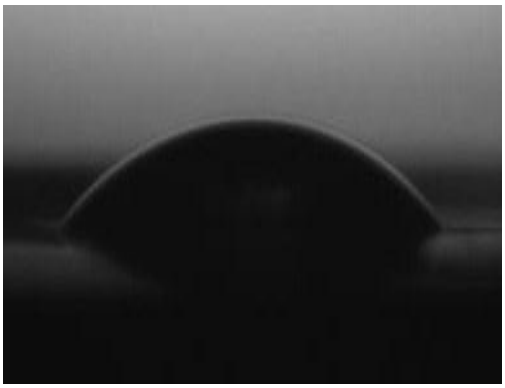

(c)

Figure 5.2. Contact Angle Image of PAH/PAA Multilayer Membrane on PSF Support ((a) Bare PSF substrate; (b) $[PAH/PAA]_{60}$; (c) $[PAH/PAA]_{120}$)

In addition, PAH/PAA membrane also show high hydrophilicity, which once again makes the membrane less susceptible to fouling. The hydrophilicity of the PAH/PAA film as indicated by contact angle measurements (see Figure 5.2) provide values of 35.5^{o} and 33.2^{o} for 60 bilayer and 120 bilayer films, respectively. In comparison the bare PSF-UF substrate is much more hydrophobic with contact angle of 80.5^{o}. The reported contact angle values of pure PAA is 5^{o} while pure PAH has the CA of 55^{o} [42, 113]. The contact angle measurements of around 34^{o} for our PAH/PAA suggest that the deposited thin film architecture may not be one of the collection of distinct bi-layers of PAH and PAA mono layers but there could rather be some degree of inter mixing of molecular chains between PAA and PAH.polyelectrolyte. Thus it is perhaps reasonable to assume that the polyelectrolyte layer by layer membranes are not truly "bi-polar" and some degree of charge mixing is to be expected between the two polyelectrolyte mono-layers.

The stability of PEM membrane has been a critical question particularly when such a membrane is exposed to high salinity or high ionic strength solutions. As shown in Figure 5.3, our investigation reveals that the deposited PAH/PAA film remains quite stable after 40 hours of testing under cross flow conditions. As can be seen from Figure 5.3, both the water flux and salt rejection remains almost constant through out the 40 hour test, which indicates that the PAH/PAA film remains intact and stable and functions smoothly under high pressure. Both 60 and 120 bi-layer PAH/PAA membranes showed similar trend of slight decrease in water flux and a slight increase in salt rejection in the first 15 to 20 hours and then remained constant. This slight change in membrane performance during

the first 15 to 20 hours most likely occurs due to polyelectrolyte chain rearrangement coupled with film compaction under relatively high feed pressure of 40 bar.

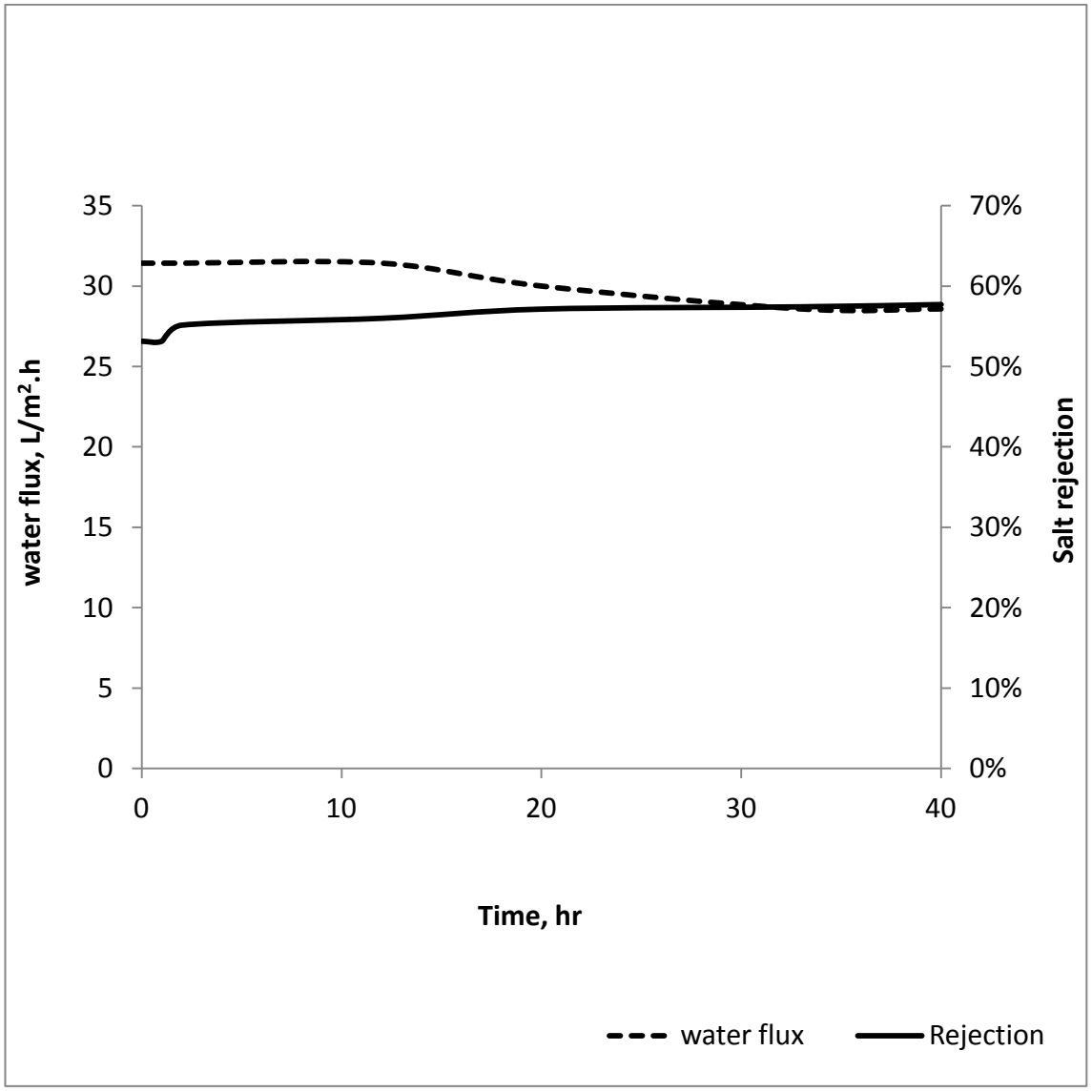

(a)

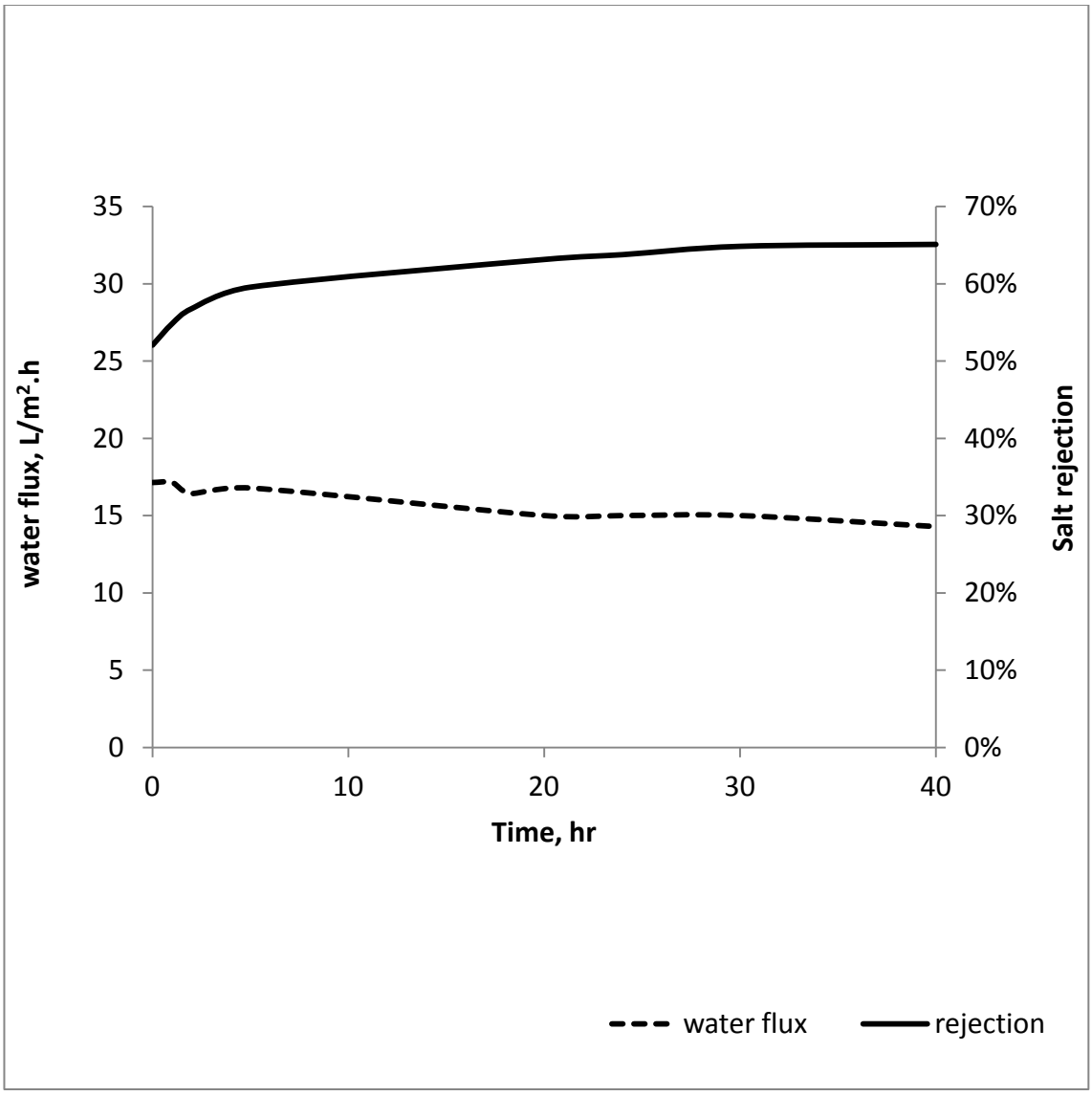

(b)

Figure 5.3. Long Term Permeation Test of PAH/PAA Multilayer Membrane. Feed solution consists of 2000 ppm NaCl, Pressure of 40 bar, Temperature of 25^{o}C, and pH of 6. ((a) $[PAH/PAA]_{60}$; (b) $[PAH/PAA]_{120}$)

Figure 5.3 also demonstrates that as the number of bilayers increase the rejection increases and the water flux decreases. This is to be expected because both permeation and rejection are, respectively, inverse and direct functions of membrane thickness. Thus any increase in the thickness of the active layer will result in a decrease in the permeate flux and increase in the salt rejection. The TEM images shown in Figure 5.4 are used for the thickness measurements and as can be seen the thickness of $[PAH/PAA]_{60}$ is about 40 nm and obviously thickness of $[PAH/PAA]_{120}$ is around 80 nm.

Another important finding of increasing the thickness of the membrane by increasing the number of bi-layers indicates that increasing the thickness has a more significant impact on water flux than on salt rejection. For instance, doubling the number of bi-layer resulted in almost 50% decrease in water flux and only about 15% increase in salt rejection. This finding suggests that perhaps salt rejection in the polyelectrolyte membranes may not involve donnan exclusion of each layer as previously believed in bipolar architecture of the film, but rather involve hindered diffusion as typically found in conventional nonporous membranes coupled with donnan exclusion of the outermost layer only. If Donnan exclusion was operative then the salt rejection should be significantly increased by adding number of polar bilayers, which obviously is not the case as indicated by Figure 5.3.

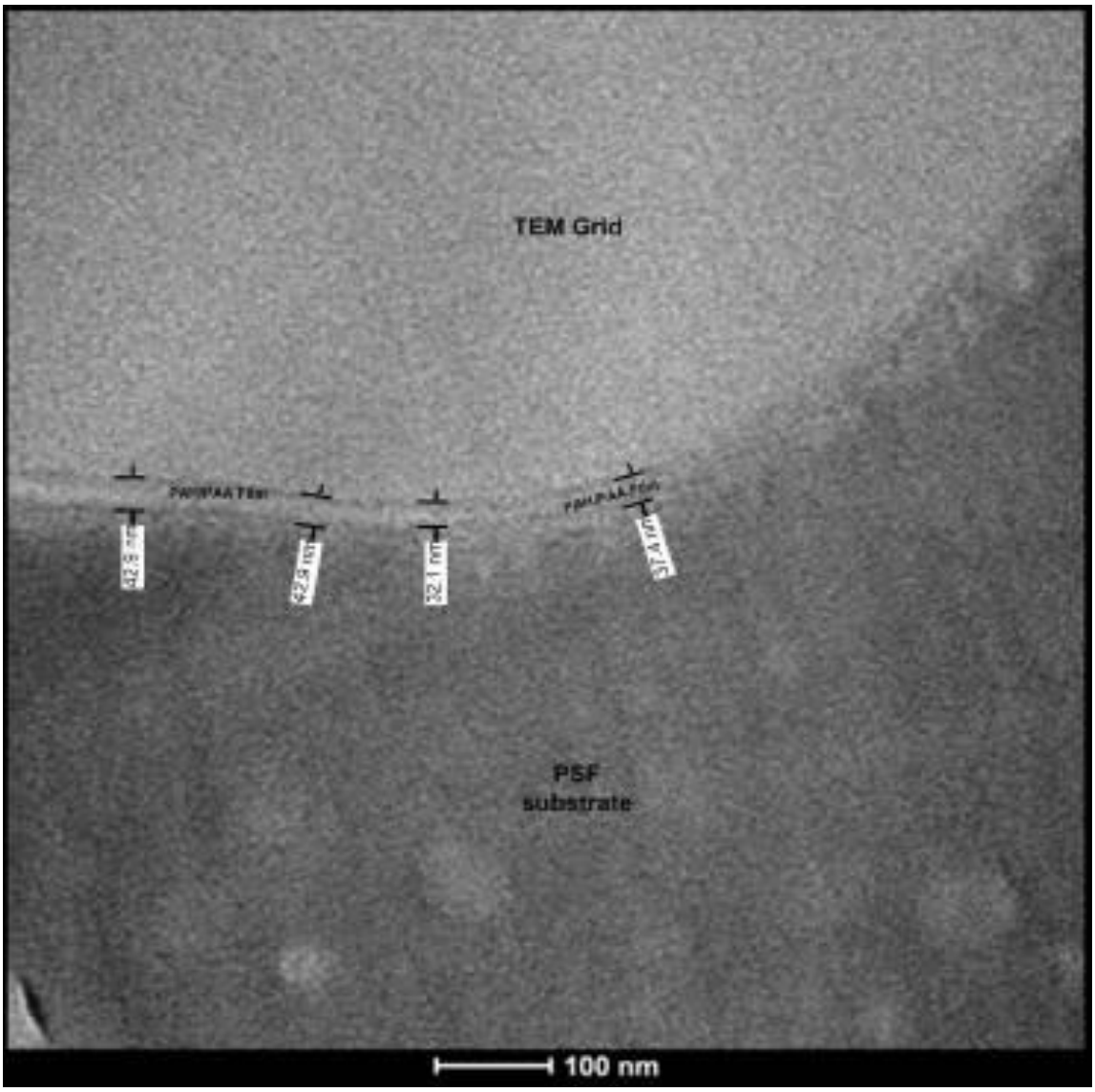

(a)

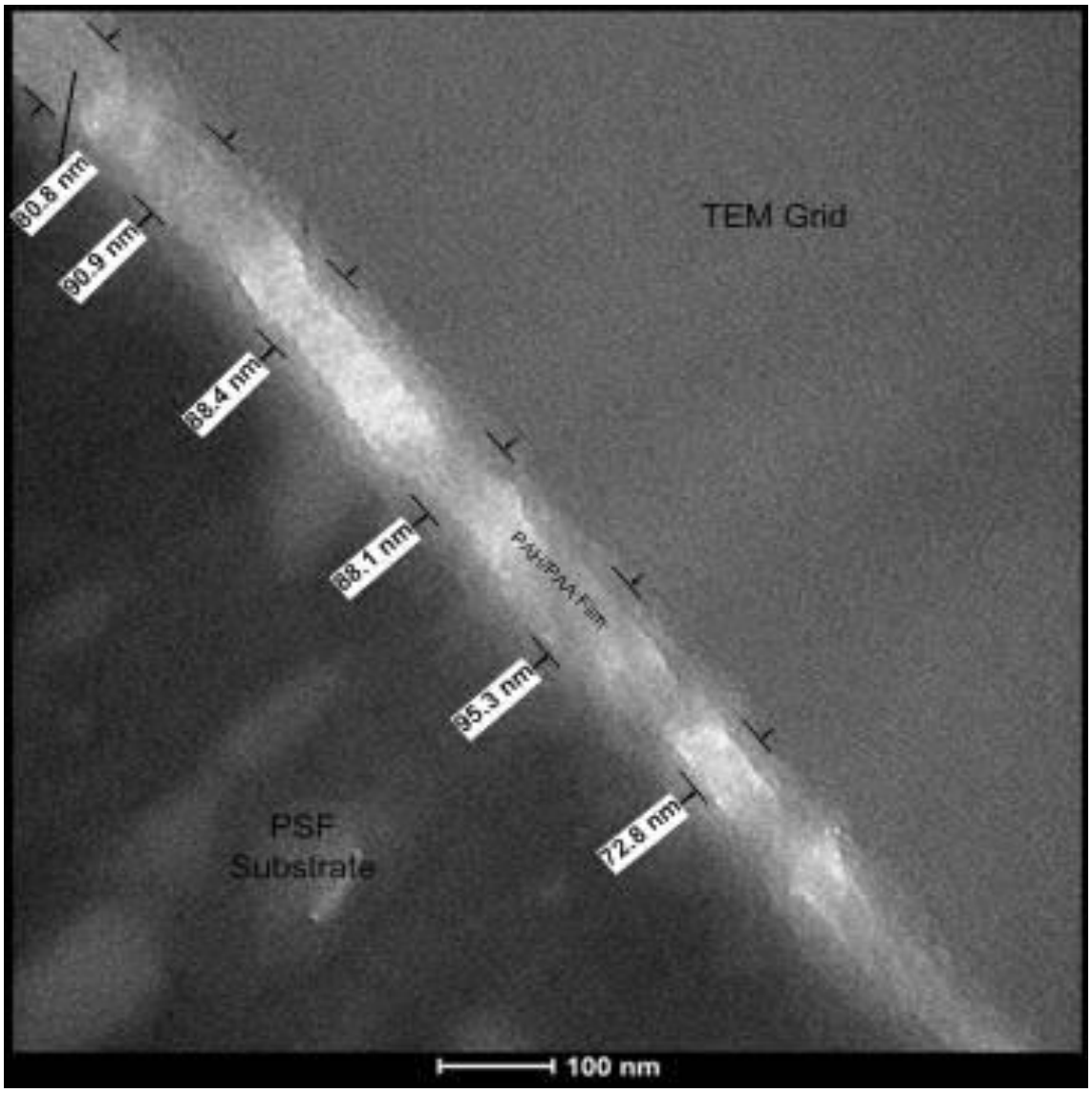

(b)

Figure 5.4. TEM Images of PAH/PAA and bare PSF Membrane (a) $[PAH/PAA]_{60}$; (b) $[PAH/PAA]_{120}$)

Figure 5.5 provides the results on the effect of feed pressure on the water flux and salt rejection for PAH/PAA membrane tested at constant feed concentration, feed temperature and feed pH. As can be seen from this figure water flux increases linearly as the pressure increases. It is known that water can pass through the membrane because of the pressure applied on the feed side. In addition, this pressure is also required to overcome the osmotic pressure thus if we extrapolate water flux plot, the line will eventually intersect X-axsis at pressure equal to osmotic pressure which is about 267 psi in our case for 2000 ppm NaCl. The effect of pressure on salt rejection is more complex and indirect. There are always channels available for salt ions to pass through the membrane. But as the pressure increases, these channels are more occupied by the water molecules than salt molecules because water molecules diffuse at a much faster rate than salt molecules. This then results in decrease in salt passage or in other word, increase in salt rejection with increase in pressure.

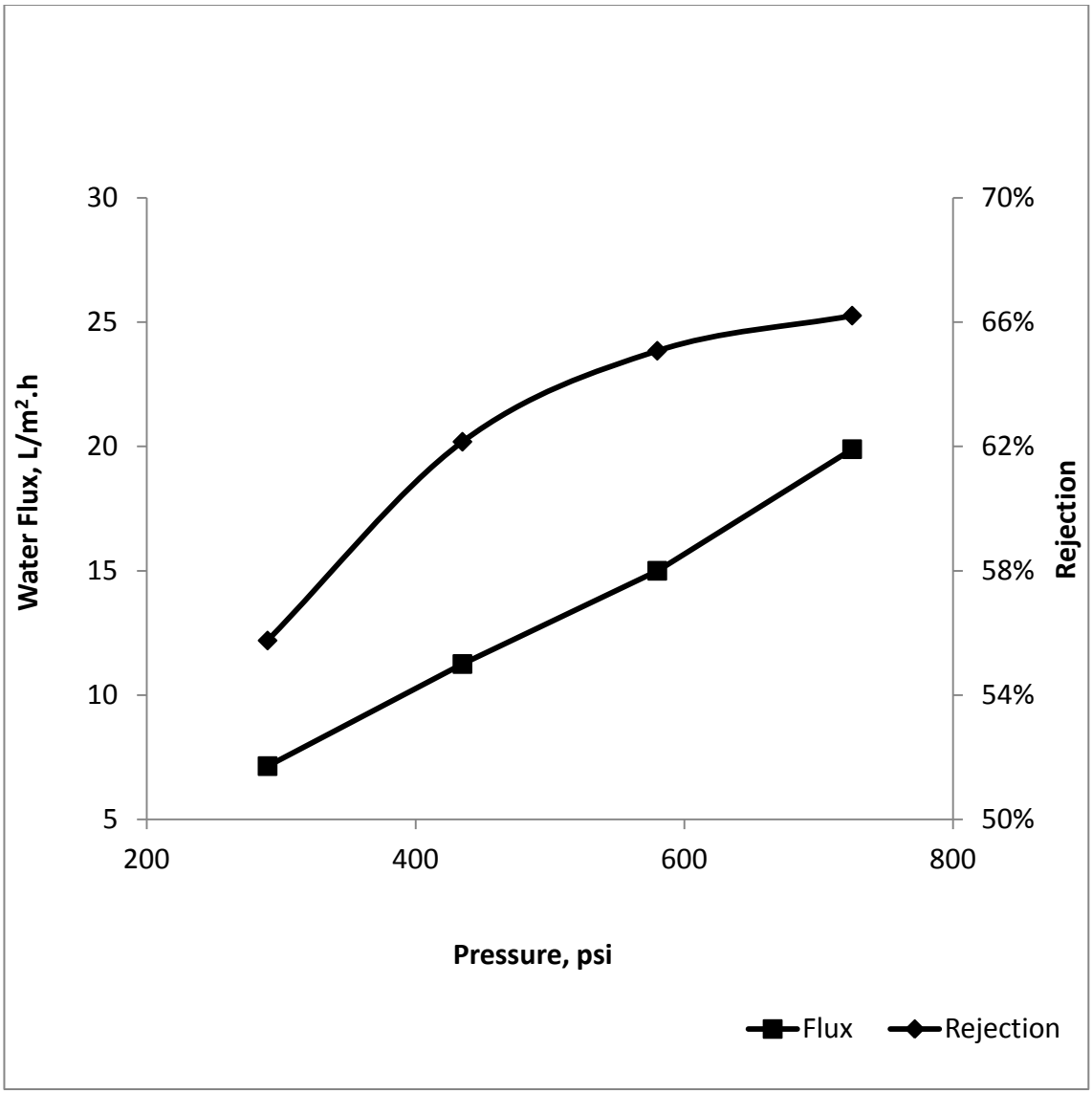
30
25
20
15
10
5
70%
66%
62%
58%
54%
50%
200
400
600
800
Water Flux, L/m².h
Rejection
Pressure, psi
Flux
Rejection

(a)

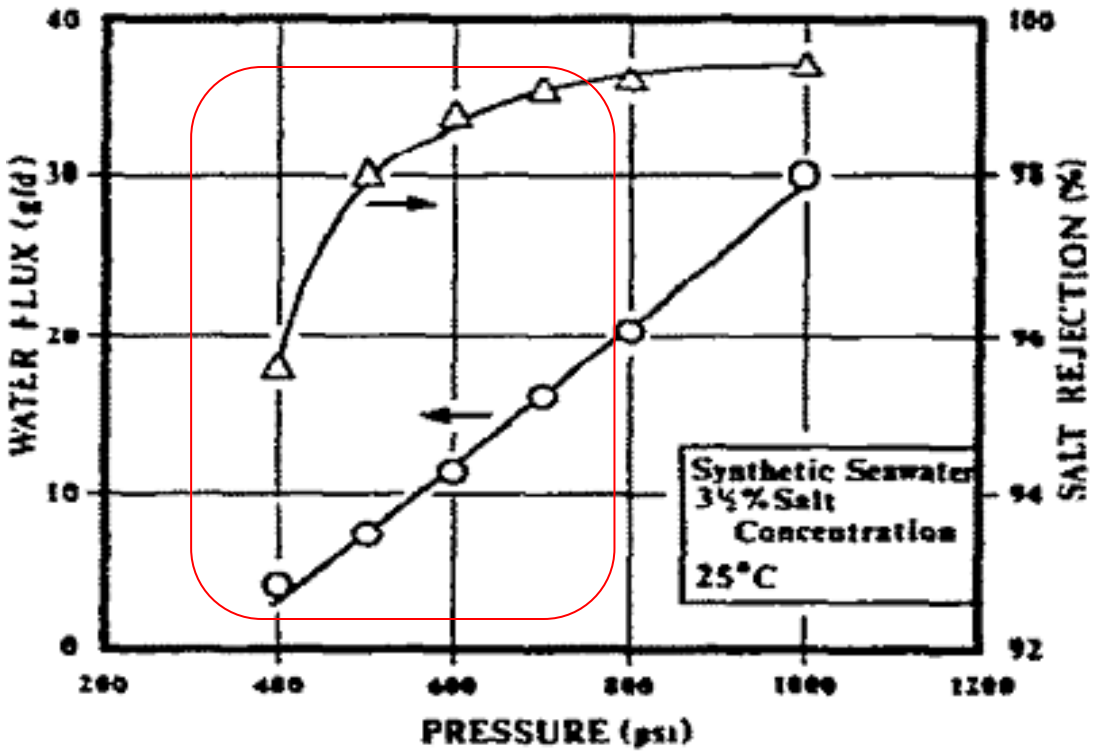

(b)

Figure 5.5. Water flux and salt rejection of (a) $[PAH/PAA]_{120}$ membrane as a function of pressure. Feed solution consists of 2000 ppm NaCl, Temperature of 25^{o}C, and pH of 6. (b) test result for FT-30 RO membrane tested at 35000 ppm NaCl and temperature of 25^{o}C [adapted from [152]]

Figure 5.5 also displays the effect of pressure on salt rejection and water flux for a commercial reverse osmosis membrane FT-30 from Film Tech. A comparison of both figures illustrates an interesting point. Focusing on the same pressure range in both figures it can be seen that the effect of pressure for our PAH/PAA membrane and commercial RO membrane FT-30 membranes show exactly the same trend for both water flux and salt rejection. It is to be noted that FT-30 which is a non-porous solution-diffusion membrane (SDM) behaves very similar to our PAH/PAA membrane, which is thus far believed to be strictly a bi-polar membrane. This similarity between the two membrane types coupled with the increase in the salt rejection with increase in the # of bi-layers in PAH/PAA tends to reinforce the argument that perhaps the polyelectrolyte membranes (PEM) behave more like SDM membranes than bi-polar membranes and thus the salt rejection in the PEM may be better characterized in terms of solution diffusion mechanism rather than the Donnan exclusion mechanism.

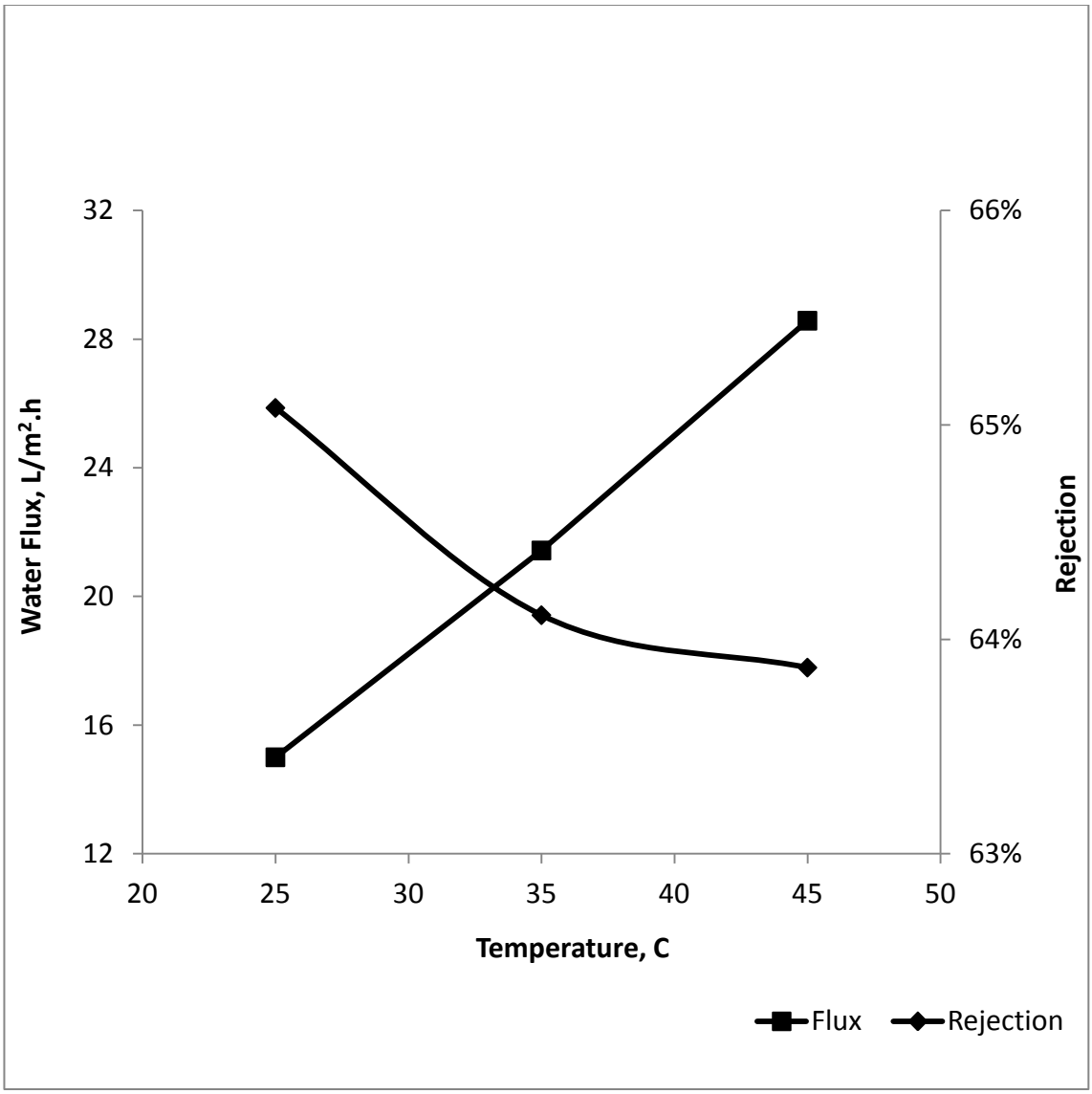
32
28
24
20
16
12
Water Flux, L/m².h
66%
65%
64%
63%
Rejection
20
25
30
35
40
45
50
Temperature, C
Flux
Rejection

(a)

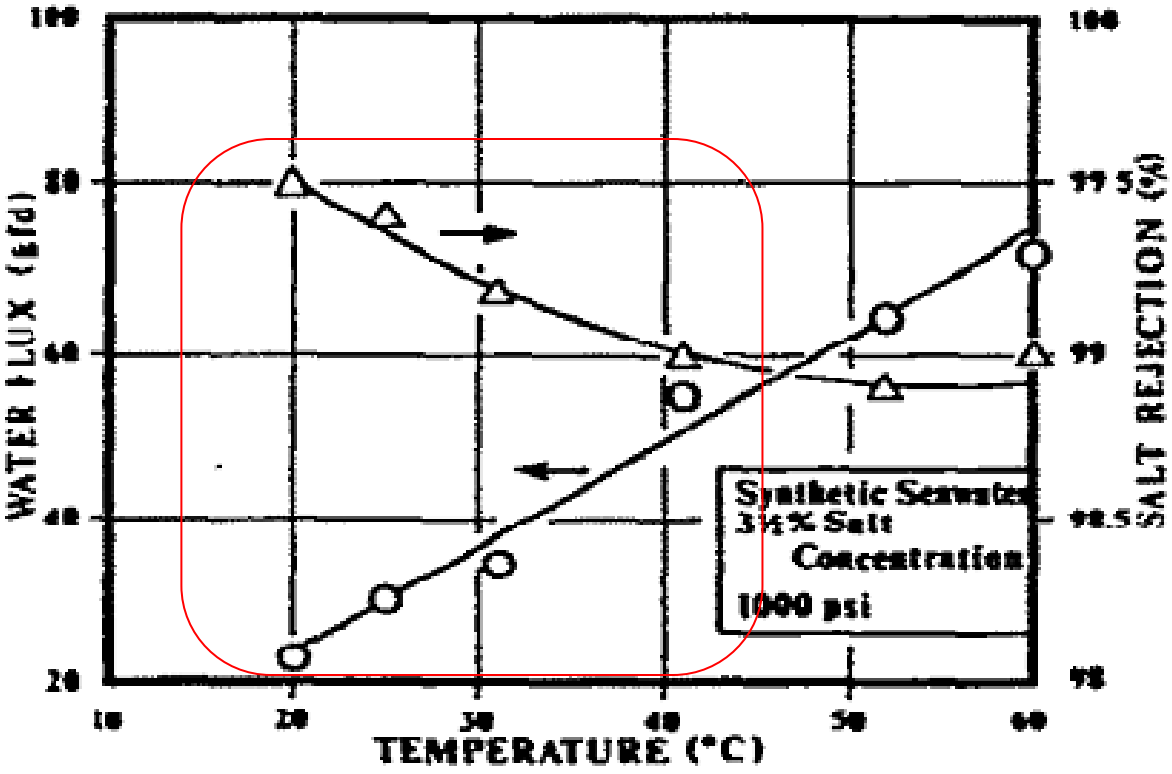

(b)

Figure 5.6. Water flux and salt rejection of (a) $[PAH/PAA]_{120}$ membrane as a function of temperature. Feed solution consists of 2000 ppm NaCl, Pressure of 40 bar, and pH of 6. (b) test result for FT-30 RO membrane tested at 35000 ppm NaCl and temperature of 25^{o}C [adapted from [152]]

The effect of temperature on water flux and salt rejection is more complex because permeability water molecules and salt ions is an activated process. It is known from solution diffusion model that permeability of solute or solvent across the membrane is function of diffusivity which is strong function of temperature. As illustrated in Figure 5.6, in our case, increasing the temperature by 20^{o}C enhances the water flux almost twice. Unfortunately, the increase of temperature also causes the increase of salt diffusivity in membrane thus reduces the salt rejection. A distinct similarity of permeation behavior between both types of membranes must be noted, which indeed provide one more evidence that PAH/PAA membrane fabricated in this work using SA-LbL behaves as a solution diffusion membrane.

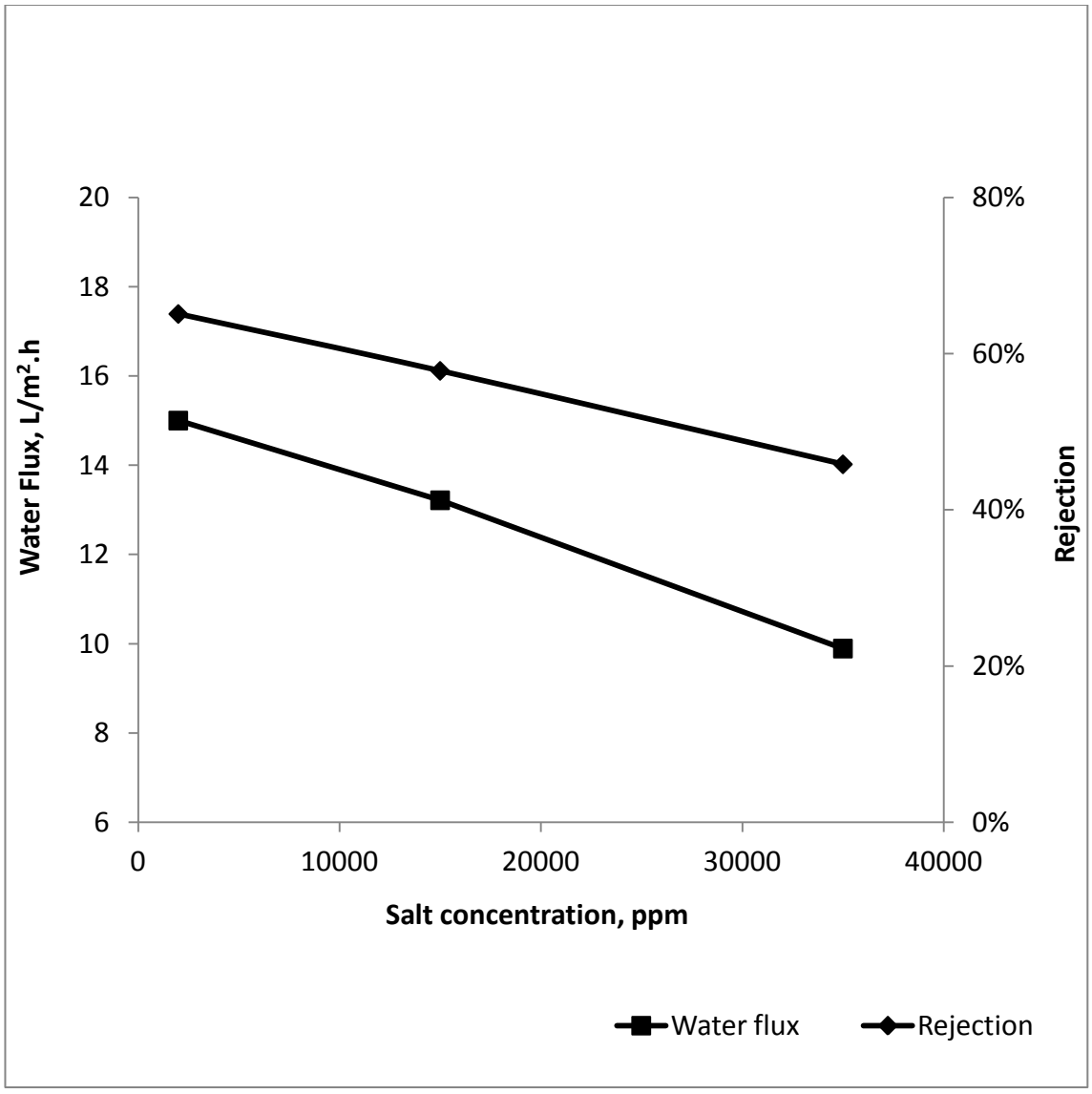
20
18
16
14
12
10
8
6
Water Flux, L/m².h
80%
60%
40%
20%
0%
Rejection
0
10000
20000
30000
40000
Salt concentration, ppm
Water flux
Rejection

(a)

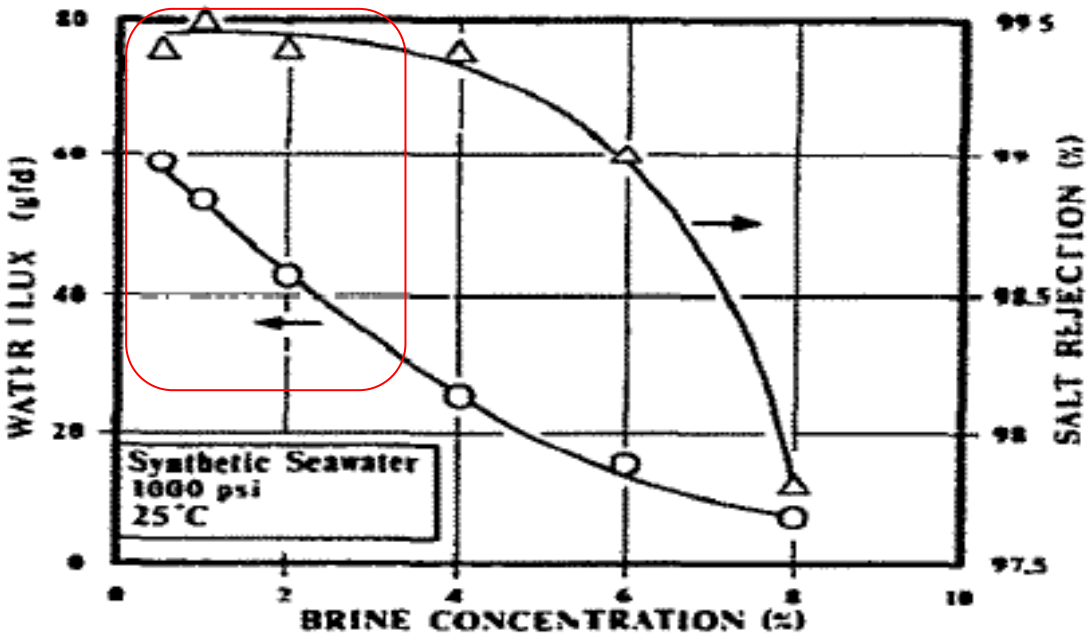

FIGURE 3. WATER FLUX AND SALT REJECTION AS A FUNCTION OF BRINE CONCENTRATION

(b)

Figure 5.7. Water flux and salt rejection of (a) $[PAH/PAA]_{120}$ membrane as a function of salt concentration. Testing condition: Pressure of 40 bar, Temperature of 25^{o}C, and pH of 6. (b) test result for FT-30 RO membrane tested at pressure of 1000 psi and temperature of 25^{o}C [adapted from [152]]

The effect of feed salt concentration on water flux and salt rejection for both the commercial RO membrane and our PAH/PAA membrane is also quite similar (see Figure 5.7). The decrease of water flux is almost linear with the increase of feed salt concentration. Increasing the salt concentration results in increasing the osmotic pressure and thus for a given feed pressure and temperature the water flux in expected to decrease with increase in salt concentration as evidenced by Figure 5.7. Increasing the salt concentration also results in the increase of driving force for salt passing through the membrane hence salt flux becomes faster. Thus increasing salt concentration leads to lower salt rejection. It is also noteworthy that the salt rejection decrease quite significantly when the PAH/PAA membrane is exposed to high salinity water. Meanwhile commercial PA membrane undergoes the same phenomenon at much higher salinity. This is because SA-LbL membrane swells more than PA membrane under such condition [99].

5.2. CONCLUSION

Our study has shown that SA-LbL PAH/PAA membrane performs quite stable under RO condition at least within 40 hours of exposure to 2000 ppm sodium chloride solution. It was noticed from membrane performance characteristics that polyelectrolyte chains rearrange themselves and they become compacted under relatively high pressure. However no performance alteration was observed after 20 hours. Our investigation on the effect of several operating condition such as pressure, temperature, and salt concentration on membrane performance also showed that SA-LbL membrane has similar characteristic to solution diffusion model.

CHAPTER SIX

NANOCLAY MODIFIED POLYAMIDE REVERSE OSMOSIS MEMBRANE

6.1. RESULT AND DISCUSSION

CS 15A is natural MNT modified with dimethyl dehydrogenated tallow (DMDT) quartenary ammonium salt. The tallow itself consists of 65 % of C18, 30% of C16 and 5% of C14. This material is more hydrophobic than natural MNT. MNT belongs to a smectite family and is categorized as 2:1 clay meaning two tetrahedral layers sandwiching one octahedral layer (see chapter two, Figure 2.2). Typical gallery spacing of MNT is about 1 – 2 nm and is expanded due to modification e.g. 3.15 nm in the case of CS-15A. During preparation thin film nanocomposite membrane, the nanoclays are dispersed in organic phase because the polyamide film builds up towards the organic phase.

Figure 6.**1** shows the XRD characteristic peaks for MNT in polyamide TFC membrane. Pure MNT is supposed to show peak at 6.85^{o} 2θ [153], however in our sample, this peak is shifted toward the smaller degree i.e. at 4.9^{O} 2θ with larger d-spacing. This is strong evidence that the MNT is intercalated [127]. It seems during 1 hour ultrasonication, TMC diffuses inside the gallery spacing and expand it. After this expansion, the other monomer i.e. MPD can easily diffuse inside the gallery and react with TMC to form polyamide. CS-15A has two characteristic peaks appear at 3^{o} and 7^{o} 2θ [154]. Figure 6.**2** shows a peak appear at 5^{o} 2θ which is believed a peak initially located at 7^{o}. The other peak i.e. 3^{o} is shifted to 2θ lower than 2^{o} which can not be

scanned using this XRD. This is again an indication that CS-15A is intercalated in polyamide membrane.

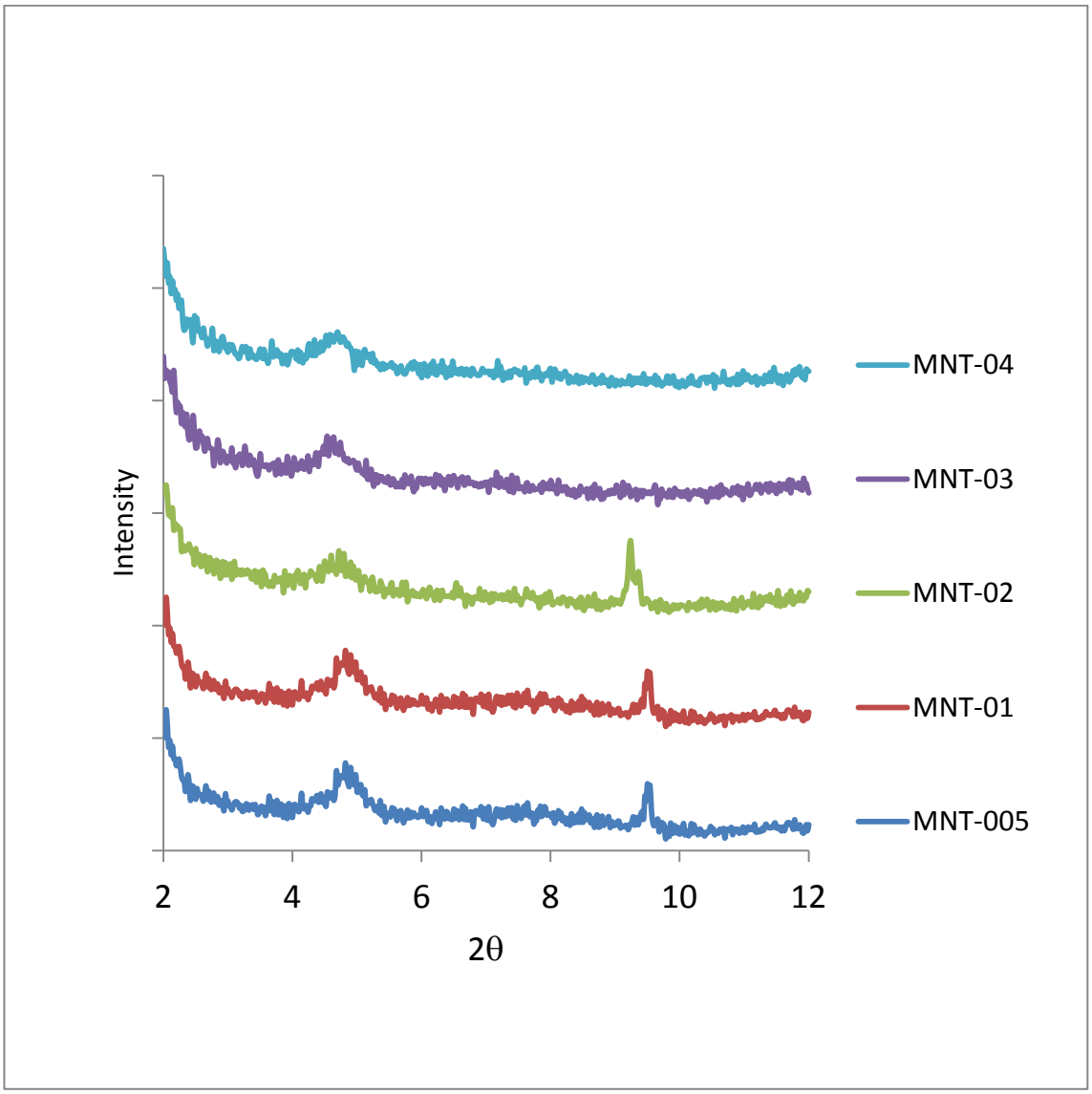

Figure 6.1. XRD Characteristic Peaks for Montmorillonite Modified Polyamide Membrane.

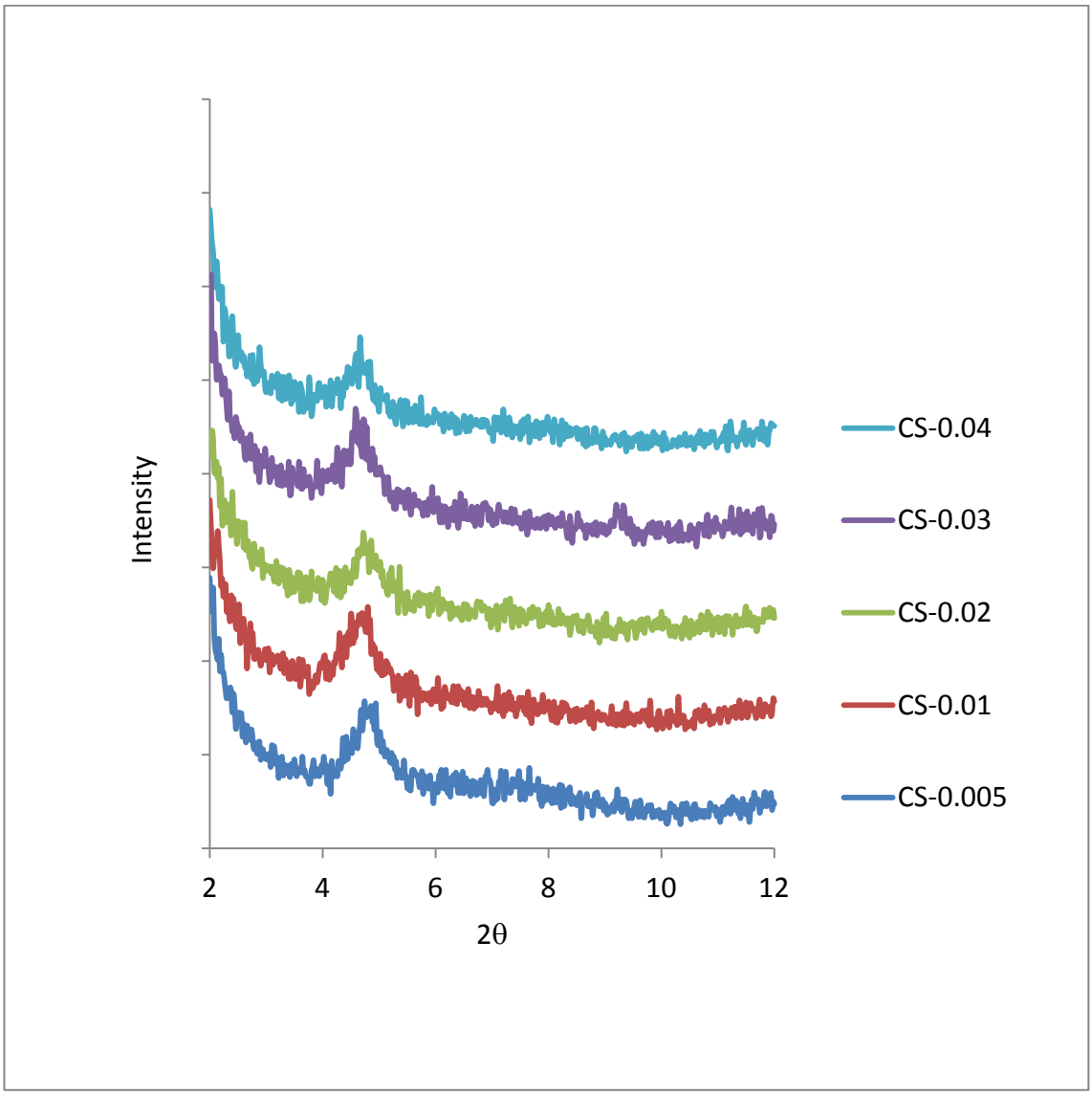

Figure 6.2. XRD Characteristic Peaks for CS-15A Modified Polyamide Membrane

TEM images show cross sectional of TFC PA membrane. We can see the highly porous PSF layer is coated with PA thin layer whose average thickness is about 250 nm. It can also be seen the membrane surface is quite rough which makes this kind of membrane prone to fouling as we have mentioned in the earlier chapter.

Despite the nanoclays are intercalated as suggested from XRD result, we can see from TEM images that MNT is not well dispersed as agglomeration occurs and results in quite big chunk. In this case, CS15A shows better dispersion. This can be explained as follows, it is well known that hydrophilic material cannot be well dispersed in organic solution whereas MNT is known for its highly hydrophilicity. Therefore, one hour ultrasonication may not be enough to disperse them in organic solvent. Even if sonication is assumed to be enough, there is also possibility for MNT to agglomerate quickly immediately the ultrasonic wave disappears. Because of the agglomeration, MNT seems trying to separate them selves from the solvent. Therefore we can see MNT is trapped between the two layers instead of embedded in PA layer.

CS15A, organically modified MNT, shows better dispersion compared to pure MNT as it becomes more hydrophobic after modification. Hence, CS15A can interact better with the organic solvent and remains dispersed during polymerization. The better interaction and dispersion makes this material can be embedded very well in PA layer.

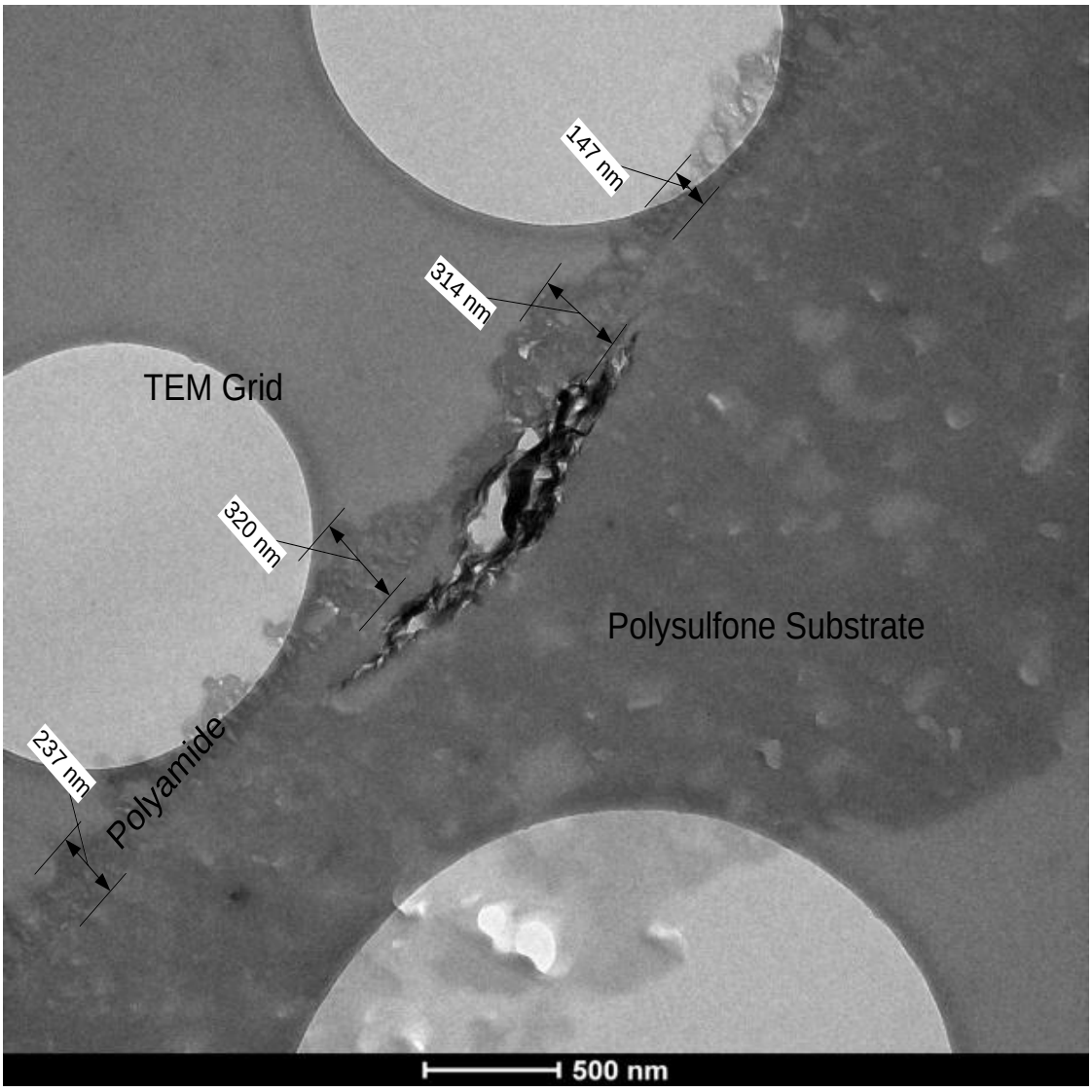

Figure 6.3. TEM image of Cross Section of MNT Modified TFC Polyamide Membrane (0.04 Wt% MNT)

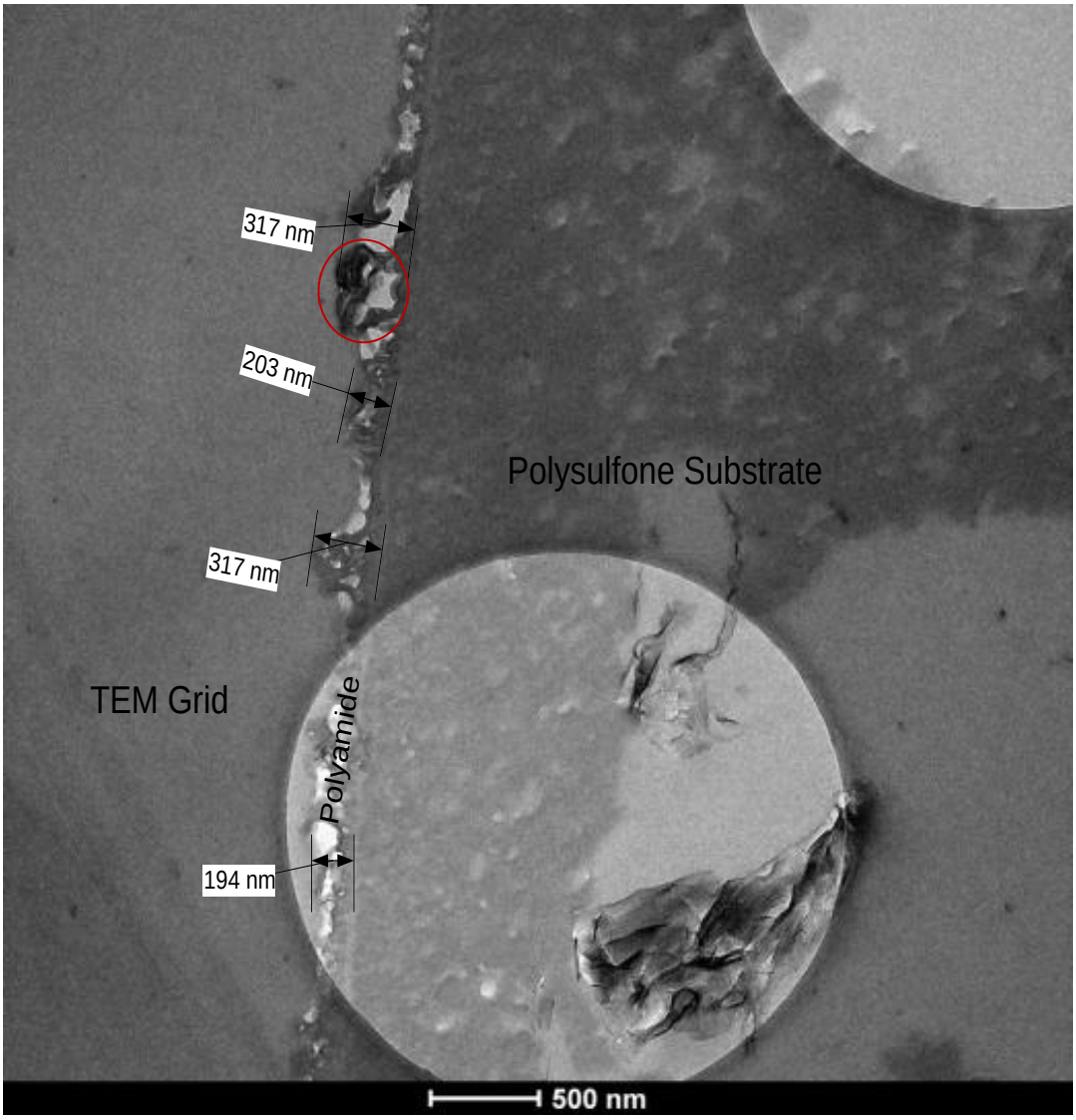

Figure 6.4. TEM image of Cross Section of CS15A Modified TFC Polyamide Membrane (0.04 Wt% CS)

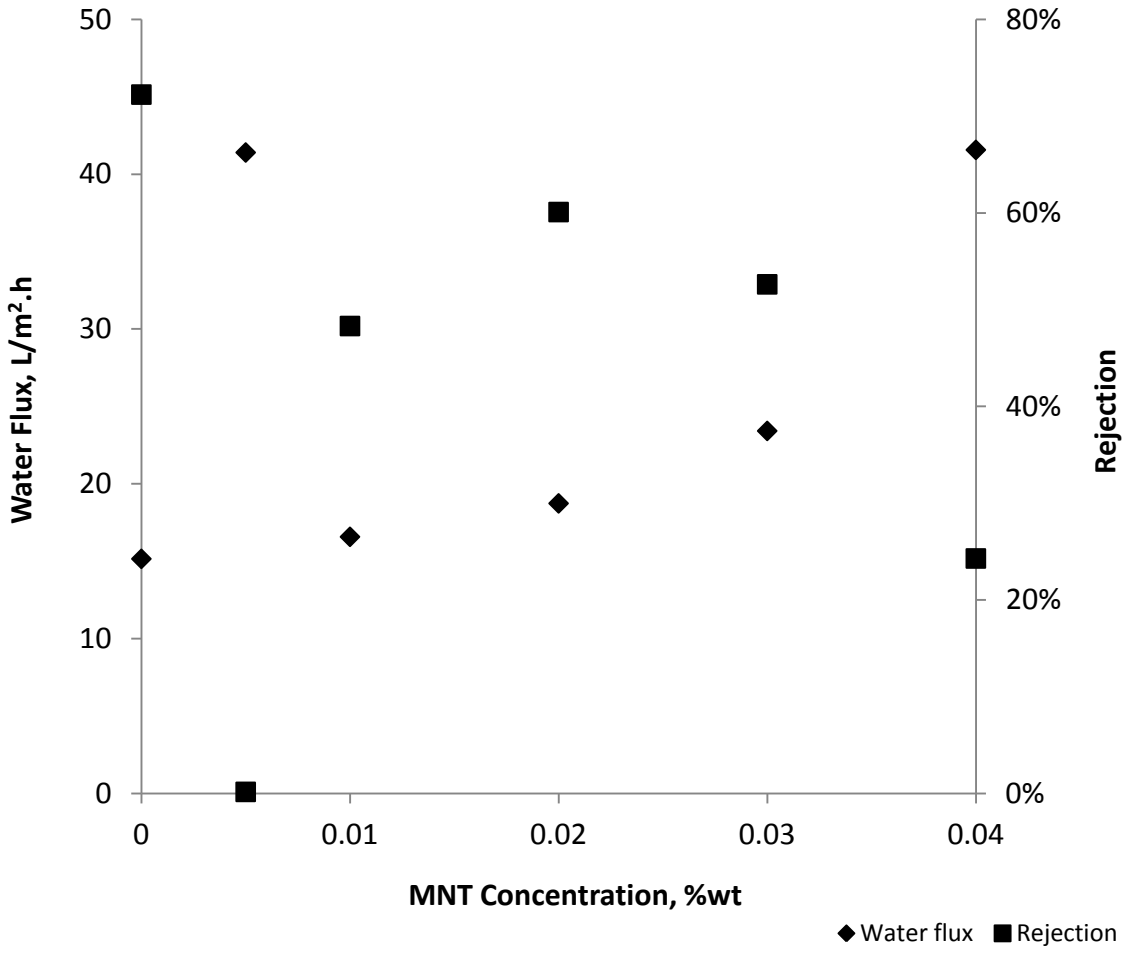
50
40
30
20
10
0
80%
60%
40%
20%
0%
Water Flux, L/m².h
Rejection
0
0.01
0.02
0.03
0.04
MNT Concentration, %wt
Water flux
Rejection

(a)

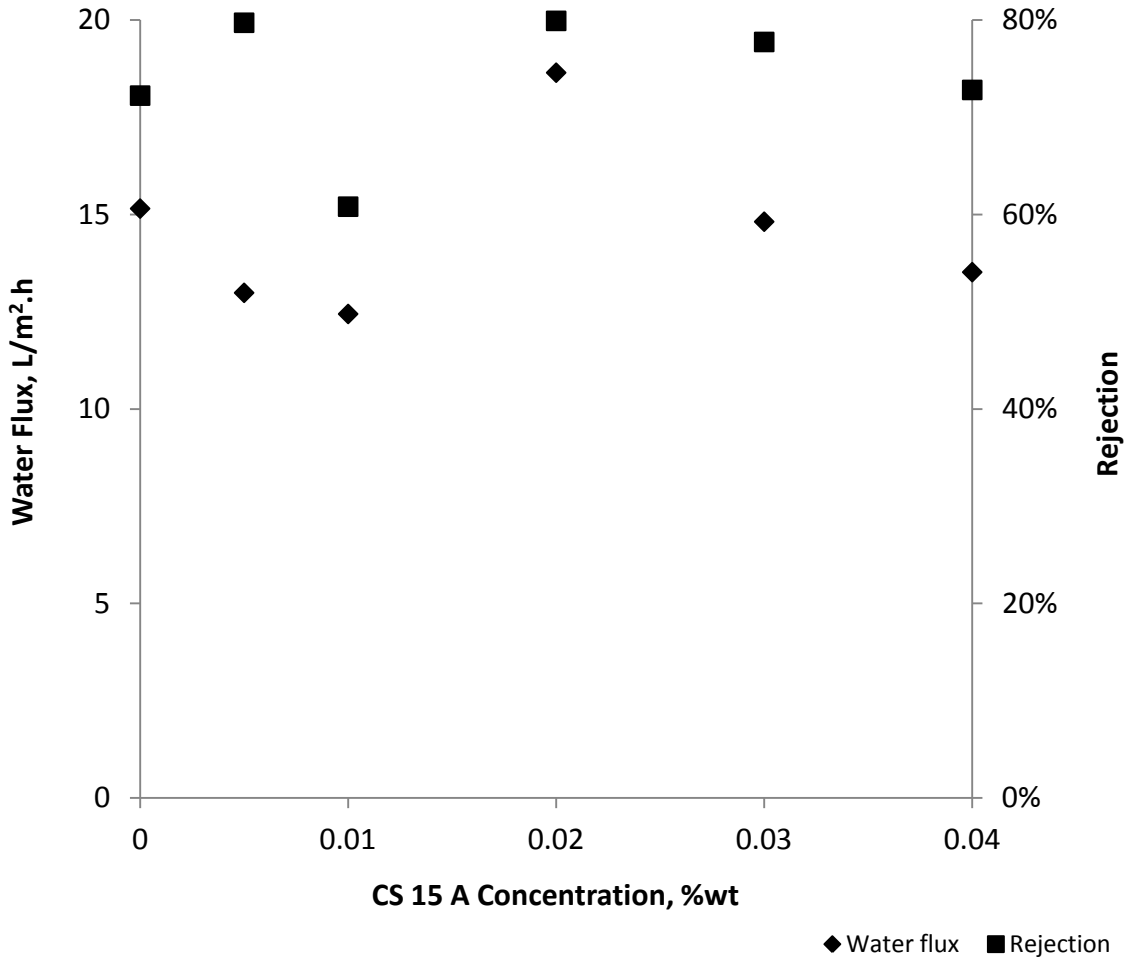

Figure 6.5. Effect of (a) MNT and (b) CS 15 A Concentration on Membrane Performance

As can be seen in **Figure 6.5**, the addition of low loading MNT into polyamide enhances the performance of the membrane. Water flux increases as the loading of MNT is increased. Apparently, the increase in water flux is likely due to more channels caused by agglomeration of MNT. The channels obviously also provide path for salt to pass through the membrane and results in significant decrease in salt rejection.

The permeation behaviour of CS15A modified TFC membrane is a bit different from MNT modified one. It seems that CS15A follows the same trend as other type of nanoclays which usually shows improved barrier properties of the polymer. Here, we can see at the beginning, the water flux decreases as CS15A loading is increased. This trend indicates the CS15A disperses and intercalated quite well thus provide turtuosity effect on the membrane that eventually improve barrier properties. However, the barrier property suddenly decreases at CS15A loading of 0.02 wt% shown by significant water flux enhancement. It seems the CS15A platelets orient themselves in such away so they do not create tortuous channels for water to pass trough the membrane. Oppositely, the platelets provide the channels for water to pass through the membrane. Surprisingly, the flux increase is coupled with the rejection increase indicating the platelet arrangement does not create larger pathways for both water and salts as found for MNT. We believe that rejection improvement is due to increase in surface charge caused by CS15A.

We start loosing the specific orientation of CS15A platelets at CS15A loading higher than 0.2 wt% however in general the platelets orientation is still good enough to at least maintain the flux and rejection above those of pristine TFC PA membrane.

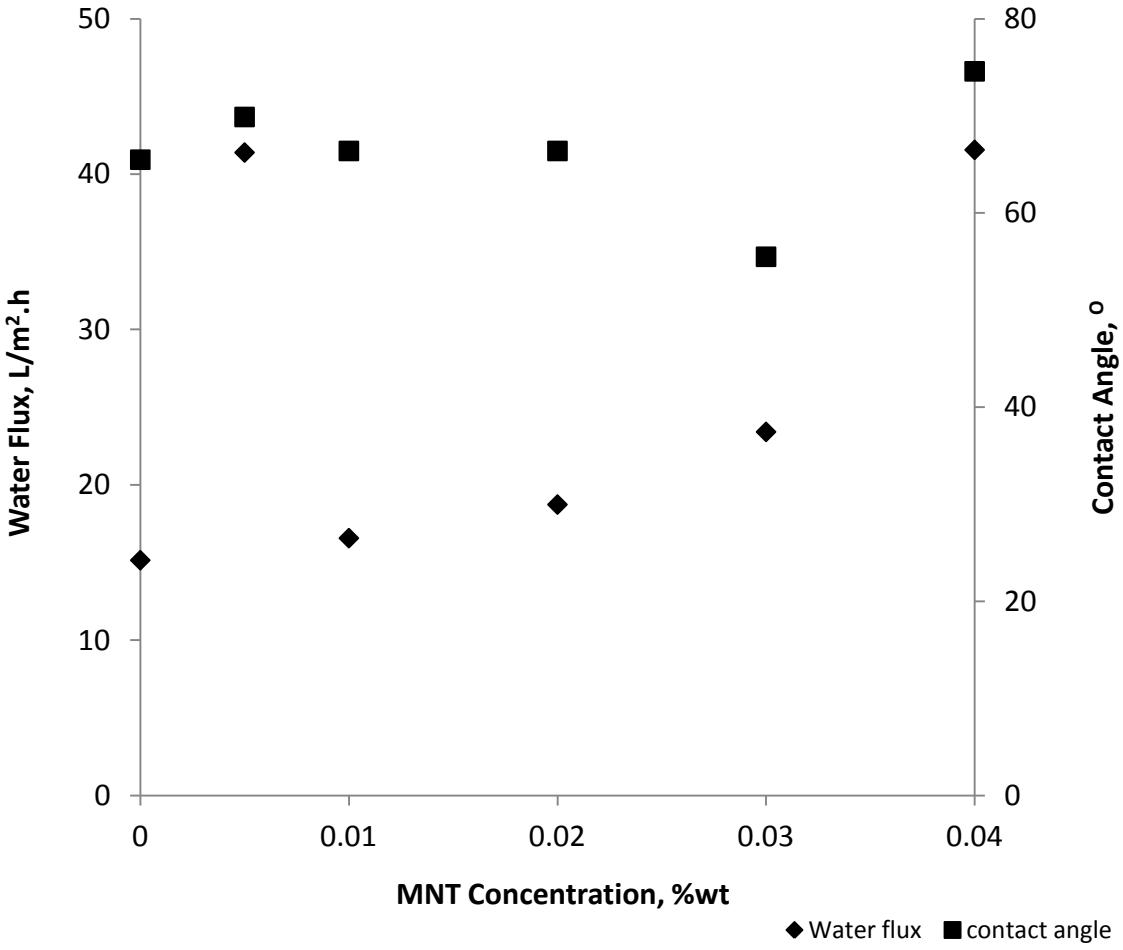
50
40
30
20
10
0
80
60
40
20
0
0
0.01
0.02
0.03
0.04
Water Flux, L/m².h
Contact Angle, °
MNT Concentration, %wt
Water flux
contact angle

(a)

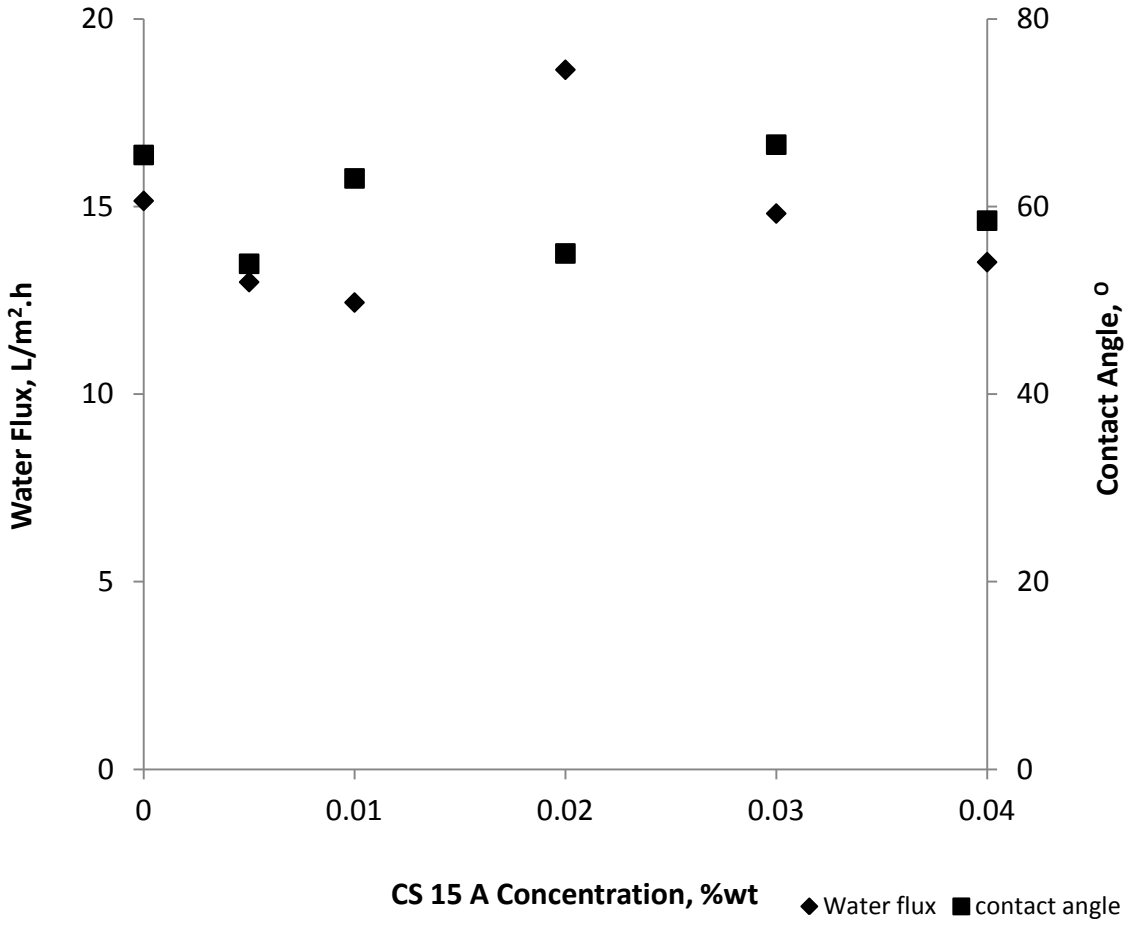

(b)

Figure 6.6. Effect of (a) MNT and (b) CS-15A Concentration on Membrane Performance and Hydrophilicity.

Figure **6.6** shows the relation between membrane hydrophilicity and its performance. Both MNT and CS15A do not seem improving the hydrophilicity. Both nanoclays modified membranes show contact angle value around 60^{o}. Contact angle depends upon not only surface hydrophilicity (or hydrophobicity) but also roughness. The contact angle value of a membrane of higher surface roughness is higher as compared to the other membrane of lower surface roughness, although both membranes are of similar hydrophilic nature [155]. In the same way, contact angle values of membranes of very high surface roughness are similar, although the membranes are somewhat different in hydrophilic nature. We believe MNT modified TFC membrane does show higher hydrophilicity than CS15A modified one, however since the membrane is very rough (our AFM measurement shows RMS roughness around 300 nm, data not shown) then the effect of roughness oppress the effect of MNT.

6.2. CONCLUSION

Two different nanoclays are introduced in polyamide RO membrane with the purpose of improving membrane performance. The result shows that cloisite 15 A can improve the flux from 15 $L/m^2.h$ to 18.65 $L/m^2.h$ with only 0.02 wt% loading and improve the rejection 72 $L/m^2.h$ to 80% $L/m^2.h$. This is due to better interaction between Cloisite 15 A and organic solvent used in polyamide synthesis. Montmorillonite nanoclays also enhance the flux tremendously but reduce the flux significantly indicating some extent of agglomeration occurs in the membrane. This happens because poor interaction between montmorillonite and organic solvent used in polyamide synthesis. This research opens up

the possibility of using other organically modified nanoclays that perhaps have better interaction with organic solvent thus more significant enhancement can be obtained.

CHAPTER SEVEN

CONCLUSIONS AND RECOMMENDATIONS

7.1. CONCLUSION

Thin film polyelectrolyte membranes have been fabricated, characterized, and tested for evaluating their performance as potential reverse osmosis membranes for water purification. The work presented in this dissertation demonstrates that SA-LbL (spin assisted layer by layer) assembly can be successfully employed as a an efficient and effective technique for depositing thin polyelectrolyte films on a given support scaffold to fabricate TFC (thin film composite) membranes. It has been shown that SA-LbL allows a good control over the film thickness, composition, and other surface properties such as roughness and hydrophilicity. It is also demonstrated that this TFC membrane fabrication via SA-LbL processing can be achieved within considerably shorter time in comparison to the conventional dip-LbL processing. It is also shown that SA-LBL does not require smooth substrates such as silicon wafer, glass, etc. but dense, homogeneous and firmly adherent films can rather be deposited on porous supports such as polysulfone ultrafiltration membrane or porous alumina etc.

Four polyelectrolyte systems have been investigated in this work, namely, PDAC/PVS, PAH/PVS, PEI/PAA and PAH/PAA. It is concluded that PAH/PAA or PAH/PVS can be considered as promising candidates as potentially new TFC membranes for RO desalination applications. These membranes show higher stability and relatively better performance compared to other two, PDAC/PVS and PEI/PAA systems as can be seen in Figure 7.1. In particular, it is known that, the polyelectrolytes with sulfonate functional

group in their backbone such as poly(styrene sulfonate) are very stable, and can even withstand under the exposure of 117000 ppm NaCl [156] with negligible swelling. It was also investigated that even at 35000 ppm NaCl many commercial RO membranes undergo quite significant swelling and obviously result in lower salt rejection [157]. Tieke and his coworkers have also shown that dip-LbL membrane consists of PVAm and PVS showed high rejection [86]. Similarly, our works using PAH/PAA membrane also showed relatively high salt rejection and stability. All of these works indeed show strong indication that LbL membrane can be very promising to replace or compete to the commercial RO membrane in the near future.

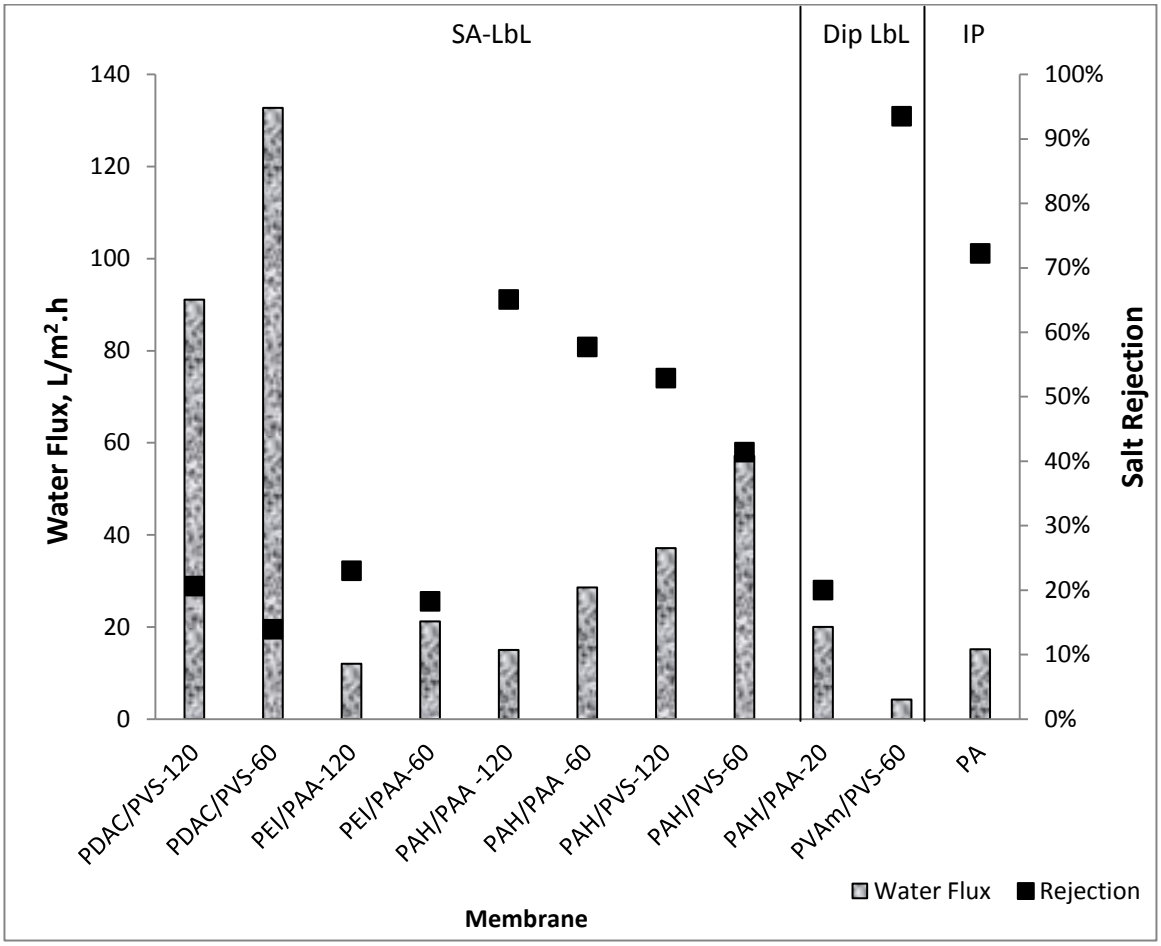

Figure 7.1. Permeation Performance of Various LbL RO and TFC RO membranes

It can be seen in Figure 7.1 that in general SA-LbL membrane shows better performance compared to dip-LbL. Their performances are even comparable to that of hand-made PA membrane made through interfacial polymerization but SA-LbL membranes have much smoother surface and more hydrophilic compared to them. I believe with better system, my membranes will be comparable to those commercial ones.

7.2. RECOMMENDATIONS

I believe that although the membranes fabricated in this work demonstrate good stability and provide comparable permeation flux as compared to the commercial RO membranes, the salt rejection remains fairly low. I recommend that the issue of low salt rejection can be addressed by cross-linking the film either chemically or thermally to make the film denser to eliminate any active sites that may act as potential paths for ion transport. Secondly, in order to improve the flux, hydrophilic nanoparticles such as nanoclays or zeolite A can be incorporated in the film as these nano particles can improve the flux without compromising the rejection [109]. Investigation of the biofouling resistance of the membranes should also be of much interest since SA-LbL membranes have all potentials to be good biofouling resistant membranes.

APPENDIX A

RAW DATA

Table A.4. Effect of pH on Bilayer Thickness of PAH/PAA Film on Silicon Wafer

Bilayer #		**bilayer thickness, nm**															
	pH of PAH	**3.5**				**5.5**				**7.5**				**9**			
	pH of PAA	**3.5**	**5.5**	**7.5**	**9**	**3.5**	**5.5**	**7.5**	**9**	**3.5**	**5.5**	**7.5**	**9**	**3.5**	**5.5**	**7.5**	**9**
6		4.68	3.80	2.23	2.98	7.28	7.58	5.50	5.33	7.85	7.80	5.38	4.75	9.90	10.35	8.78	6.30
7		5.20	4.80	3.73	3.10	8.15	7.80	5.55	4.80	9.83	7.93	6.00	5.45	10.75	10.08	9.05	8.25
average		4.94	4.30	2.98	3.04	7.71	7.69	5.53	5.06	8.84	7.86	5.69	5.10	10.33	10.21	8.91	7.28

Table A.5. Effect of pH on Monolayer Thickness of PAH and PAA

	monolayer thickness, nm															
pH of PAH	**3.5**				**5.5**				**7.5**				**9**			
pH of PAA	**3.5**	**5.5**	**7.5**	**9**	**3.5**	**5.5**	**7.5**	**9**	**3.5**	**5.5**	**7.5**	**9**	**3.5**	**5.5**	**7.5**	**9**
PAH	2.11	1.99	1.88	1.84	3.69	4.00	3.44	2.51	4.56	3.49	2.00	2.66	5.16	6.83	5.09	3.71
PAA	2.83	2.31	1.10	1.20	4.03	3.69	2.09	2.55	4.28	4.38	3.69	2.44	5.16	3.39	3.83	3.56

Table A.6. Effect of Spin Speed on PAH/PAA Multilayer Film Thickness and Surface Roughness

(pH of PAH and of PAA = 3.5, Concentration of PAH and of PAA = 0.01 M)

	Bilayer Thickness and RMS roughness, nm		
RPM	**with rinsing**	**without rinsing**	**RMS**
2000	6.05	8.28	4.45
3000	5.51	7.35	3.61
4000	5.10	6.23	3.44
5000	4.83	5.58	3.31

Table A.7. PAH/PAA Multilayer Film Growth

(pH of PAH and PAA = 3.5, Spin Speed = 2000 rpm, Concentration of PAH and of PAA = 0.01 M)

# bilayer	Thickness, nm
0.5	2.30
1.5	7.00
2.5	11.50
3.5	16.70
4.5	21.75
5.5	26.55
6	28.93
6.5	31.23
7	34.50
7.5	36.43
10	51.05
15	75.27
20	89.70
30	131.59

Table A.8. Effect of Concentration on Thickness and Surface Roughness

(pH of PAH and of PAA = 3.5, Spin Speed = 2000 rpm)

Concentration, M	Thickness and Roughness	
	Bilayer, nm	RMS, nm
0.005	3.93	1.79
0.01	5.80	1.82
0.025	7.85	1.93
0.050	8.92	2.48

Table A.9. Permeation Performance of PDAC/PVS Multilayer Membrane

(pH of PDAC = 3.5 and pH of PVS = 9, Spin Speed = 3000 rpm, Concentration of PDAC and of PVS = 0.01 M)

(Feed Water Concentration = 2000 ppm , pressure = 580 psi, temperature = 25^{o}C, Feed Water pH = 6)

Bilayer #	**60**			**120**		
Run	**Time,min**	**Flux, L/m^2.h**	**Rejection**	**Time,min**	**Flux, L/m^2.h**	**Rejection**
1	0			0		
	120	121.43		120	107.14	
	180	121.43	14.88%	180	107.14	19.96%
	240	121.43	14.64%	240	107.14	20.20%
2	0			0		
	120	135.71		120	71.43	
	180	135.71	13.35%	180	78.57	20.25%
	240	142.86	12.52%	240	78.57	21.58%

Table A.10. Permeation Performance of PAH/PVS Multilayer Membrane

(pH of PAH = 3.5 and pH of PVS = 9, Spin Speed = 3000 rpm, Concentration of PAH and of PVS = 0.01 M)

(Feed Water Concentration = 2000 ppm , pressure = 580 psi, temperature = 25^{o}C, Feed Water pH = 6)

60			**120**		
Time,min	**Flux, L/m^2.h**	**Rejection**	**Time,min**	**Flux, L/m^2.h**	**Rejection**
0			0		
120	57.14	43.39%	120	35.71	57.92%
180	57.14	41.26%	180	37.14	53.45%
240	57.14	41.53%	240	37.50	52.31%

Table A.11. Permeation Performance of PAH/PAA Multilayer Membrane

(pH of PAH = 3.5 and pH of PAA = 9, Spin Speed = 3000 rpm, Concentration of PAH and of PVS = 0.01 M)

(Feed Water Concentration = 2000 ppm , pressure = 580 psi, temperature = 25^{o}C, Feed Water pH = 6)

60			**120**		
Time,min	**Flux, L/m^2.h**	**Rejection**	**Time,min**	**Flux, L/m^2.h**	**Rejection**
0			0		
120	31.43	53.15%	120	17.14	54.85%
180	31.43	55.15%	180	16.86	56.79%
240	31.43	55.15%	240	16.79	59.56%

Table A.12. Permeation Performance of PEI/PAA Multilayer Membrane

(pH of PEI = 3.5 and pH of PAA = 9, Spin Speed = 3000 rpm, Concentration of PEI and of PAA= 0.01 M)

(Feed Water Concentration = 2000 ppm , pressure = 580 psi, temperature = 25^{o}C, Feed Water pH = 6)

60			**120**		
Time,min	**Flux, L/m^2.h**	**Rejection**	**Time,min**	**Flux, L/m^2.h**	**Rejection**
0			0		
120	21.43	18.26%	120	12.00	23.00%
180	20.95	18.26%	180	12.00	23.00%
240	21.43	18.26%	240	12.00	23.00%

Table A.13. Long Term Permeation Performance of PAH/PAA Multilayer Membrane

(pH of PAH = 3.5 and pH of PAA = 9, Spin Speed = 3000 rpm, Concentration of PAH and of PAA = 0.01 M)

(Feed Water Concentration = 2000 ppm , pressure = 580 psi, temperature = 25^{o}C, Feed Water pH = 6)

60			**120**		
Time,h	**Flux, L/m^2.h**	**Rejection**	**Time,h**	**Flux, L/m^2.h**	**Rejection**
0	31.43	53.15%	0	17.14	52.08%
1	31.43	53.15%	1	17.14	54.85%
2	31.43	55.15%	2	16.86	56.79%
12	30.00	56.00%	5	16.79	59.56%
20	28.57	57.15%	20	15.00	63.13%
33	28.57	57.43%	30	15.00	64.83%
40	28.57	57.72%	40	15.00	65.08%

Table A.14. Effect of Pressure on PAH/PAA Membrane Performance

(120 Bilayer, pH of PAH = 3.5 and pH of PAA = 9, Spin Speed = 3000 rpm, Concentration of PAH and of PAA = 0.01 M)

(Feed Water Concentration = 2000 ppm , temperature = 25^{o}C, Feed Water pH = 6)

Pressure, Psi	**Flux, L/m^2.h**	**Rejection**
725	19.89	66.21%
580	15.00	65.08%
435	11.25	62.15%
290	7.14	55.76%

Table A.15. Effect of Temperature on PAH/PAA Membrane Performance

(120 Bilayer, pH of PAH = 3.5 and pH of PAA = 9, Spin Speed = 3000 rpm, Concentration of PAH and of PAA = 0.01 M)

(Feed Water Concentration = 2000 ppm , Pressure = 580 Psi, Feed Water pH = 6)

Temperature, ^{O}C	**Flux, L/m^2.h**	**Rejection**
25	15.00	65.08%
35	21.43	64.11%
45	28.57	63.87%

Table A.16. Effect of Feed Salt Concentration on PAH/PAA Membrane Performance

(120 Bilayer, pH of PAH = 3.5 and pH of PAA = 9, Spin Speed = 3000 rpm, Concentration of PAH and of PAA = 0.01 M)

(Feed Water Concentration = 2000 ppm , pressure = 580 psi, temperature = 25^{o}C, Feed Water pH = 6)

Feed Conc, ppm	**Flux, L/m^2.h**	**Rejection**
2000	15.00	65.08%
15000	13.21	57.80%
35000	9.89	45.83%

Table A.17. Effect of Curing Time and Temperature on Permeation Performance of Polyamide Thin Film Composite Membrane

(Feed Water Concentration = 2000 ppm , pressure = 580 psi, temperature = 25^{o}C, Feed Water pH = 6)

Time, h	**TW-0-RT**		**TFC-TW-0 (105^{O}C, 60 s)**		**TFC-TW-0 (105^{O}C, 90 s)**	
	Flux, L/m^2.h	**Rejection**	**Flux, L/m^2.h**	**Rejection**	**Flux, L/m^2.h**	**Rejection**
1	8.94	68.91%	13.64	88.97%	14.68	66.00%
2	8.88	71.38%	14.29	90.24%	15.00	69.64%
3	8.94	73.46%	14.29	91.38%	15.25	71.48%
4	8.93	75.22%	15.01	91.94%	15.47	72.46%
5	8.51	77.47%	13.93	92.52%	15.36	73.87%

Table A.18. Effect of Cloisite 15A Loading on Permeation Performance of Polyamide Thin Film Nanocomposite Membrane

(Feed Water Concentration = 2000 ppm , pressure = 580 psi, temperature = 25^{o}C, Feed Water pH = 6)

Time, h	**Weight %**									
	0.005		**0.01**		**0.02**		**0.03**		**0.04**	
1	12.44	75.30%	11.51	55.92%	18.67	73.78%	15.06	73.32%	13.82	67.62%
2	13.39	77.34%	12.55	58.28%	18.80	76.52%			13.58	68.85%
3	13.09	78.47%	12.91	60.03%	18.80	79.36%			13.25	70.64%
4	12.99	79.44%	12.76	60.69%	18.88	80.39%	14.83	76.17%	13.46	71.92%
5	13.03	80.03%	12.49	61.40%	18.08	79.68%	14.55	76.40%	13.48	72.71%

Table A.19. Effect of Montmorillonite Loading on Permeation Performance of Polyamide Thin Film Nanocomposite Membrane

(Feed Water Concentration = 2000 ppm , pressure = 580 psi, temperature = 25^{o}C, Feed Water pH = 6)

Time, h	**Weight %**									
	0.005		**0.01**		**0.02**		**0.03**		**0.04**	
1	45.84	-1.16%	17.26	44.18%	20.07	52.13%	25.43	46.53%	44.41	19.47%
2	43.29	1.10%	17.05	45.96%	19.74	55.99%	23.29	51.44%	42.86	21.10%
3	40.62	-0.74%	16.45	47.89%	18.80	58.17%	23.23	53.81%	41.21	21.78%
4	39.32	-0.79%	16.13	51.49%	17.28	60.58%	22.74	56.44%	39.87	22.51%
5	37.93	0.16%	15.97	52.01%	17.78	61.42%	22.38	54.85%	39.50	23.19%

APPENDIX B

SPINGROWER & PERMEATION CELL

SPIN-GROWER™

Description

The absolute Nano SpinGrower is a versatile desktop-scale tool for deposition of multilayer thin films from liquid solutions, including via layer-by-layer (LbL) assembly. Applications include production of multilayer nanostructured thin films and nanocomposite coatings from charged polymers, nanoparticles (metallic, semiconducting, insulating), nanofibers (nantoubes, nanowires), nanoplatelets (e.g., grapheme, clays), and other supramolecular species. The system accommodates substrates with diameters up to 6 inches (15.2 cm) and achieves assembly times an order of magnitude faster than conventional dip LbL systems, with film bi-layer thickness comparable to that from traditional techniques. Products from the Spin Grower also display more highly ordered structures compared to dip-coated LbL films. The SpinGrower is a fully automated system and can be preprogrammed for an indefinite number of layers, with control of the deposition sequence and dispensed volume.

Specification

The SpinGrower overall system specifications and components are listed in the below tables.

Table A.2.20. Basic System Specification

Specification	Value
Substrate spin speed	0-10,000 rpm
Maximum fluid injection rate	1.2 mL/s
Maximum substrate diameter	15.2 cm
Number of solutions	5
Reservoir capacity	2 L
Solution pH range	1-10

Table A.2.21. System Components

Component	Description
Spin Coater (1)	Special Coating Systems G3P-8
Peristaltic Pumps (5)	Watson-Marlow 300 series high precision OEM
Pump Tubing	Watson-Marlow Bioprene Tubing ID 1/16", Wall Thickness 1/16"
Data Acquisition Boards (3)	National Instruments USB 6008
24 V 10 A DC Power source (1)	Acopian Gold box Unregulated DC power supply
Fluid Delivery (1)	Loc-Line Modular Hose System

Reservoir Bottles (5)	Nalgene 2 L bottles
Pump rack (1)	14 gauge sheet aluminium rack
Electronics rack (1)	PVC junction box
Chuck adaptor (2)	Delrin microscope slide adaptor with viton o-ring

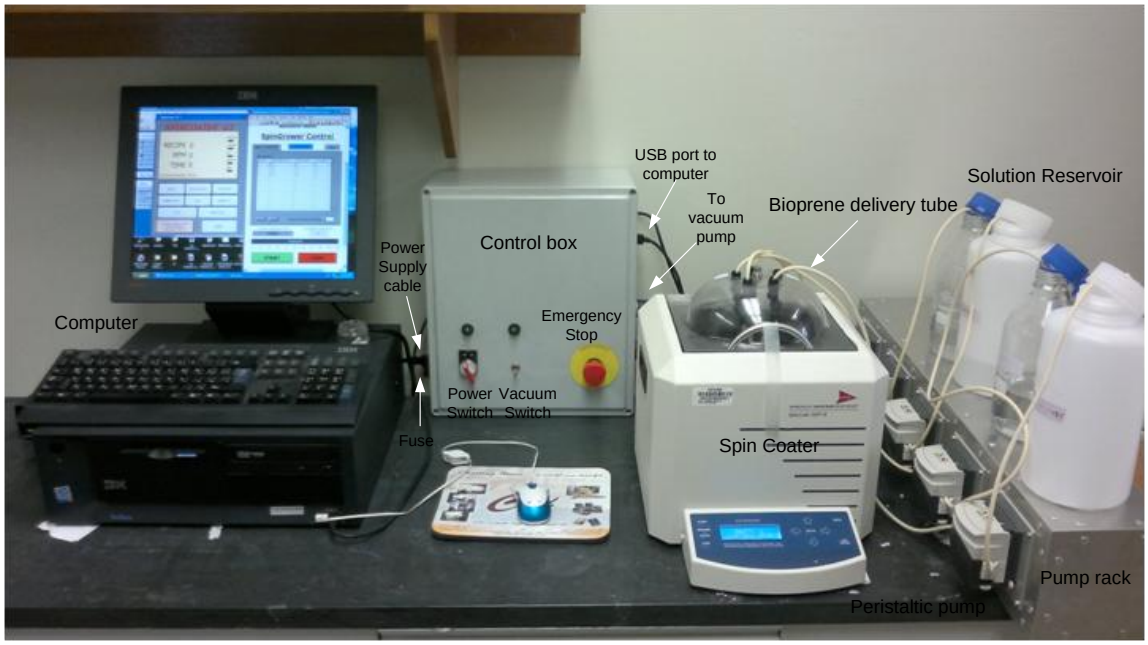

Figure B.7. SpinGrower Full System Set-up

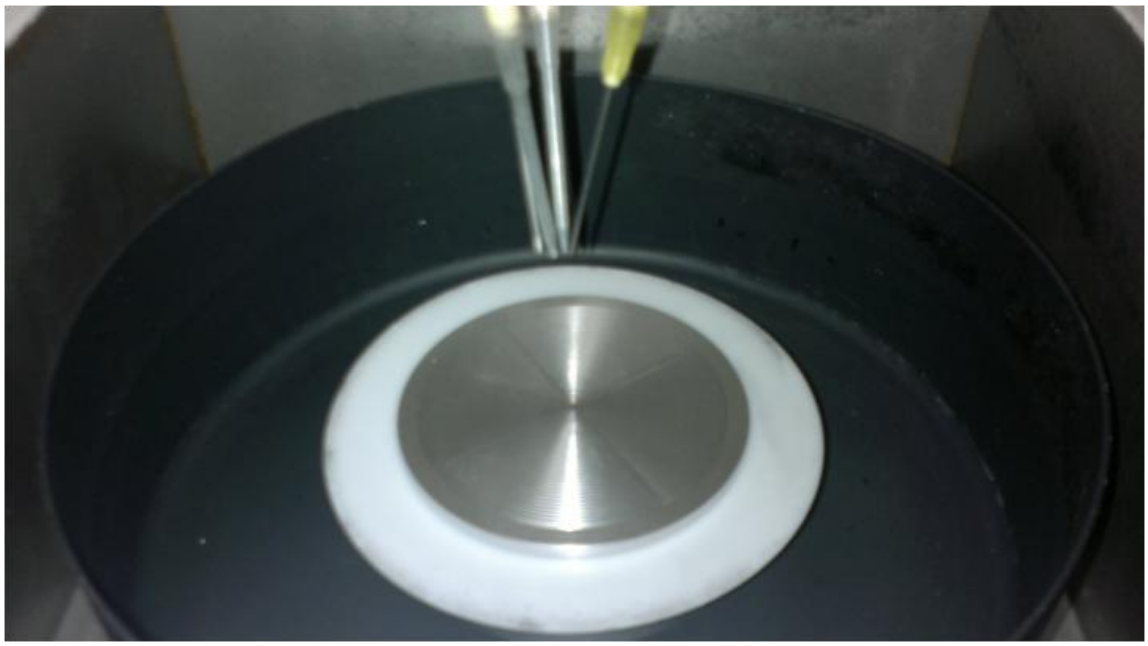

Figure B.8. Spin Coater

Calibration

There are two parts for the calibration, namely the ‘No-Drip Calibration’ and the ‘Rate Calibration’. The user needs to be on the proper tab for each kind of calibration as the calibration routines are slightly different.

1. The pump must be calibrated for proper reverse time after fluid deposition to ensure no excess dripping occurs during the film making process. Run the program ‘SpinGrower Control.vi’ and click on calibration tab as shown in **Figure B.9**.

Figure B.9. Front panel of SpinGrower Control.vi

A new window will appear as shown Figure B.10 . Under the ‘No-Drip nlowest reverse time for which the pump completely prevents all drips and the fluid meniscus is flush with the end of the output tube. Plot the reverse time versus the pump speed and fit a second order polynomial trend line to the data. The coefficients of the equation should be keyed into the space provided under the No-Drip Calibration tab. Repeat this for each pump. Save all changes before exiting the calibration panel.

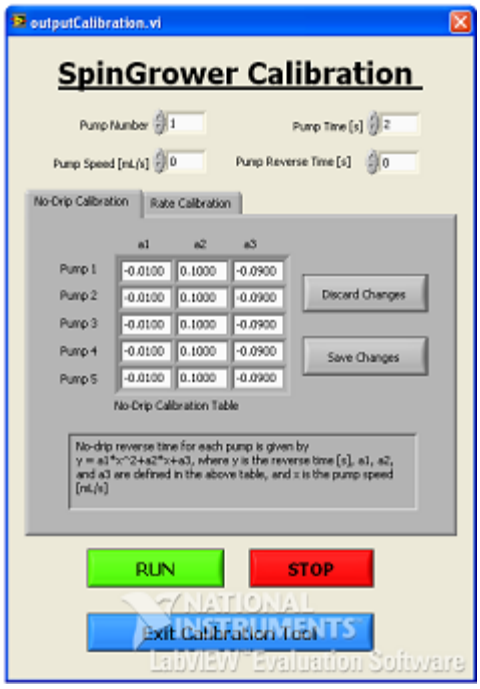

Figure B.10. No-Drip Calibration Panel

2. The pumps must also be calibrated to inject the proper amount of fluid. Run the program 'SpinGrower Control.vi' and click on calibration. A new window will appear as shown in **Figure B.11** below. Under the 'Rate Calibration' tab, specify the pump number, run time, and speed. For each run, unject the fluid into a beaker, and determine the mass of the injected fluid. Plot the expected mass versus actual mass and fit a linear trend line through the data points. Change the value of the first column to the slope of the line and the value of the second column to the intercept of the line. Test to make sure the proper volume is being deposited, and reiterate the calibration if necessary. Repeat this for each pump. Save all changes before exiting the calibration panel.

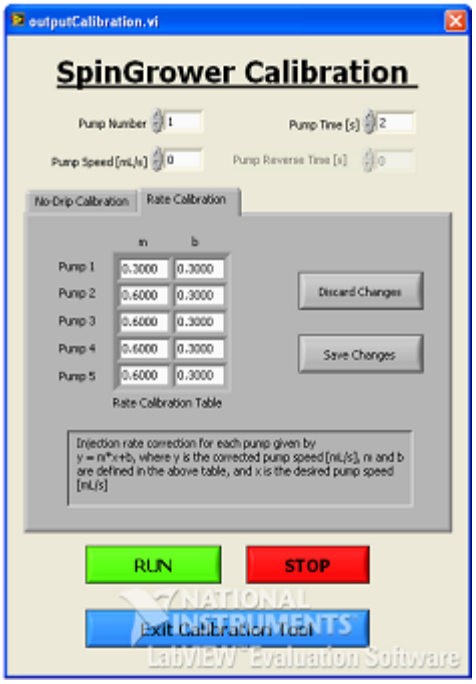

Figure B.11. Rate Calibration Panel

Operation

After the system has been set up and calibrated, operations for making a film simply requires filling the reservoirs with desired solutions and running the SpinGrower Control Program. It is recommended to calibrate the system before each operation for the optimum performance and accuracy of the SpinGrower. It is important to know that the SpinGrower Control Program can only control the liquid flow rate, injection time and number of sequence. It does not control the spin speed which is controlled by other software so called G3P-PC. This software can be installed on the computer but it is also available in the spin coater itself. Before starting the program, it is mandatory to turn on the spincoater otherwise the program will crash and required to exit. In the main panel of G3P software, the user will find the following command buttons:

- Center Button: spins slowly (50 rpm) for 5 secondes, with vacuum on the chuck, to allow the user to check the centering of the sample.
- Change Recipe Button: lets the user to call a different recipe to run form those saved in the spinner.
- Stop button stops the spinner in mid-recipe.
- Vacuum On/Off button will turn the vacuum off whenever a recipe is not running.
- Start button begins running the recipe selected in the window.
- Clear button is used when a recipe has crasehed for some reason for examples: physical intervention with rotation, communication loss, vacuum loss, etc. Clicking this resets the recipe and spinner.
- Edit Recipe button goes to a new window where the user can type or use the up/down arrows to select another recipe number and then takes the user to edit existing recipes or creates new ones.
- Exit button exits the program and returns to windows program.

As mentioned, the new window appears after clicking edit recipe button. In this new window the user will find

- Open Recipe File lets the user select an existing file to edit.
- Clear Steps sets all values for selected steps to zero. This is important when the user creates a new recipe from scratch. User can have 20 different steps that can also be cleared by keying the number of the steps needed to be cleared.
- Save to PC makes a recipe file in the PC but not in the spinner. The file can be loaded to the spinner later.

- Read from spin coater asks for the recipe number then loads it into the computer so that the user can review, change or save it.
- Write to spin coater asks for recipe number where the user wants to save it. This will overwrite anything that is already in the spinner at that number, so make sure that the user knows where you want to place/write the recipe.
- Exit takes back the user to the main window panel.

Aside from the above buttons, the user can also modify the recipe steps in the same window:

- Ramp (0 to 25.5 seconds), this number tells the spin coater how many seconds to take to accelerate or decelerate to the desired speed (RPM). If Ramp is set to zero, the spin coater will try to comply but if the required change of speed is too great, a motion error may occur.
- RPM (0 to 9999 RPM), this number is the rotational speed for the spin coater for this step.
- Dwell (0 to 999 seconds), this is how long to spn at the RPM the user just selected.
- Dispense (None, coating, edge, solvent, N2), this dispense function will be turned on at the beginning of Dwell. Its duration is controlled by the Time variable.
- Time (0 to 10 seconds), this setting will determine how low the dispense function will be turned on. If Dispense function is set to none then Time setting does nothing.

After the recipe is ready, we can transfer our attention to the SpinGrower Control program and do the following:

1. Fill the solution reservoirs with the desired solutions.

2. Purge the fluid lines to ensure no contamination occurs due to residues in the lines.
3. Position the Loc-Line tubing to the desired fluid deposition location, center the substrate onto the chuck in the spin coater, and then close the spin coater lid.
4. Run the SpinGrower.Control.vi program. Here the user may specify entire sequence with the pumps injecting in arbitrary order and the recipe can be saved for later use.
5. Input the parameters for the film by specifying the pump number, pump speed, pump time, dry time, and number of iterations. These values will control each solution's injection rate and time, the dry time between layers, the sequence of solutions, and the number of layers desired.
6. Start the spin coater by clicking Start button in G3P software. After the spin coater reach the desired speed, click on Start button in SpinGrower Control program.
7. If a sequence needs to be aborted, click on the Stop button.
8. To perform an emergency stop, hit the red emergency stop button located at the front of the control box (see Figure B.7).

Example of Sample Preparation

For example the procedure to prepare 60 bilayers of PAA and PAH is as follows

1. Prepare PAA and PAH solution of 0.01 M based on their repeating unit.
2. Place the solutions in the solution reservoirs. Note: make sure you put the solutions in sequence for example if you want to deposit PAA first before PAH then place the solution in the following order: PAA in the first solution reservoir

followed by deionized water in the second reservoir, PAH in the third one, and again deionized water in the fourth one. It is also important to place the reservoirs according to pump sequence.

3. Place the support/substrate in the spin coater (see Figure B.**8**). Note: if your sample can not be hold by vacuum for example membranes then use another light flat base and stick or glue the samples to that base then put the base in the spin coater.
4. Close the spincoater lid and make sure it is properly closed otherwise you may encounter unexpected error during film preparation.
5. Turn on the spin coater.
6. Transfer your attention to the G3P and SpinGrower control software. Key the required information to the software. For example the spin speed of 3000 rpm, flow rate of 0.4 mL/sec for 7 sec for the pumps that are going to be used for delivering PAA and PAH solution and flow rate of 0.4 mL/sec for 20 sec for the pumps that are going to be used for delivering washing water, number of deposition of 60. Note: it is important to provide enough Dwell time so the spin coater does not stop while number of film deposition is still not yet accomplished.
7. Click start button in G3P software and wait until the spincoater reaches desired speed i.e. 3000 rpm then click start button in SpinGrower software.
8. After film deposition is accomplished, click stop button in G3P software if the spin coater is still running. Open the lid and take the sample out from the spin coater.
9. Clean the spin coater after use to avoid corrosion and blockage of vacuum line.

STERLITECH CF042 PERMEATION CELL

The Sterlitech CF042 membrane cell is a lab scale cross flow filtration unit that is designed to provide fast and accurate performance data with minimal amounts of product, expense, and time. The CF042 can be used in a variety of applications and with a variety of membranes.

Specification

Table B.22. System Specification

Component	Description
Effective Membrane Area	42 cm^2 (9.207 cm x 4.572 cm) Outer Dimensions : 12.7 cm x 10 cm x 8.3 cm
Cell Body	Stainless steel (CF042SS316) and PTFE (CF042)
Top and Bottom Plate	316L Stainless Steel
Quick Release Knobs	Stainless Steel
Support	20 micron sintered 316L Stainless Steel
O-rings	Buna (Viton Available)
Maximum Pressure	69 bar (1000 psi) for PTFE version
Maximum Operating Temp	80ºC
pH Range	Membrane Dependent

Principle of Operation:

The permeation cell setup can be seen in Figure B.12 and Figure B.13. A single piece of rectangular membrane is installed in the base of the cell. The two cell components are assembled using the stainless steel studs as guides. Use the "quick-release" hand nuts to tighten the components together. The feed stream is pumped from the user supplied feed vessel to the feed inlet. The feed inlet is located on the cell bottom. Flow continues through a manifold into the membrane cavity. Once in the cavity, the solution flows tangentially across the membrane surface. Solution flow is fully user controlled and is laminar or turbulent depending upon the fluid viscosity and fluid velocity. A portion of the solution permeates the membrane and flows through the permeate carrier, which is located on top of the cell. The permeate flows to the center of the cell body top, is collected in a manifold and then flows out the permeate outlet connection into a user supplied permeate collection vessel. The concentrate stream, which contains the material rejected by the membrane, continues sweeping over the membrane and collects in the manifold. The concentration then flows out the concentrate tube into a vessel or back into the feed vessel.

Figure B.12. CF042-Permeation Cell Setup

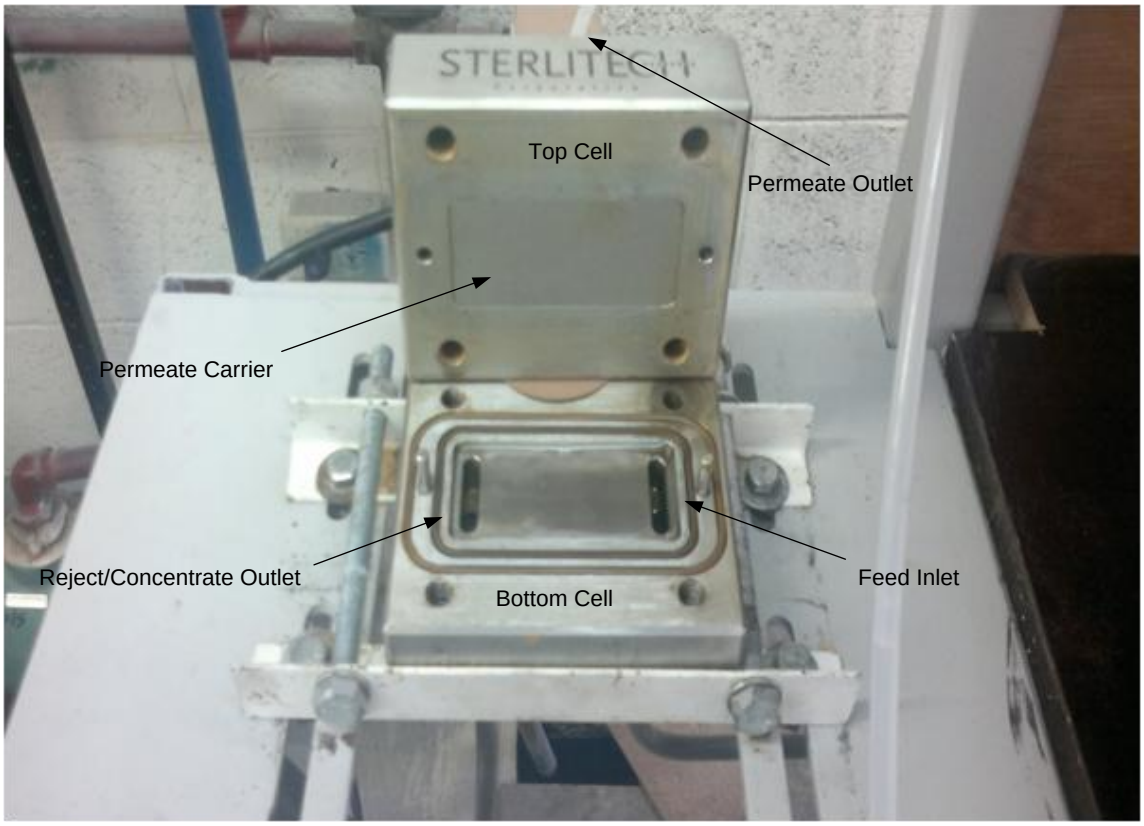

Figure B.13. Stainless Steel CF042SS316 Permeation Cell

Example of Membrane Testing

All membranes in this work were tested at 2000 ppm NaCl, pressure of 40 bar, temperature of 25^{o}C, pH of 6.

1. Prepare 2000 ppm NaCl Solution as much as 20 L by dissolving 40 gram NaCl and place the solution in the feed tank. Close the lid of the feed tank.
2. Put the membrane sample (11 cm x 7 cm) in the cell. Make sure the active side facing down. Tight the cell very well.
3. Turn on the chiller and set the chiller temperature at 0^{o}C. Wait until the temperature of the feed around 15^{o}C.
4. Start the pump by pressing black switch on the right side of permeation table.
5. Increase the pressure gradually until the desired pressure achieved.
6. Fine tune the chiller temperature (typically around 10 - 15 ^{o}C) in order to maintain feed temperature at 25^{o}C.
7. Collect the sample from permeate tube at specific time using volumetric glass for example for 10 or 15 mL and measure the time to collect the sample.

References

[1] M.A. Montgomery, M. Elimelech, Water And Sanitation in Developing Countries: Including Health in the Equation, Environmental Science & Technology, 41 (2007) 17-24.

[2] S. Pfister, A. Koehler, S. Hellweg, Assessing the Environmental Impacts of Freshwater Consumption in LCA, Environmental Science & Technology, 43 (2009) 4098-4104.

[3] M.A. Shannon, P.W. Bohn, M. Elimelech, J.G. Georgiadis, B.J. Marinas, A.M. Mayes, Science and technology for water purification in the coming decades, Nature, 452 (2008) 301-310.

[4] L.F. Greenlee, D.F. Lawler, B.D. Freeman, B. Marrot, P. Moulin, Reverse osmosis desalination: Water sources, technology, and today's challenges, Water Research, 43 (2009) 2317-2348.

[5] W. Neil M, Distillation plant development and cost update, Desalination, 136 (2001) 3-12.

[6] R. Borsani, S. Rebagliati, Fundamentals and costing of MSF desalination plants and comparison with other technologies, Desalination, 182 (2005) 29-37.

[7] C. Fritzmann, J. Lowenberg, T. Wintgens, T. Melin, State-of-the-art of reverse osmosis desalination, Desalination, 216 (2007) 1-76.

[8] K.V. Reddy, N. Ghaffour, Overview of the cost of desalinated water and costing methodologies, Desalination, 205 (2007) 340-353.

[9] R.J. Petersen, Composite reverse osmosis and nanofiltration membranes, Journal of Membrane Science, 83 (1993) 81-150.

[10] I. Moch, Hollow fiber Permeators and reverse osmosis, in: Desalination and Water Reuse, 1992, pp. 30-37.

[11] J. Johnson, M. Busch, Engineering Aspects of Reverse Osmosis Module Design in: IDS Annual Conference, Israel, 2009, pp. 39-72.

[12]http://www.thepurchaseadvantage.com/page/TPA/CTGY/Toray_RO_Membranes.html, in.

[13] Y.S. Lee, Self-Assembly and Nanotechnology: a Force Balance Approach, John Wiley & Sons, Inc, New Jersey, 2008.

[14] I. Langmuir, The Constitution and Fundamental Properties of Solids and Liquids. II Liquids.1, Journal of the American Chemical Society, 39 (1917) 1848-1906.

[15] K.B. Blodgett, Films Built by Depositing Successive Monomolecular Layers on a Solid Surface, Journal of the American Chemical Society, 57 (1935) 1007-1022.

[16] G.D. Rose, J.A. Quinn, Gas transport through supported Langmuir-Blodgett multilayers, Journal of Colloid and Interface Science, 27 (1968) 193-207.

[17] B. Tieke, Langmuir–Blodgett membranes for separation and sensing, Advanced Materials, 3 (1991) 532-541.

[18] M.D. Conner, V. Janout, I. Kudelka, P. Dedek, J. Zhu, S.L. Regen, Perforated monolayers: fabrication of calix[6]arene-based composite membranes that function as molecular sieves, Langmuir, 9 (1993) 2389-2397.

[19] R.A. Hendel, L.-h. Zhang, V. Janout, M.D. Conner, J.T. Hsu, S.L. Regen, Insight into the Permeation Selectivity of Calix[n]arene-Based Langmuirâˆ’Blodgett Films:â€‰ Importance of Headgroup Association and the Solid Phase, Langmuir, 14 (1998) 6545-6549.

[20] G.B. Khomutov, Interfacially formed organized planar inorganic, polymeric and composite nanostructures, Advances in Colloid and Interface Science, 111 (2004) 79-116.

[21] C.R. Martin, M. Nishizawa, K. Jirage, M. Kang, Investigations of the Transport Properties of Gold Nanotubule Membranes, The Journal of Physical Chemistry B, 105 (2001) 1925-1934.

[22] C.R. Martin, M. Nishizawa, K. Jirage, M. Kang, S.B. Lee, Controlling Ion-Transport Selectivity in Gold Nanotubule Membranes, Advanced Materials, 13 (2001) 1351-1362.

[23] M. Wirtz, C.R. Martin, Template-Fabricated Gold Nanowires and Nanotubes, Advanced Materials, 15 (2003) 455-458.

[24] J.C. Hulteen, K.B. Jirage, C.R. Martin, Introducing Chemical Transport Selectivity into Gold Nanotubule Membranes, Journal of the American Chemical Society, 120 (1998) 6603-6604.

[25] K.B. Jirage, J.C. Hulteen, C.R. Martin, Effect of Thiol Chemisorption on the Transport Properties of Gold Nanotubule Membranes, Analytical Chemistry, 71 (1999) 4913-4918.

[26] S. Yu, S.B. Lee, M. Kang, C.R. Martin, Size-Based Protein Separations in Poly(ethylene glycol)-Derivatized Gold Nanotubule Membranes, Nano Letters, 1 (2001) 495-498.

[27] S. Yu, S.B. Lee, C.R. Martin, Electrophoretic Protein Transport in Gold Nanotube Membranes, Analytical Chemistry, 75 (2003) 1239-1244.

[28] M.-S. Kang, C.R. Martin, Investigations of Potential-Dependent Fluxes of Ionic Permeates in Gold Nanotubule Membranes Prepared via the Template Method, Langmuir, 17 (2001) 2753-2759.

[29] S.B. Lee, C.R. Martin, pH-Switchable, Ion-Permselective Gold Nanotubule Membrane Based on Chemisorbed Cysteine, Analytical Chemistry, 73 (2001) 768-775.

[30] J.C. Love, L.A. Estroff, J.K. Kriebel, R.G. Nuzzo, G.M. Whitesides, Self-Assembled Monolayers of Thiolates on Metals as a Form of Nanotechnology, Chemical Reviews, 105 (2005) 1103-1170.

[31] R.K. Iler, Multilayers of colloidal particles, Journal of Colloid and Interface Science, 21 (1966) 569-594.

[32] G. Decher, J.D. Hong, J. Schmitt, Buildup of ultrathin multilayer films by a self-assembly process: III. Consecutively alternating adsorption of anionic and cationic polyelectrolytes on charged surfaces, Thin Solid Films, 210-211 (1992) 831-835.

[33] Y. Lvov, G. Decher, H. Mohwald, Assembly, Structural Characterization, and Therml-Behavior of Layer-by-Layer Deposited Ultrathin Films of Poly(Vinyl Sulfate) and Poly(Allylamine), Langmuir, 9 (1993) 481-486.

[34] J. Schmitt, T. Grunewald, G. Decher, P.S. Pershan, K. Kjaer, M. Losche, Internal Structure of Layer-by-Layer Adsorbed Polyelectrolyte Films-A Neutran and X-Ray Reflectivity Study, Macromolecules, 26 (1993) 7058-7063.

[35] Y. Lvov, H. Haas, G. Decher, H. Mohwald, A. Mikhailov, B. Mtchedlishvily, E. Morgunova, B. Vainshtein, Successive Deposition of Alternate Layers of Polyelectrolytes and A Charged Virus, Langmuir, 10 (1994) 4232-4236.

[36] J. Schmitt, G. Decher, W.J. Dressick, S.L. Brandow, R.E. Geer, R. Shashidhar, J.M. Calvert, Metal nanoparticle/polymer superlattice films: Fabrication and control of layer structure, Advanced Materials, 9 (1997) 61-&.

[37] G.B. Sukhorukov, H. M◌hwald, G. Decher, Y.M. Lvov, Assembly of polyelectrolyte multilayer films by consecutively alternating adsorption of polynucleotides and polycations, Thin Solid Films, 284-285 (1996) 220-223.

[38] G. Decher, Fuzzy nanoassemblies: Toward layered polymeric multicomposites, Science, 277 (1997) 1232-1237.

[39] Y. Shimazaki, M. Mitsuishi, S. Ito, M. Yamamoto, Preparation of the Layer-by-Layer Deposited Ultrathin Film Based on the Charge-Transfer Interaction, Langmuir, 13 (1997) 1385-1387.

[40] Y. Shimazaki, M. Mitsuishi, S. Ito, M. Yamamoto, Preparation and Characterization of the Layer-by-Layer Deposited Ultrathin Film Based on the Charge-Transfer Interaction in Organic Solvents, Langmuir, 14 (1998) 2768-2773.

[41] C. Helm, M. Lösche, H. Möhwald, G. Decher, J. Schmitt, Fine-Tuning of the film thickness of ultrathin multilayer films composed of consecutively alternating layers of anionic and cationic polyelectrolytes, in: Trends in Colloid and Interface Science VI, Springer Berlin / Heidelberg, 1992, pp. 160-164.

[42] S.S. Shiratori, M.F. Rubner, pH-Dependent Thickness Behavior of Sequentially Adsorbed Layers of Weak Polyelectrolytes, Macromolecules, 33 (2000) 4213-4219.

[43] K. B¼scher, K. Graf, H. Ahrens, C.A. Helm, Influence of Adsorption Conditions on the Structure of Polyelectrolyte Multilayers, Langmuir, 18 (2002) 3585-3591.

[44] J.B. Schlenoff, S.T. Dubas, T. Farhat, Sprayed Polyelectrolyte Multilayers, Langmuir, 16 (2000) 9968-9969.

[45] G.M. Nogueira, D. Banerjee, R.E. Cohen, M.F. Rubner, Spray-Layer-by-Layer Assembly Can More Rapidly Produce Optical-Quality Multistack Heterostructures, Langmuir, 27 7860-7867.

[46] K.C. Krogman, N.S. Zacharia, S. Schroeder, P.T. Hammond, Automated Process for Improved Uniformity and Versatility of Layer-by-Layer Deposition, Langmuir, 23 (2007) 3137-3141.

[47] A. Izquierdo, S.S. Ono, J.C. Voegel, P. Schaaf, G. Decher, Dipping versus Spraying:â€‰ Exploring the Deposition Conditions for Speeding Up Layer-by-Layer Assembly, Langmuir, 21 (2005) 7558-7567.

[48] J. Cho, K. Char, J.D. Hong, K.B. Lee, Fabrication of Highly Ordered Multilayer Films Using a Spin Self-Assembly Method, Advanced Materials, 13 (2001) 1076-1078.

[49] S.-S. Lee, J.-D. Hong, C.H. Kim, K. Kim, J.P. Koo, K.-B. Lee, Layer-by-Layer Deposited Multilayer Assemblies of Ionene-Type Polyelectrolytes Based on the Spin-Coating Method, Macromolecules, 34 (2001) 5358-5360.

[50] P.A. Chiarelli, M.S. Johal, J.L. Casson, J.B. Roberts, J.M. Robinson, H.L. Wang, Controlled Fabrication of Polyelectrolyte Multilayer Thin Films Using Spin-Assembly, Advanced Materials, 13 (2001) 1167-1171.

[51] S. Vozar, Y.-C. Poh, T. Serbowicz, M. Bachner, P. Podsiadlo, M. Qin, E. Verploegen, N. Kotov, A.J. Hart, Automated spin-assisted layer-by-layer assembly of nanocomposites, Rev Sci Instrum., 80(2) (2009) 023903.

[52] E. Kharlampieva, V. Kozlovskaya, J. Chan, J.F. Ankner, V.V. Tsukruk, Spin-Assisted Layer-by-Layer Assembly: Variation of Stratification as Studied with Neutron Reflectivity, Langmuir, 25 (2009) 14017-14024.

[53] C. Jiang, B.M. Rybak, S. Markutsya, P.E. Kladitis, V.V. Tsukruk, Self-recovery of stressed nanomembranes, Applied Physics Letters, 86 (2005) 121912-121913.

[54] C. Jiang, V.V. Tsukruk, Freestanding Nanostructures via Layer-by-Layer Assembly, Advanced Materials, 18 (2006) 829-840.

[55] Y.-H. Lin, C. Jiang, J. Xu, Z. Lin, V.V. Tsukruk, Robust, fluorescent, and nanoscale freestanding conjugated films, Soft Matter, 3 (2007) 432-436.

[56] C. Jiang, S. Markutsya, V.V. Tsukruk, Compliant, Robust, and Truly Nanoscale Free-Standing Multilayer Films Fabricated Using Spin-Assisted Layer-by-Layer Assembly, Advanced Materials, 16 (2004) 157-161.

[57] H. Dautzenberg, Polyelectrolyte Complex Formation in Highly Aggregating Systems. 1. Effect of Salt:â€‰ Polyelectrolyte Complex Formation in the Presence of NaCl, Macromolecules, 30 (1997) 7810-7815.

[58] C. Brender, M. Danino, Screening in Short Polyelectrolyte Chains. A Monte Carlo Study, The Journal of Physical Chemistry, 100 (1996) 17563-17567.

[59] R. Baker, Membrane technology and applications, McGraw-Hill, New York ; London, 2000.

[60] S. Loeb, S. Sourirajan, Sea Water Demineralization by Means of an Osmotic Membrane, in: Saline Water Conversionâ€”II, AMERICAN CHEMICAL SOCIETY, WASHINGTON, D. C., 1963, pp. 117-132.

[61] L.F. Song, M. Elimelech, Theory of Concentration Polarization in Cross-Flow Filtration, Journal of the Chemical Society-Faraday Transactions, 91 (1995) 3389-3398.

[62] J.G. Wijmans, S. Nakao, J.W.A. Vandenberg, F.R. Troelstra, C.A. Smolders, Hydrodynamic Resistance of Concentration Polarization Boundary-Layers in Ultrafiltration, Journal of Membrane Science, 22 (1985) 117-135.

[63] C. Fritzmann, J. Lowenberg, T. Wintgens, T. Melin, State-of-the-art of reverse osmosis desalination, Desalination, 216 (2007) 1-76.

[64] K.C. Khulbe, T. Matsuura, S. Singh, G. Lamarche, S.H. Noh, Study on fouling of ultrafiltration membrane by electron spin resonance, Journal of Membrane Science, 167 (2000) 263-273.

[65] S.S. Sablani, M.F.A. Goosen, R. Al-Belushi, M. Wilf, Concentration polarization in ultrafiltration and reverse osmosis: a critical review, Desalination, 141 (2001) 269-289.

[66] M.C. Porter, Concentration Polarization with Membrane Ultrafiltration, Industrial & Engineering Chemistry Product Research and Development, 11 (1972) 234-&.

[67] V. Gekas, B. Hallstrom, Mass-Transfer in the Membrane Concentration Polarization Layer under Turbulent Cross Flow .1. Critical Literature-Review and Adaptation of Existing Sherwood Correlations to Membrane Operations, Journal of Membrane Science, 30 (1987) 153-170.

[68] M.S.H. Bader, J.N. Veenstra, Analysis of concentration polarization phenomenon in ultrafiltration under turbulent flow conditions, Journal of Membrane Science, 114 (1996) 139-148.

[69] Z.V.P. Murthy, S.K. Gupta, Estimation of mass transfer coefficient using a combined nonlinear membrane transport and film theory model, Desalination, 109 (1997) 39-49.

[70] J.P. Agrawal, Souriraj.S, Reverse Osmosis, Industrial and Engineering Chemistry, 61 (1969) 62-&.

[71] N. Lakshminarayanaiah, Transport phenomena in artificial membranes, Chem Rev, 65 (1965) 491-565.

[72] R.W. Laity, An Application of Irreversible Thermodynamics to the Study of Diffusion, Journal of Physical Chemistry, 63 (1959) 80-83.

[73] D.R. Paul, Reformulation of the solution-diffusion theory of reverse osmosis, Journal of Membrane Science, 241 (2004) 371-386.

[74] P. Mukherjee, A.K. SenGupta, Some observations about electrolyte permeation mechanism through reverse osmosis and nanofiltration membranes, Journal of Membrane Science, 278 (2006) 301-307.

[75] T.K. Sherwood, P.L.T. Brian, R.E. Fisher, Desalination by Reverse Osmosis, Industrial & Engineering Chemistry Fundamentals, 6 (1967) 2-&.

[76] A.E. Yaroshchuk, Solution-Diffusion-Imperfection Model Revised, Journal of Membrane Science, 101 (1995) 83-87.

[77] W.S.W. Ho, K.K. Sirkar, Membrane handbook, Van Nostrand Reinhold, New York, 1992.

[78] H.G. Burghoff, K.L. Lee, W. Pusch, Characterization of Transport across Cellulose-Acetate Membranes in the Presence of Strong Solute-Membrane Interactions, Journal of Applied Polymer Science, 25 (1980) 323-347.

[79] K.S. Spiegler, O. Kedem, Thermodynamics of hyperfiltration (reverse osmosis): criteria for efficient membranes, Desalination, 1 (1966) 311-326.

[80] M. Soltanieh, W.N. Gill, REVIEW OF REVERSE OSMOSIS MEMBRANES AND TRANSPORT MODELS, Chemical Engineering Communications, 12 (1981) 279 - 363.

[81] P.A. Chiarelli, M.S. Johal, D.J. Holmes, J.L. Casson, J.M. Robinson, H.-L. Wang, Polyelectrolyte Spin-Assembly, Langmuir, 18 (2001) 168-173.

[82] J. Cho, S.-H. Lee, H. Kang, K. Char, J. Koo, B.H. Seung, K.-B. Lee, Quantitative analysis on the adsorbed amount and structural characteristics of spin self-assembled multilayer films, Polymer, 44 (2003) 5455-5459.

[83] S.-S. Lee, K.-B. Lee, J.-D. Hong, Evidence for Spin Coating Electrostatic Self-Assembly of Polyelectrolytes, Langmuir, 19 (2003) 7592-7596.

[84] L. Krasemann, B. Tieke, Selective Ion Transport across Self-Assembled Alternating Multilayers of Cationic and Anionic Polyelectrolytes, Langmuir, 16 (1999) 287-290.

[85] J.L. Stair, J.J. Harris, M.L. Bruening, Enhancement of the Ion-Transport Selectivity of Layered Polyelectrolyte Membranes through Cross-Linking and Hybridization, Chemistry of Materials, 13 (2001) 2641-2648.

[86] W. Jin, A. Toutianoush, B. Tieke, Use of Polyelectrolyte Layer-by-Layer Assemblies as Nanofiltration and Reverse Osmosis Membranes, Langmuir, 19 (2003) 2550-2553.

[87] B.W. Stanton, J.J. Harris, M.D. Miller, M.L. Bruening, Ultrathin, Multilayered Polyelectrolyte Films as Nanofiltration Membranes, Langmuir, 19 (2003) 7038-7042.

[88] M.D. Miller, M.L. Bruening, Controlling the Nanofiltration Properties of Multilayer Polyelectrolyte Membranes through Variation of Film Composition, Langmuir, 20 (2004) 11545-11551.

[89] R.H. Lajimi, A.B. Abdallah, E. Ferjani, M.S. Roudesli, A. Deratani, Change of the performance properties of nanofiltration cellulose acetate membranes by surface adsorption of polyelectrolyte multilayers, Desalination, 163 (2004) 193-202.

[90] R. Malaisamy, M.L. Bruening, High-Flux Nanofiltration Membranes Prepared by Adsorption of Multilayer Polyelectrolyte Membranes on Polymeric Supports, Langmuir, 21 (2005) 10587-10592.

[91] S.U. Hong, R. Malaisamy, M.L. Bruening, Optimization of flux and selectivity in Cl-/SO42- separations with multilayer polyelectrolyte membranes, Journal of Membrane Science, 283 (2006) 366-372.

[92] S.U. Hong, R. Malaisamy, M.L. Bruening, Separation of Fluoride from Other Monovalent Anions Using Multilayer Polyelectrolyte Nanofiltration Membranes, Langmuir, 23 (2007) 1716-1722.

[93] S.U. Hong, L. Ouyang, M.L. Bruening, Recovery of phosphate using multilayer polyelectrolyte nanofiltration membranes, Journal of Membrane Science, 327 (2009) 2-5.

[94] W. Ritcharoen, P. Supaphol, P. Pavasant, Development of polyelectrolyte multilayer-coated electrospun cellulose acetate fiber mat as composite membranes, European Polymer Journal, 44 (2008) 3963-3968.

[95] H.-Y. Deng, Y.-Y. Xu, B.-K. Zhu, X.-Z. Wei, F. Liu, Z.-Y. Cui, Polyelectrolyte membranes prepared by dynamic self-assembly of poly (4-styrenesulfonic acid-co-maleic acid) sodium salt (PSSMA) for nanofiltration (I), Journal of Membrane Science, 323 (2008) 125-133.

[96] J.B. Schlenoff, H. Ly, M. Li, Charge and Mass Balance in Polyelectrolyte Multilayers, Journal of the American Chemical Society, 120 (1998) 7626-7634.

[97] J.B. Schlenoff, S.T. Dubas, Mechanism of Polyelectrolyte Multilayer Growth:â€‰ Charge Overcompensation and Distribution, Macromolecules, 34 (2001) 592-598.

[98] L. Shao, J.L. Lutkenhaus, Thermochemical properties of free-standing electrostatic layer-by-layer assemblies containing poly(allylamine hydrochloride) and poly(acrylic acid), Soft Matter, 6 (2010) 3363-3369.

[99] T.R. Farhat, J.B. Schlenoff, Ion Transport and Equilibria in Polyelectrolyte Multilayers, Langmuir, 17 (2001) 1184-1192.

[100] A.A. Antipov, G.B. Sukhorukov, H. Möhwald, Influence of the Ionic Strength on the Polyelectrolyte Multilayers' Permeability, Langmuir, 19 (2003) 2444-2448.

[101] J.K. Holt, H.G. Park, Y. Wang, M. Stadermann, A.B. Artyukhin, C.P. Grigoropoulos, A. Noy, O. Bakajin, Fast Mass Transport Through Sub-2-Nanometer Carbon Nanotubes, Science, 312 (2006) 1034-1037.

[102] M. Ishiguro, T. Matsuura, C. Detellier, Reverse osmosis separation for a montmorillonite membrane, Journal of Membrane Science, 107 (1995) 87-92.

[103] L. Li, J. Dong, T.M. Nenoff, R. Lee, Desalination by reverse osmosis using MFI zeolite membranes, Journal of Membrane Science, 243 (2004) 401-404.

[104] G.r. Turgut M, Permselectivity of zeolite filled polysulfone gas separation membranes, Journal of Membrane Science, 93 (1994) 283-289.

[105] R. Kiyono, G.H. Koops, M. Wessling, H. Strathmann, Mixed matrix microporous hollow fibers with ion-exchange functionality, Journal of Membrane Science, 231 (2004) 109-115.

[106] D.Q. Vu, W.J. Koros, S.J. Miller, Mixed matrix membranes using carbon molecular sieves: I. Preparation and experimental results, Journal of Membrane Science, 211 (2003) 311-334.

[107] J.P.G. Villaluenga, M. Khayet, M.A. LÃ³pez-Manchado, J.L. Valentin, B. Seoane, J.I. Mengual, Gas transport properties of polypropylene/clay composite membranes, European Polymer Journal, 43 (2007) 1132-1143.

[108] S.A. Hashemifard, A.F. Ismail, T. Matsuura, Effects of montmorillonite nano-clay fillers on PEI mixed matrix membrane for CO2 removal, Chemical Engineering Journal, 170 316-325.

[109] B.-H. Jeong, E.M.V. Hoek, Y. Yan, A. Subramani, X. Huang, G. Hurwitz, A.K. Ghosh, A. Jawor, Interfacial polymerization of thin film nanocomposites: A new concept for reverse osmosis membranes, Journal of Membrane Science, 294 (2007) 1-7.

[110] H.S. Lee, S.J. Im, J.H. Kim, H.J. Kim, J.P. Kim, B.R. Min, Polyamide thin-film nanofiltration membranes containing TiO2 nanoparticles, Desalination, 219 (2008) 48-56.

[111] A. GarcÃ-a, S. Eceolaza, M. Iriarte, C. Uriarte, A. Etxeberria, Barrier character improvement of an amorphous polyamide (Trogamid) by the addition of a nanoclay, Journal of Membrane Science, 301 (2007) 190-199.

[112] J. Choi, M.F. Rubner, Influence of the Degree of Ionization on Weak Polyelectrolyte Multilayer Assembly, Macromolecules, 38 (2004) 116-124.

[113] D. Yoo, S.S. Shiratori, M.F. Rubner, Controlling Bilayer Composition and Surface Wettability of Sequentially Adsorbed Multilayers of Weak Polyelectrolytes, Macromolecules, 31 (1998) 4309-4318.

[114] M. Elzbieciak, M. Kolasinska, S. Zapotoczny, R. Krastev, M. Nowakowska, P. Warszynski, Nonlinear growth of multilayer films formed from weak polyelectrolytes, Colloids and Surfaces A: Physicochemical and Engineering Aspects, 343 (2009) 89-95.

[115] M. Amara, H. Kerdjoudj, Modification of cation-exchange membrane properties by electro-adsorption of polyethyleneimine, Desalination, 155 (2003) 79-87.

[116]http://www.sigmaaldrich.com/catalog/ProductDetail.do?lang=en&N4=447013|ALDRICH&N5=SEARCH_CONCAT_PNO|BRAND_KEY&F=SPEC.

[117] http://en.wikipedia.org/wiki/Poly%28acrylic_acid%29.

[118] http://www.chemical-reagent.com/products/Poly%28vinyl-sulfate-potassium-salt%29/, in.

[119]http://www.sigmaaldrich.com/catalog/ProductDetail.do?lang=en&N4=283215|ALDRICH&N5=SEARCH_CONCAT_PNO|BRAND_KEY&F=SPEC.

[120]http://www.sigmaaldrich.com/catalog/ProductDetail.do?lang=en&N4=522376|ALDRICH&N5=SEARCH_CONCAT_PNO|BRAND_KEY&F=SPEC&cm_sp=Customer_Favorites-_-Detail_Page-_-Text-522376.

[121] http://en.wikipedia.org/wiki/PolyDADMAC.

[122]http://www.polysciences.com/Catalog/Department/Product/98/categoryId__283/PageIndex__5/search__polyethyleneimine/productId__49/.

[123] http://en.wikipedia.org/wiki/Polyethylenimine.

[124] http://www.sterlitech.com/bench-scale-equipment/flat-sheet-membranes/ultrafiltration-uf-membrane.html.

[125] http://en.wikipedia.org/wiki/Polysulfone.

[126] http://en.wikipedia.org/wiki/Wafer_%28electronics%29.

[127] D.R. Paul, L.M. Robeson, Polymer nanotechnology: Nanocomposites, Polymer, 49 (2008) 3187-3204.

[128] M. Nyström, P. Järvinen, Modification of polysulfone ultrafiltration membranes with UV irradiation and hydrophilicity increasing agents, Journal of Membrane Science, 60 (1987) 275-296.

[129] D. Birnie, S. Hau, D. Kamber, D. Kaz, Effect of ramping-up rate on film thickness for spin-on processing, Journal of Materials Science: Materials in Electronics, 16 (2005) 715-720.

[130] http://en.wikipedia.org/wiki/Attenuated_total_reflectance.

[131] N.S. Zacharia, D.M. DeLongchamp, M. Modestino, P.T. Hammond, Controlling Diffusion and Exchange in Layer-by-Layer Assemblies, Macromolecules, 40 (2007) 1598-1603.

[132] V.V. Tsukruk, V.N. Bliznyuk, D. Visser, A.L. Campbell, T.J. Bunning, W.W. Adams, Electrostatic deposition of polyionic monolayers on charged surfaces, Macromolecules, 30 (1997) 6615-6625.

[133] S. Fujita, S. Shiratori, The initial growth of ultra-thin films fabricated by a weak polyelectrolyte layer-by-layer adsorption process, Nanotechnology, 16 (2005) 1821-1827.

[134] P.A. Chiarelli, M.S. Johal, J.L. Casson, J.B. Roberts, J.M. Robinson, H.L. Wang, Controlled fabrication of polyelectrolyte multilayer thin films using spin-assembly, Advanced Materials, 13 (2001) 1167-+.

[135] J. Cho, K. Char, J. Hong, K. Lee, Fabrication of multilayer films using a spinning process, Growth, Evolution and Properties of Surfaces, Thin Films and Self-Organized Structures. Symposium (Mater.Res. Soc. Symposium Proceedings Vol.648), (2001) P6.25.21-25|xv+602.

[136] P. Yimsiri, M.R. Mackley, Spin and dip coating of light-emitting polymer solutions: Matching experiment with modelling, Chemical Engineering Science, 61 (2006) 3496-3505.

[137] D. Meyerhofer, Characteristics of resist films produced by spinning, Journal of Applied Physics, 49 (1978) 3993-3997.

[138] P.A. Patel, A.V. Dobrynin, P.T. Mather, Combined Effect of Spin Speed and Ionic Strength on Polyelectrolyte Spin Assembly, Langmuir, 23 (2007) 12589-12597.

[139] S.S. Lee, K.B. Lee, J.D. Hong, Evidence for spin coating electrostatic self-assembly of polyelectrolytes, Langmuir, 19 (2003) 7592-7596.

[140] T. Mauser, C. Déjugnat, G.B. Sukhorukov, Reversible pH-Dependent Properties of Multilayer Microcapsules Made of Weak Polyelectrolytes, Macromolecular Rapid Communications, 25 (2004) 1781-1785.

[141] J.L. Lutkenhaus, K. McEnnis, P.T. Hammond, Nano- and Microporous Layer-by-Layer Assemblies Containing Linear Poly(ethylenimine) and Poly(acrylic acid), Macromolecules, 41 (2008) 6047-6054.

[142] G.V. Duarte, B.V. Ramarao, T.E. Amidon, Polymer induced flocculation and separation of particulates from extracts of lignocellulosic materials, Bioresource Technology, 101 (2010) 8526-8534.

[143] Colloid-Polymer Interactions, American Chemical Society, 1993.

[144] X. Feng, M. Leduc, R. Pelton, Polyelectrolyte complex characterization with isothermal titration calorimetry and colloid titration, Colloids and Surfaces A: Physicochemical and Engineering Aspects, 317 (2008) 535-542.

[145] F. Caruso, A.S. Susha, M. Giersig, H. Möhwald, Magnetic Core–Shell Particles: Preparation of Magnetite Multilayers on Polymer Latex Microspheres, Advanced Materials, 11 (1999) 950-953.

[146] L. Shao, J.L. Lutkenhaus, Thermochemical properties of free-standing electrostatic layer-by-layer assemblies containing poly(allylamine hydrochloride) and poly(acrylic acid), Soft Matter, 6 3363-3369.

[147] T. Shintani, A. Shimazu, S. Yahagi, H. Matsuyama, Characterization of methyl-substituted polyamides used for reverse osmosis membranes by positron annihilation lifetime spectroscopy and MD simulation, Journal of Applied Polymer Science, 113 (2009) 1757-1762.

[148] H. Ju, A.C. Sagle, B.D. Freeman, J.I. Mardel, A.J. Hill, Characterization of sodium chloride and water transport in crosslinked poly(ethylene oxide) hydrogels, Journal of Membrane Science, 358 131-141.

[149] W. Xie, H. Ju, G.M. Geise, B.D. Freeman, J.I. Mardel, A.J. Hill, J.E. McGrath, Effect of Free Volume on Water and Salt Transport Properties in Directly Copolymerized Disulfonated Poly(arylene ether sulfone) Random Copolymers, Macromolecules, 44 4428-4438.

[150] A. Bondi, van der Waals Volumes and Radii, The Journal of Physical Chemistry, 68 (1964) 441-451.

[151] J.Y. Park, D.R. Paul, Correlation and prediction of gas permeability in glassy polymer membrane materials via a modified free volume based group contribution method, Journal of Membrane Science, 125 (1997) 23-39.

[152] J.E. Cadotte, R.J. Petersen, R.E. Larson, E.E. Erickson, A new thin-film composite seawater reverse osmosis membrane, Desalination, 32 (1980) 25-31.

[153] A.Q. Wang, N. D'Souza, T.D. Golden, Ceramic montmorillonite nanocomposites by electrochemical synthesis, Applied Clay Science, 42 (2008) 310-317.

[154] A.K. Nikolaidis, D.S. Achilias, G.P. Karayannidis, Synthesis and Characterization of PMMA/Organomodified Montmorillonite Nanocomposites Prepared by in Situ Bulk Polymerization, Industrial & Engineering Chemistry Research, 50 571-579.

[155] D. Rana, T. Matsuura, Surface Modifications for Antifouling Membranes, Chemical Reviews, 110 2448-2471.

[156] S.T. Dubas, J.B. Schlenoff, Swelling and Smoothing of Polyelectrolyte Multilayers by Salt, Langmuir, 17 (2001) 7725-7727.

[157] J. Yang, S. Lee, E. Lee, J. Lee, S. Hong, Effect of solution chemistry on the surface property of reverse osmosis membranes under seawater conditions, Desalination, 247 (2009) 148-161.

VITA

- Farid Fadhillah
- Born in Bontang, 15/6/1978
- Received Bachelor degree (S.T.) in Chemical Engineering from Gadjah Mada University, Indonesia in December 2002.
- Received Master degree (M.T.) in Chemical Engineering from Gadjah Mada University, Indonesia in September 2005.
- Joined King Fahd University of Petrleum & Minerals in February 2007.
- Worked as Lecturer-B at King Fahd University of Petroleum & Minerals.
- Received Doctor of Philosophy degree in Chemical Engineering from King Fahd University of Petroleum & Minerals in April 2012.
- Email: faridfad@kfupm.edu.sa or farid.fadhillah@ymail.com